Feasibility study of Fiber Reinforced Polymer Railway Bridges

MASTER OF SCIENCE THESIS

For the degree of Master of Science in Structural Engineering at Delft University of Technology

Swaraj Sharma

Steel and Composites Section

Faculty of Civil Engineering and Geo-Sciences

TU Delft

Graduation Committee

Prof.Dr. Milan Veljkovic (Chairman)
Department of Structural Engineering, Steel and Composite Structures
Faculty of Civil Engineering and Geosciences
Delft University of Technology

Dr.M.Pavlovic
Department of Structural Engineering, Steel and Composite Structures
Faculty of Civil Engineering and Geosciences
Delft University of Technology

Peter Konijnenbelt (MSc)
Senior Structural Engineer at Arcadis BV
Delft University of Technology

Dr.ir.FP van der Meer
Department of Structural Engineering, Computational Mechanics
Faculty of Civil Engineering and Geosciences
Delft University of Technology

Ir.L.J.M Houben (Coordinator)
Department of Structural Engineering, Road and Railway Engineering
Faculty of Civil Engineering and Geosciences
Delft University of Technology

Table of Contents

Preface

Dear Reader,
This thesis marks the completion of my Masters in Structural Engineering at the Faculty of Civil Engineering and Geosciences, Delft University of Technology. This research has been performed under the supervision of dr.Marko Pavlovic and Peter Konijnenbelt (MSc).

I would like to convey my gratitude to the Steel and Composite Structures section initiative towards research excellence. They gave me the freedom to explore the subject, and also for supporting and guiding me when needed. I would also like to extend my gratitude to employees from Arcadis, who helped me throughout my work and guided me whenever I was struck. I am deeply indebted to prof.Milan Veljkovic and dr.ir.FP van der Meer for their support in the graduation work.

I would like to thank my close friends here in Delft, Hemant, Swaraj, Dhruv, Ravi and other international students who have made my stay in Delft extraordinary. My utmost gratitude to my parents for believing in my dream and providing me with endless love and support, without which I would not have reached this far in my life. Special thanks to Swastik and Sakshi for their care and understanding.

Nearly two years ago, I started with my Masters in Structural Engineering. I never imagined that my dream to understand this fascinating field of structures would bring me here. It has inspired me to take on this challenge and equipped me with the tools to make a difference, albeit small, through this research and the projects to come.

Swaraj Sharma
Delft,
The Netherlands

Summary

The Netherlands has one of the busiest rail network in the Europe (Oliver Wyman, 2016) that is growing rapidly due to the limited rail network and improved inter-connectivity with road and marine transportation mode. Because of intensifying rail traffic and ageing rail bridge infrastructure (Archives: Arcadis), the rail bridge infrastructure comprising of steel bridges is deteriorating. The simple old and small span steel railway bridges have approached their service life and are outdated according to OVS guidelines in terms of safety, repair and inspection. In addition, the issue of structural degradation because of corrosion, noise emission in the neighborhood and fatigue resistance adds to the severity of this scenario.

A static linear assessment of one of the old steel railway bridges with I-girder section is made to have a look at the impact of increased frequency. The assessment is based on the method of calculating fatigue damage using equivalence factors for a stress range and NEN8701-2015 code for the assessment of existing bridge structures in the Netherlands. The top flange of the I-beam with holes can be treated as a structural element with holes subjected to bending and axial forces and checked for fatigue stresses against detail category 90 (Table 8.1, EN1993-1-9). The damage of 1.3 is observed on the top flange when the bridge is just 44 years old. Another issue with the existing bridge is the lack of function requirements like passenger path for accidental evacuation, repair path and noise absorbing elements for the neighborhood. Alternate solutions for the upgrading of service life are discussed and studied in the literature study section.

The Common solution in The Netherlands is to replace them with heavier steel bridge or a concrete slab bridge (heavier). The increased weight of the new steel railway bridge structure is about 33% higher than the existing steel rail bridge. Due to the increased weight of the bridge structure, the foundation may need upgrading as well, which is expensive and takes more time. In-order to re-use the existing foundation and shorten the construction period, the alternative solution for the redundant old short span steel railway bridge is to replace it with the FRP material structure. Glass Fibers Polymer materials have a high strength to weight ratio, while 70 percent lighter than conventional steel structures. This reduces the dead load of bridge structure as compared to the existing steel bridge and existing foundations can be reused. FRP's inherit low Young's modulus due to the resin in the laminate. Therefore, the design of such bridges to restraint heavier rail loadings is stiffness based.

A literature study is made to consider the state of the art FRP bridge decks available in the market and manufacturing processes involved. A study into EN1991-2-2003 and OVS00030-06 is made to determine the design criteria for the bridges. In addition, a study about the application of the FRP laminates for the railway bridge, behavior of FRP under static ULS and fatigue conditions is done. To fit the new FRP bridge under the existing scenario, the influence of embedded rail system and ballast track system on the bridge is understood.

Subsequently, conceptual design of FRP bridges is made to choose the final desired shape of the structure. Then using these shapes, a combination of FRP-steel and only FRP material bridge forms comprising of ballast rail track system and embedded rail track system is made using OVS guidelines. The respective design is based on short term deflection criteria using approximate material values from the literature. A comparison between these structural forms is made based on deflection and critical areas for fatigue like connections. Form II and Form III comprising of only FRP material are considered for preliminary analysis to study the feasibility of only FRP bridge.

Accordingly, the laminate analysis is performed using an online tool to determine Young's modulus and strength values of the ply lay-up considered for this application. The ply lay-up is designed per CUR,96 recommendations and from the manufacturing point of view such that there are no warping stresses, shear-extension and shear-bending coupling within the plies. The results of this tool are verified by the properties given in JRC,2016 for bi-directional ply.

The preliminary design of bridge follows the conceptual design using the customized ply laminate properties in the thesis study where the influence of creep on FRP material and the existing depth using the feasible rail track system is considered. The final geometric lay-out of these forms are presented including functional requirements consideration. Form II (ballast track system) is optimized by studying the effect of webs orientation in the structure to increase stiffness and reduce material consumption. The variation study and the deflection calculation is done by using the ABAQUS. Both the forms are modelled in ABAQUS.

After the preliminary design of the bridge, the bridge is checked for ULS loadings against their expected failure modes per JRC, 2016.The checks for the failure modes are within the safety ratio of 1 for both these bridges. The shear stresses at the supports have the maximum stresses. The results are verified by hand calculations made for Timoshenko beam model with similar bridge properties. The embedded rail track system bridge structure is finally chosen for feasibility analysis as the depth requirement of this bridge is within the allowable allowance and the weight is low by 1.5 times less than the bridge with ballast.

Although, fatigue resistance of FRP material is high as evident due to their application in aerospace industry. But the nature of fatigue phenomena in the civil application of this material is still unknown due to the various application of this material in the industry and different range of loads encountered. For analysis, critical details are obtained from the static analysis. This is followed by obtaining influence line diagram and moving set of real fatigue load models mentioned in Annex, EN1991-2. Rainfall counting method is used and stress-histogram plots are obtained for bending, shear and normal stresses respectively. Further, the damage is calculated using Miner's rule. The damage for all the details is low making sure that the service life of 100 years is easily achievable for the FRP bridge.

In the end, a revised design of Form III is made with serviceability (deflection) as the governing criterion observed from the above analysis performed. The geometry is optimized to have reduced mass and limiting deflections. The weight of the final revised FRP bridge is 2.4 times the new steel railway bridge per structural elements.

List of Figures

Ply		Micromec	Fiber		Matrix		Fraction		Thickness [mm]	Density [kg/m3]
ID	Name		Fiber ID	Fiber name	Matrix ID	Matrix name	type	amount [%]		
1	UD ply	yes	1	E-Glass	1	Polyester	fiber volume	55	0,8	1.953,5

List of Tables

1

Introduction

1.1 Background

The importance of public transport in the Netherlands can be dated back to 17th century when Dutch people used horse-drawn carts and track boats. Since then, the concept of public transport extended from waterways (canals) to bus-services and trams. It was in 1929 when railways developed in the country. The tradition of public transport started from 17th century continued to the 21st century, as evident from the development of high-speed rail lines and a dense complimentary urban network of buses and trams.

To understand the influence of public transport in the normal life of working Dutch people, the figure 1 below compares the commutes made by the passenger. From this figure, it can be observed that the around 10% of the population favours travel by trail mode(train/tram/metro) within Netherlands. This results in 2.4% of the traffic in the country.

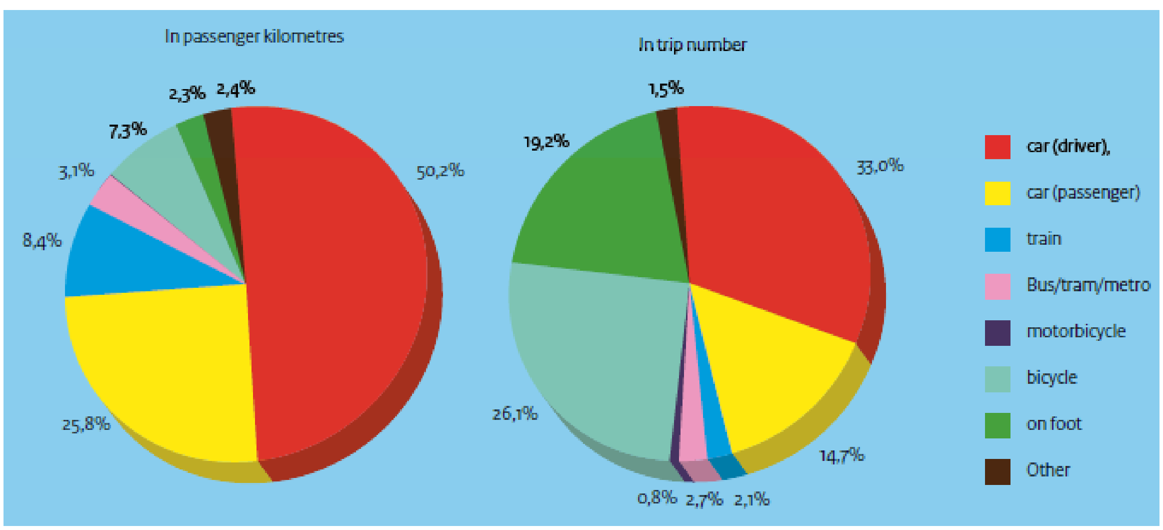

Figure 1 Passenger kilometers performed and trip number (Source: Mobiliteitsonderzoek Nederland)

Interestingly, the role of the rail transport is not only limited to the citizens but also contribute to the economy of the country. Figure 2 shows that 1% of the goods are transported by rail mode within the country and around 8% at intra-country level

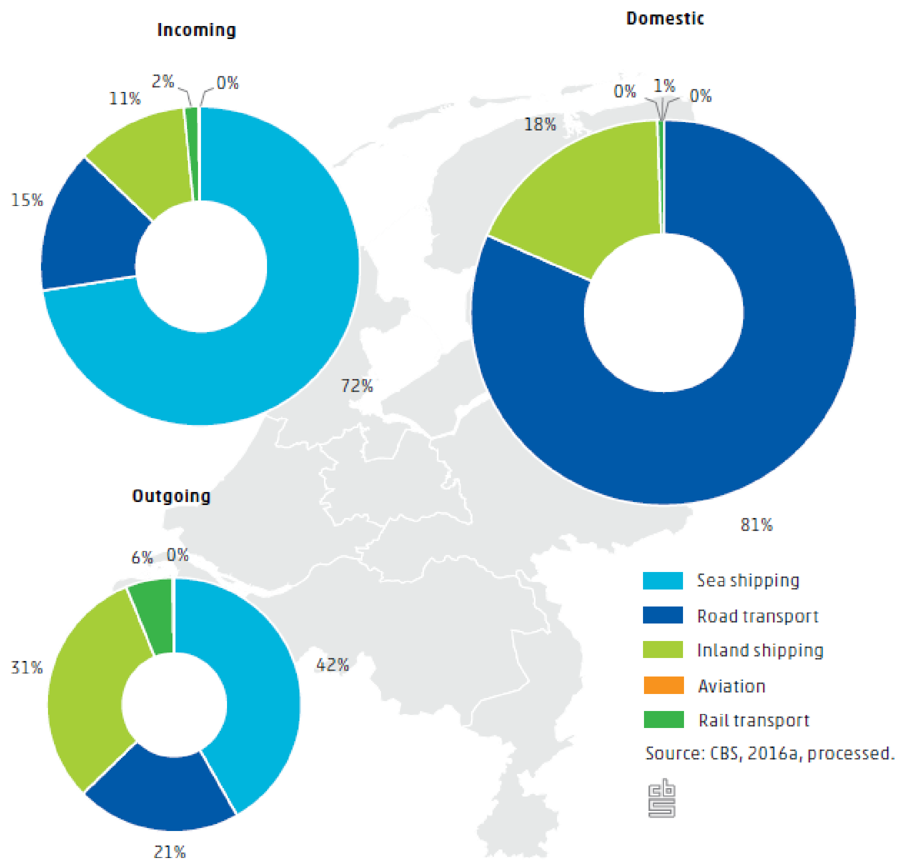

Figure 2 Goods transported in The Netherlands (Source: CBS,2016)

Overall, the study can say that the rail transport plays an important role in Dutch society and provides an easy and convenient way of travel. The rapid increase in the passengers carried by rail every 5 years in Figure 3 testifies the dependence of Dutch society on rail mode of communication.

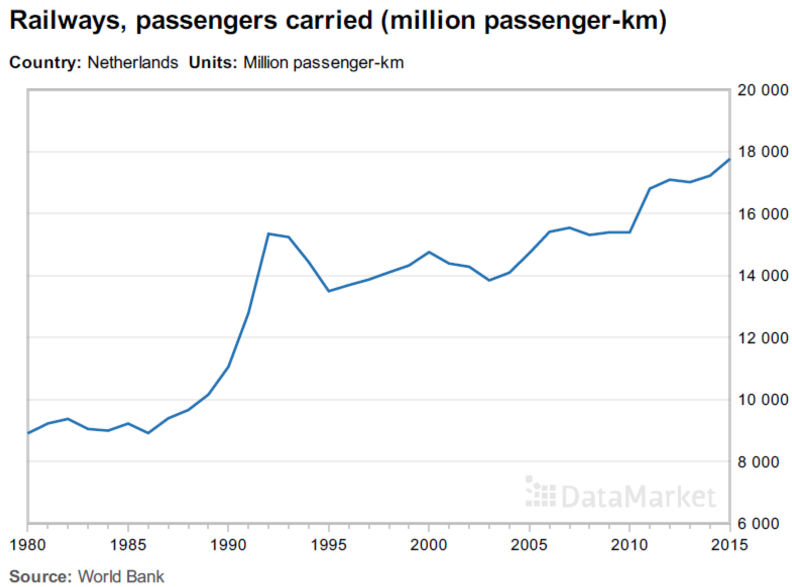

Figure 3 Railway passenger- kilometer per year (Source: World Bank)

1.2 Rail traffic scenario in The Netherlands

The Netherlands has one of the busiest rail network in the Europe (Oliver Wyman, 2016) that is growing rapidly due to the limited rail network and improved inter-connectivity with road and marine transportation mode. Figure 4 below shows that The Netherlands has the highest train density per Day among all the European countries in 2014.

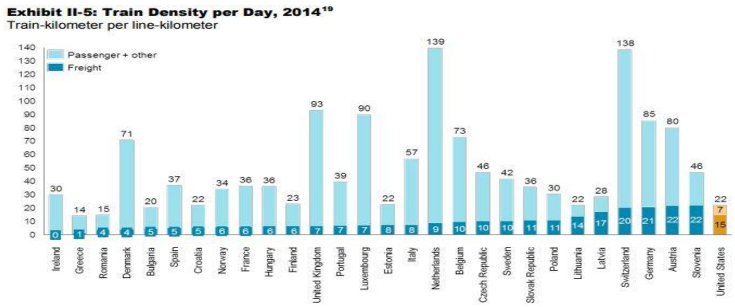

Figure 4 Train Density per Day (Source: Oliver Wyman,2016)

Due to limited land and increased train density, it is expected to have higher rail line density in the country to enable smooth flow of passengers and freight transport. Figure 5 shows the railway line density for the year 2012 among the European nations. One can observe that The Netherlands is among the countries with densest railway lines in the Europe.

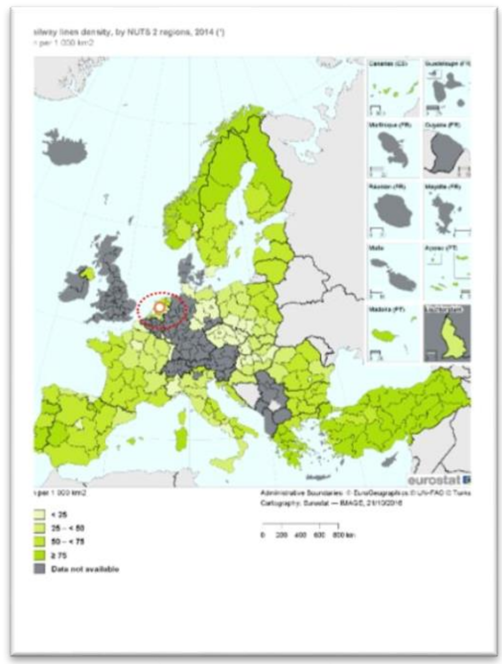

Figure 5 Railway lines density in Europe (Source: Eurostat)

Therefore, one can conclude from these above-mentioned figures that the Netherlands has the busiest and intensified rail network in the Europe.

1.3 Rail infrastructure in The Netherlands

To sustain a society which is dependent upon rail mode transportation for its daily operational need, the rail infrastructure has a huge role to play in it. Since the setting up of railways till present, the emphasis has been laid on the installation of new assets that aid in running more number of trains at a faster speed and safe operation.

Examples of such modernisation are electrification and upgradation of Rotterdam to Zevenaar and Zevenaar to Emmerich to 25kV 50Hz trunk freight line for smooth transfer of goods.

Large scale conversion of railway lines has been made in the past. Upgradation of existing lines of Amsterdam to Brussel to high speed line of 2400V.The existing 1.5kV dc system throughout the country is proposed to extend till 25kV as well.

In the context of rolling stock, to sustain high speed lines new rolling stock like ICE3M and TGV etc. have been ordered to work/working on the proposed 25kV lines.

Additionally, catenary infrastructure has also been upgraded or proposed for some left rail sections to get adapted to 25kV. The existing signalling system is being replaced with more modern European Train Control system.

It is important to consider that infrastructure modernisation of high speed rolling stock along with the electrical stock is for an increase in train frequency in The Netherlands and introduction of high speed lines to reduce travel time. The idea of emphasising on such modernisation acts is to make a comparison with the upgradation of existing rail bridge infrastructure. Though a lot of upgradation activities have been taken place by Dutch government the story of bridge infrastructure which will pave the way for high speed and uninterrupted rail movement is mostly ignored due to lack of knowledge about the hidden failure causing mechanisms. Until 2000, Rijkswaterstaat had no idea about the faster wearing out of the steel bridges in the country due to a combination of increasing traffic density and local wheel loads resulting in fatigue. It was in 2000 when Rijkswaterstaat in combination with TU delft lead a program to calculate the state and lifespan of these bridge to take appropriate measures (NWO).Therefore, the upgradation of bridge rail infrastructure is lacking behind its peers.

1.3.1 Steel rail bridges

In the Netherlands, most of the civil rail infrastructure especially bridges were built in the 1960s and 1970s. According to a study done by TNO (TNO TIME, 2017), around 70% of such bridges were constructed before 1980.By that time, these bridges were estimated to be 50-80 years old. Thus, the Dutch rail infrastructure is approaching their service life or has reached. To have a better understanding of such scenario, an overview of year of construction of steel railway bridges constructed in The Netherlands is shown in figure 6. This figure shows the age composition of 974 steel bridges operational in The Netherlands.

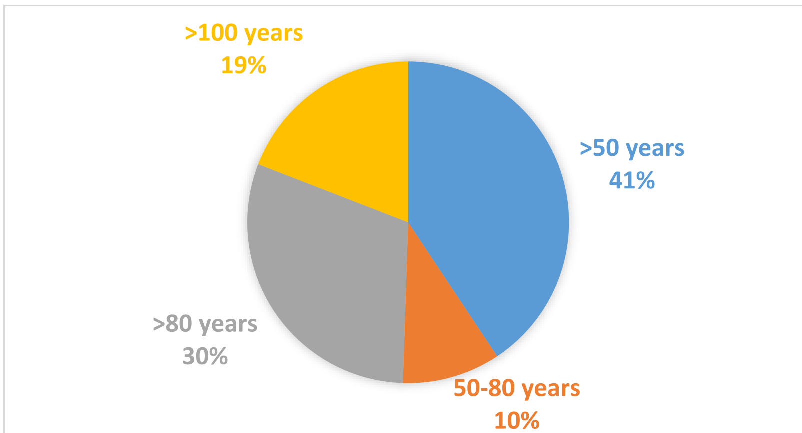

Figure 6 Age Composition of Steel Bridges in The Netherlands (Source: Arcadis: archives)

From the above figure 6, it can be observed that around 19% of the steel bridges have already exceeded their service life whereas around 30% of them are near to their end life. In fact, in upcoming years this will add more to the aging numbers. Therefore, the ageing of steel rail bridge infrastructure is a concern for the Netherlands government and rail infrastructure.

Out of all the rail bridges described above in Figure 6, most of them comprise of double I-girder steel rail bridges. This is evident from the figure 7 shown below which shows the type of small span steel rail bridges out of the total 974 steel rail bridges in the country.

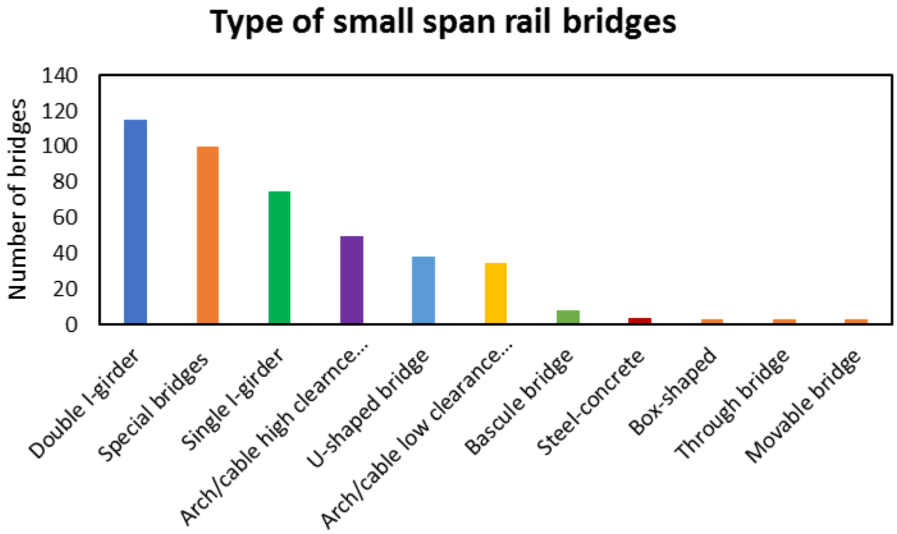

Figure 7 Type of small span rail bridges (Source: Arcadis, archives)

A close look into the age of these bridges (Figure 8) reveals about their service life which has been exceeded or are near to exceed. Figure 9 shows the span and number of such bridges that are small.

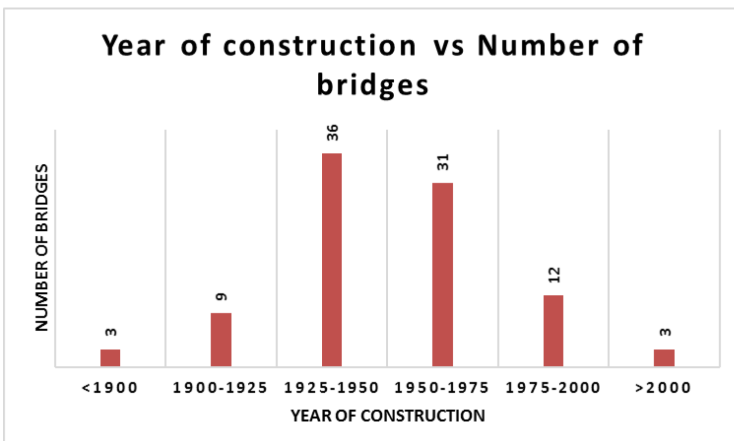

Figure 8 Year of construction of small span steel rail bridges

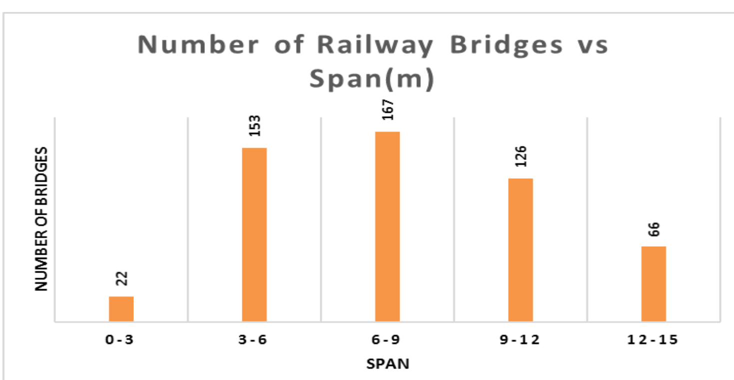

Figure 9 No of Railway Bridges vs Span(m) (Archives: Arcadis, NL)

This situation is critical in terms of the safe and reliable operation of steel railway bridges in the country. In the light of increasing rail density in the country, thereby increase in passage of trains across the bridge, this might lead to a critical situation. This should be dealt urgently by assessing the structural integrity of these bridge infrastructures which have extended beyond /approaching their service life in the Netherlands.

1.4 Evolution of rail traffic loads

Since various rail bridges have aged as reported in the section 1.3.1, the burden of the traffic has also increased from the 18th century to the present.

For the ULS design of steel bridges, a load model is used that represents the equivalent axle load of a train. As the type of axles of trains has evolved with time, so as the load models to present the impact of actual train load for ultimate strength and optimum design of bridges. An overview of the traffic load model for steel bridge in the Netherlands for the time between 1963-2002 and 2002 to present is shown in figure 10 and 11. For the period between 1963-2002, VOSB-1963 was used for the design of steel bridges in The Netherlands.

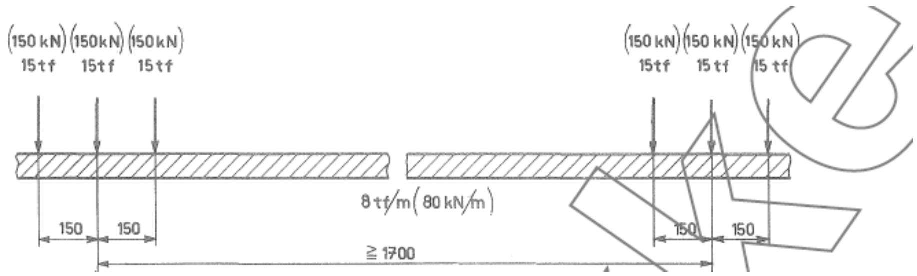

Figure 10 Rail load model (VOSB1963)

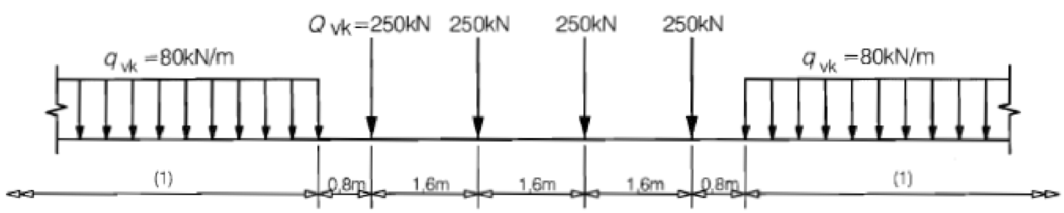

Figure 11 LM 71 (EN 1991-2-2003)

From the above figures, it can be seen that the load positions and magnitude have changed. The value of concentrated load has increased from 150kN to 250kN though the magnitude of UDL load remains the same. The impact of such changes will be observed in the next section.

1.4.1 Comparison of load models

In this section, the study will compare the influence of the load models from VOSB,1963 and EN1991-2-2003 on the bending moment acting on a HE650B simply supported beam of length varying from 5-15m span for comparison. The objective of the comparison is to observe how do these load models affect the ultimate strength of a bridge as a function of their span length. The bridge is modelled as a beam for simplified comparison.

Figure 12 shows the plot of bending moment of HE650B beam with varying span when subjected to load model from VOSB,1963 and EN1991-2-2003 under the ultimate limit state. For comparison, the VOSB load is multiplied by S and B factor which is defined as:

$$S(Impact\ coefficient) = 1 + \left(\frac{60}{100 + L}\right), where\ L\ is\ span\ in\ meters$$

$$B(Load\ coefficient) = 0.6 + \left(\frac{40}{100 + L}\right), where\ L\ is\ span\ in\ meters$$

Load model from EN1991-2-2003 is multiplied by load coefficient $\alpha = 1.21$ and dynamic coefficient for carefully maintained tracks $\varphi = \frac{1.44}{L^{0.5} - 0.2} + 0.82$, $where\ L\ is\ the\ span\ in\ meters.$

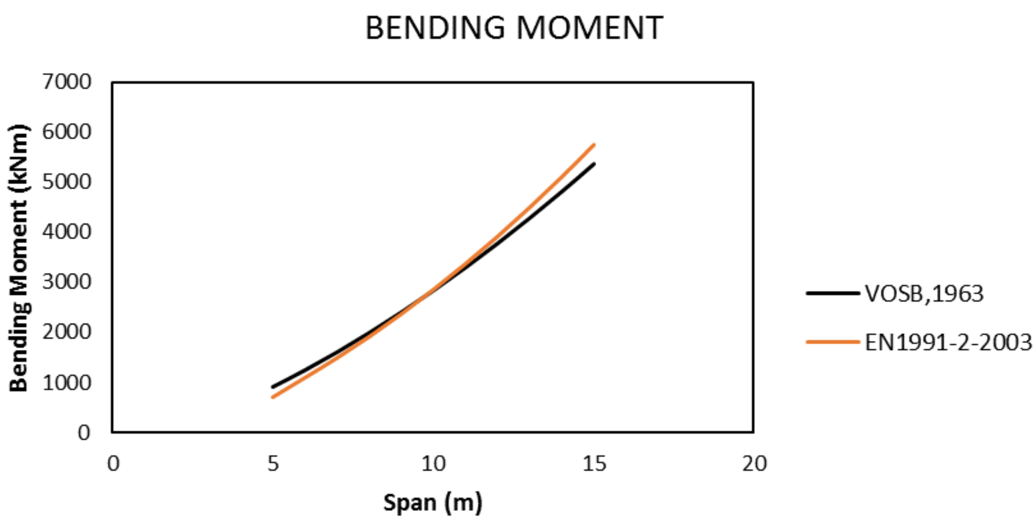

Figure 12 BM comparison due to VOSB,1963 & EN1991-2-2003

The difference in the bending moment ratio of these loads is studied in terms of their ratio to observe the net difference in figure 13. From the figure 13, one can observe that for the bridges of the span between 8-12m, there is no difference. Both the load models result in equal stress on the beam. The reason being the inclusion of load coefficient α, which is given in Eurocode so that the behavior of old and new steel bridge is same for passing trains. For other span ranges, there is a slight difference of an average of 2-3%, which can be observed in figure 13.

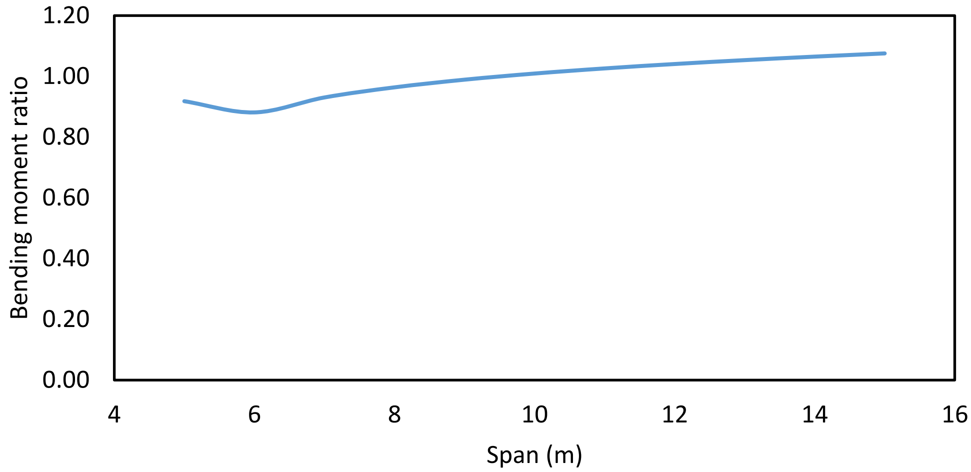

Figure 13 BM ratio for different spans

1.4.1.1 Verification of results

To authenticate the variation shown in the plots presented in figure 12 and 13, a small study is made. Loads with same magnitude(kN) as mentioned in figure 10 and 11 are modelled in Staad Pro software and bending moments are obtained for the load models from 1963 and 2002 codes. The affinity towards using Staad Pro software is because of its availability to the student at the moment. Other software can be used as well. Figure 14 and 15 shows the schematic diagram of the loads modelled for VOSB and EN respectively acting on a HE650B beam.

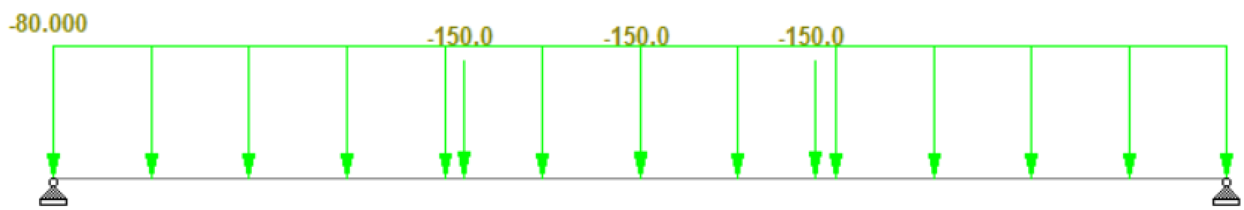

Figure 14Load magnitude and load positions for VOSB,1963 in Staad

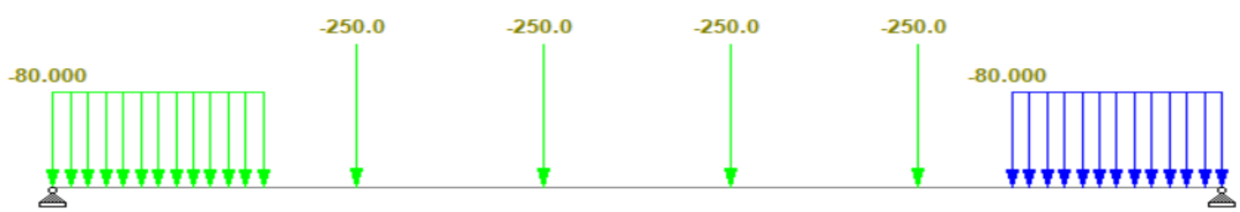

Figure 15 Load magnitude and load positions for EN1991-2-2003 in Staad

Results:

The analysis in the software is performed to calculate the bending strength and deflection. Figure 16 and 17 compare the bending moment from VOSB and European code respectively on a HE650B beam.

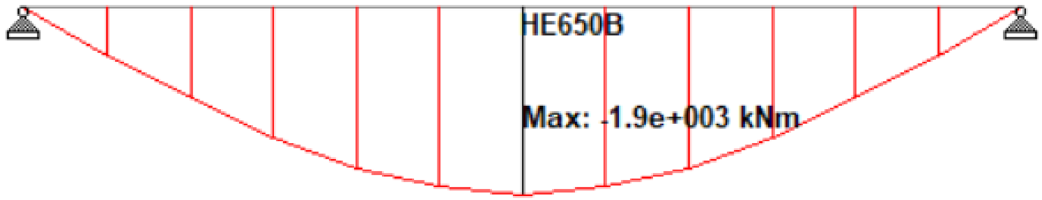

Figure 16 Resulting bending moment from VOSB,1963 load model

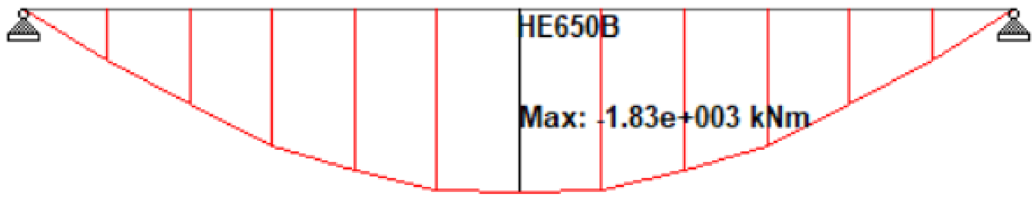

Figure 17 Resulting bending moment from LM71, EN1991-2-2003

As expected the bending moment is maximum around then mid-span. Table 1 compares the final results obtained from the above figures.

VOSB,1963 load model		
Maximum Bending moment (BM) at mid-span (x=5m)		1900 kNm
Design BM: $M_{ed} = BM * S * B$		2827.2 kNm
S (Impact fact)	1.55	1(a),art15,VOSB,1963
B (Load factor)	0.96	3,art14,VOSB,1963
LM 71 EN1991-2-2003		
Maximum Bending moment (BM) at mid-span (x=5m)		1830kNm
Design BM: $M_{ed} = BM * \alpha * \varphi$		2856.45kNm
α	1.21	cl6.3.2(3) ,EN1991-2-2003
φ	1.29	Table A.1.2(B),NEN 8701-2015

Table 1 Comparison between VOSB,1963 and EN1991-2-2003 load model

The results of maximum factored bending moment from table 1 suggest that the bending moment resulting from load model of VOSB,1963 is 1.01 times the LM71 from the current Eurocode. The results from Staad Pro gives the same ratio as from the plot in figure 13. This implies that the structural integrity of the structure with the evolution of load models should not be an issue for steel railway bridges. With the inclusion of material factors for VOSB,1963 that have a same significance as the partial safety factor, the ratio might vary. But the variation would not be much.

1.4.2 Frequency of trains

It is obvious from that fact that the public transport in the last 100 years has expanded and evolved by huge number as discussed in section 1.1 and 1.2. Due to this expansion, the rail traffic has also increased over this period of time. To understand the depth of incrementation of the traffic, UIC regression data based on real trains for Europe has been plotted in the figure18 for the time between 1900-1990.The plot shows that the traffic has increased exponentially over the period by 70%. The impact of this increase in frequency can be critical especially for the steel railway bridges which were not upgraded as required against the other rail infrastructure for modernization. The increased frequency would result in an increase in a number of cyclic stresses due to the passage of trains. This increment is important because since the bridges are designed for the service life of 100 years but the traffic expansion (number/speed) increased at much higher pace.

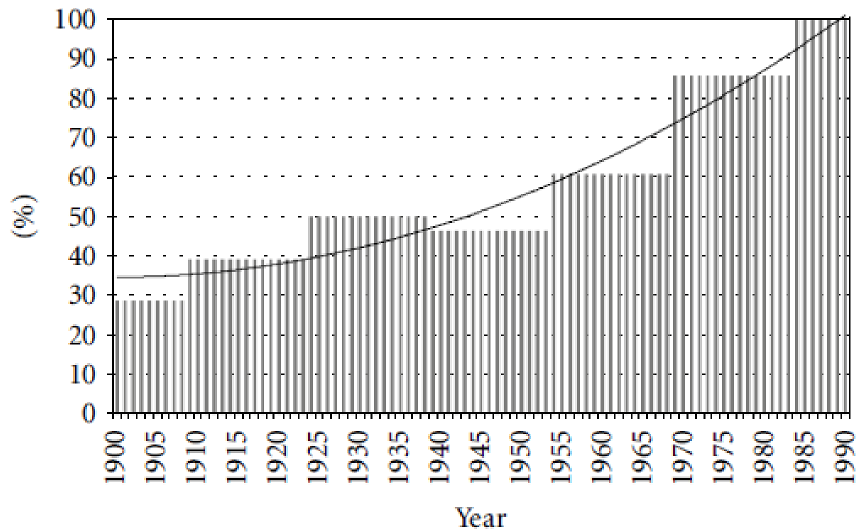

Figure 18 Traffic increment regression based on UIC real train

In the early 18th -19th century, the concept of fatigue stresses was not considered at all. In VOSB-1963, it was considered through magnification factors but critical fatigue classes and criteria for fatigue design was not considered at that time. Due to the intensification of rail traffic as described in section 1.2, the existing bridge infrastructure designed according to old codes experienced an increase in cyclic stresses. This increase in cyclic stresses can be critical for the service life of these bridges in the form of cracks at connections and degrade the strength of the steel structures. According to art 69 VOSB,1963 code for design of steel bridges in the older times, fatigue was considered as a function of R value and no fatigue classes for connections or details were developed. This did not predict the exact fatigue behaviour of steel structures and connections involved. Though the design of the bridges for ultimate limit strength still holds structural integrity these cyclic stresses are more critical even if they are much lower in magnitude. This concept of fatigue was developed in early 19th century by Wohler and applied to Eurocodes in detail by 1991.

To understand the impact of this increased frequency, increased speed and higher axle loads it is important to compare the different trains that were in service in the last 100 years. The data from UIC website can be used to understand the scenario, though it may not be accurate for The Netherlands due to lack of information in the archives. This data (Figure 19) about historical loadings have been assumed from UIC779-1 for fatigue analysis, which gives us the the idea about the type of trains, axle loads involved and their frequency to perform fatigue analysis in the absence of related information about historic trains.

From figure 19 it can be seen that the frequency of trains from 1900-1968 has increased by 112%. From figure 8, it can be observed that most of the small span (10-15m) steel railway bridges were constructed between 1925-1975. Therefore, the frequency of trains from the mid time period of 1950-1990 has increased by 65%. This implies the number of cyclic stresses increased by 65% (train/day) too on these steel bridges, which were designed using VOSB,1938 and VOSB,1963.

The point of focus is that these bridges are still in operation till now. The EN-1991-2-2003 recommends considering the real train models for 25ton traffic as depicted in figure 21. From this, one can compare that the number of cycles of stresses due to the passage of the real trains (A03, figure 20) from 1900 to till date has increased roughly by more than 10 times (axles/day) considering figure 21. At the same time, the magnitude of these trains has increased from 140kN (A03) to 250kN (Fatigue type 5model) by 78% in last 100 years. Thereby, cyclic stresses and fatigue can be critical and further investigation of such steel bridges should be placed as per their service life.

Period	Train/day	Type	UIC ref.	Train type [%]	Train/day for type
1900–1908	34,3	Tot.			
	17,2	Passenger	A03	100%	17,2
	17,2	Freight	A04	100%	17,2
1909–1923	47,2	Tot.			
	23,6	Passenger	A05	60%	14,1
			A06	40%	9,4
	23,6	Freight	A07	100%	23,6
1924–1938	60,0	Tot.			
	30,0	Passenger	A08	60%	18,0
			A09	40%	12,0
	30,0	Freight	A07	60%	18,0
			A10	40%	12,0
1939–1953	55,7	Tot.			
	27,8	Passenger	A11	50%	13,9
			A12	50%	13,9
	27,8	Freight	A10	60%	16,7
			A13	40%	11,1
1954–1968	72,8	Tot.			
	36,4	Passenger	A14	25%	9,1
			A15	17%	6,2
			A17	33%	12,0
			A18	25%	9,1
	36,4	Freight	A16	40%	14,6
			A20	60%	21,9
1969–1983	102,8	Tot.			
	51,4	Passenger	A14	28%	14,4
			A18	36%	18,5
			A19	36%	18,5
	51,4	Freight	A20	40%	20,6
			A21	60%	30,9
1984–1990	120,0	Tot.			
	60,0	Passenger	S01	56%	33,6
			S02	44%	26,4
	60,0	Freight	S03	37%	22,2
			S04	37%	22,2
			S05	13%	7,8
			S06	13%	7,8

Figure 19 Historical data of real trains from 1900-1990 (UIC 779-1)

Period	Train	Train/day	Tractor (L) carriage (Ci)	kN/axle	$n°$ axles	$n°$ carriage	Axles/day	ΣF [kN]	$n°$ Axles/year
1900–1908	A03	17,2	L	140,00	3	1	51,5	420	$1{,}9E+04$
		17,2	L	120,00	2	1	34,3	240	$1{,}3E+04$
		17,2	L	100,00	1	1	17,2	100	$6{,}3E+03$
		17,2	C1	50,00	3	6	308,9	900	$1{,}1E+05$
						Tot.	411,8	1660	$1{,}5E+05$

Figure 20 A03 train data (Pellegirino, 2012)

Train type	Number of trains/day	Mass of train [t]	Traffic volume [10^6t/year]
5	6	2160	4,73
6	13	1431	6,79
11	16	1135	6,63
12	16	1135	6,63
	51		24,78

Figure 21 Fatigue load models EN1991-2-2003

Similarly, vibrations of railway bridges is another concept that has been completely ignored in the early 19th century. In VOSB-1963, this is again considered through dynamic amplification factors which were developed for the speed of trains lower than the present speed of trains. Figure 22 shows the allowable speed of trains on the railway tracks of the Netherlands.

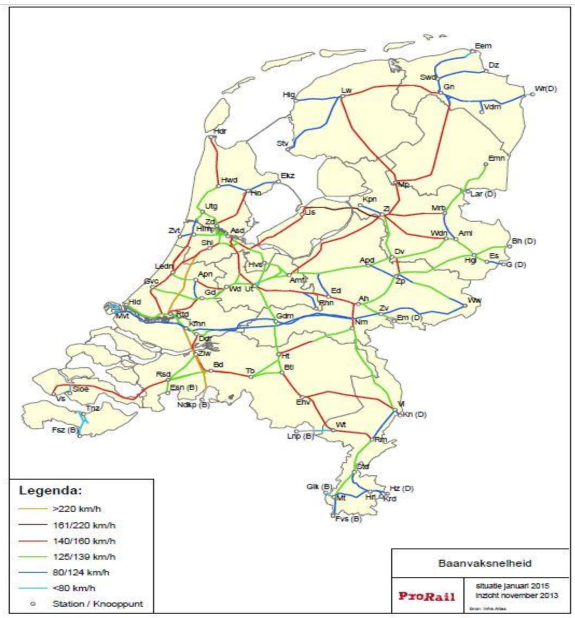

Figure 22 Speed of Trains in The Netherlands

In addition, these rail tracks would now be subjected to much higher rail speeds according to EU inter-connection strategy as can be seen in figure 23. This could convert the situation from critical to catastrophic at any time of service. These high-speed trains amplify stresses by huge magnitudes for which these old bridges were not designed.

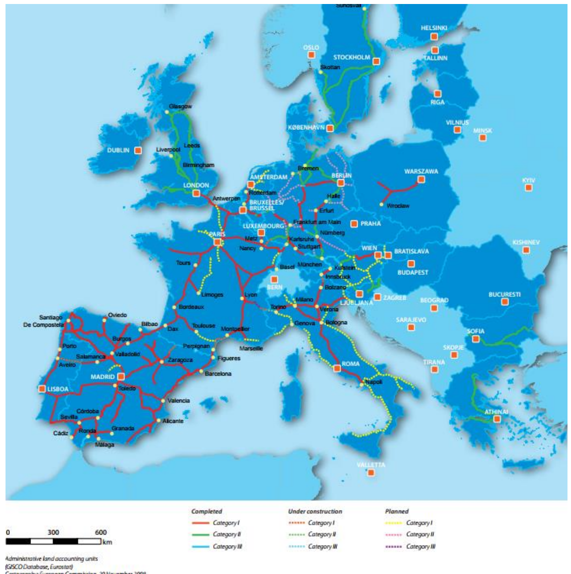

Figure 23 Proposed HSL in Europe

1.5 Case study

Till now, it can be summarized that the small span steel rail bridges are approaching their service life or have exceeded and with the increased intensity of rail traffic over time, they may be prone to fatigue. To understand the impact of the stress amplifications factors over time, an assessment study of one of these small span steel double-I girder bridge is made using NEN8701-2015 code. This code lays the guidelines for the assessment of the existing structures in The Netherlands.

1.5.1 Overview of the bridge

For the evaluation, a double I-girder small span bridge (Figure 24 & 25) has been used. In figure 7, one can observe that around 12 of such double I girder bridges have reached their expected life. Around 36 of double girder bridges would be reaching their service life in about 10-15 years. These bridges in the meantime would be subjected to higher railway loadings as compared to original design loads with the increase in frequency and speed of the railway traffic in the country. This creates a critical scenario of the ageing railway bridge structure and increasing traffic with higher speeds, that could be unsafe to human demands. This bridge is one of the old steel I- girder steel railway bridges with a small span of 10.625m laid across the railway network lines throughout the country.

Due to the unavailability of the drawings of old bridges with service life near to 100 years, the following bridge constructed in 1973 has been chosen for evaluation. The assessment of this bridge would throw light on the current scenario of steel railway bridges in the country and give an idea about their structural capacity in terms of strength, stiffness and fatigue.

In figure 24, one can see the old steel railway bridge of 10.625m span on the railway line Zwolle to Herfte. Figure 24 also shows the geometrical dimensions and figure 25 shows the cross-section of the bridge.

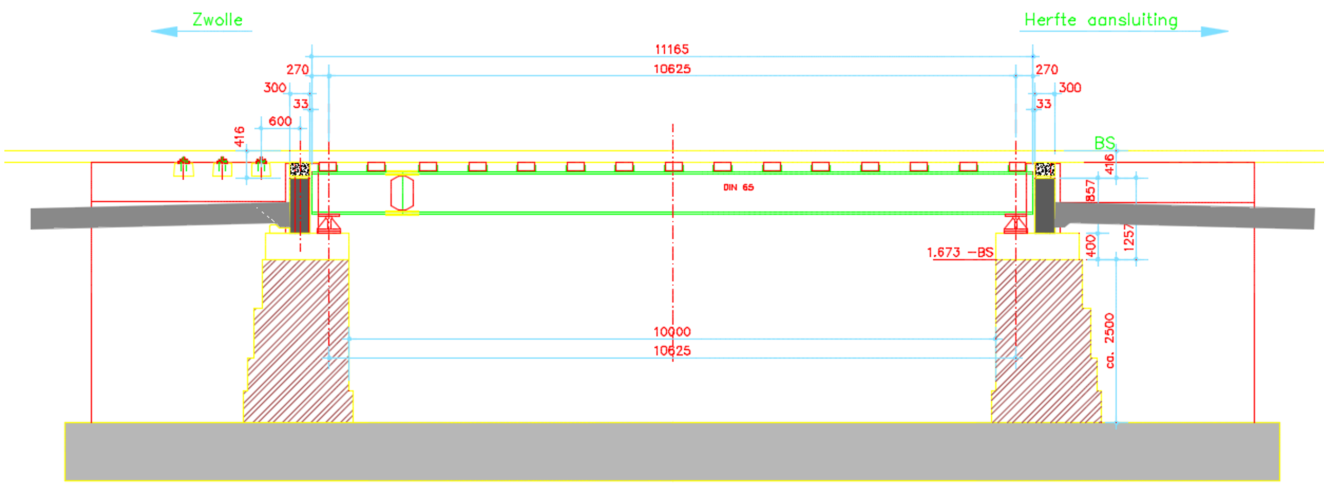

Figure 24 Section of the bridge along the span

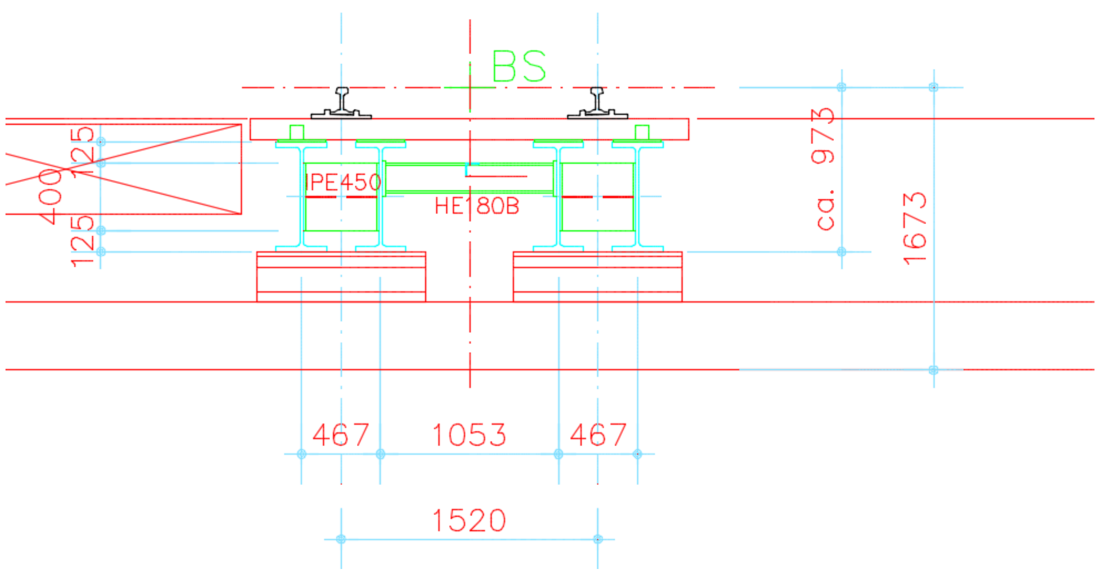

Figure 25 cross-section of the bridge

In figure 24, one can see that the clear span of the bridge is 10.625m supported on the masonry foundation. From figure 25, it can be observed that the cross-section consists of four I-girders that bear the railway loadings and provide strength to the bridge. A cross-beam is laid between the girder2 and girder 3(starting from left) and another cross beam has been laid between girder 1-2 and girder 3-4 in for stability. The load is transferred from each rail supported on the timber sleeper to the two girders just below it. The connection between the cross-beams and the I-shaped girders is bolted. Similarly, the connection between the timber sleeper and I girder is bolted with M16 bolts. Table 2 below gives the information about the structural properties of the bridge elements present.

Type of the structure element	Structural Properties
I-girder	HE650B, S235
Cross beam between 2-3 girders	HE180B,600mm spacing, S235
Cross beam between 1-2 & 3-4 girders	IPE450,600mm spacing, S235

Table 2 Structural Element properties of the Bridge

1.5.2 Assessment

The table 3 below shows the results of the assessment done for the bridge incorporating NEN 8700-2015, NEN8701-2015, EN1991-2-2003, OVS00030-6. *The assessment is just a preliminary initial evaluation of bridge considering linear elastic analysis only.* A single I-girder is analyzed for the LM71 loading, which is shared equally by the four I-girders in the cross-section of the bridge. The properties of the HE650B beam considered here is presented below in Table 3.

Geometrical Properties	
h	650 mm
b	300 mm
t_f	31 mm
t_{wo}	16 mm
A	28600 mm^2
Section Properties	
W_y	6.48E+6 mm^3
I_y	2.11E+9 mm^4

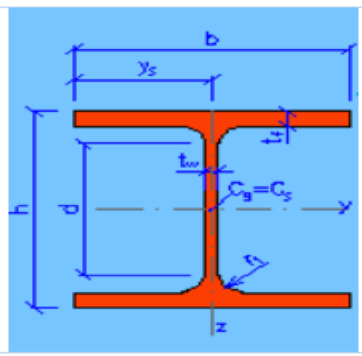

Table 3 Geometric and Section Properties of HE650B I-section (www.statictools.eu, n.d.)

1.5.2.1 Load distribution

In order to assess the structural integrity of the whole bridge structure, the load distribution needs to be configured for accurate analysis. The existing bridge is to be investigated against LM71 load model from EN1991-2-2003.The position of loads for LM 71 are shown in figure 11, section 1.4.1. These loads are defined for the whole bridge structure; hence these loads are divided by 4 (4 I-girders) to obtain load magnitudes (250/4 =62.5kN & 80/4=20kN) for only one girder of the existing bridge structure.

To attain maximum bending moment acting on the bridge, the critical load position for LM71 acting on a generalized beam is derived in Annex A. From the derivation, it can be concluded that the maximum bending moment for the beam of 10.625m is obtained at a distance of 0.4m between the mid-span of the bridge and the equivalent resultant load of the LM71. The concentrated load is distributed as per 6.3.6.1 (1) EN1991-2-2003, where the load is distributed longitudinally as shown in figure 26. For this the distance, 'a' is taken as 600mm, the distance between the rail support points/sleeper.Q_{vi} for this assessment would be 62.5kN.

After considering the above recommendations, the resulting load model configuration acting on a HE650B beam of 10.625m is shown below in figure 27.

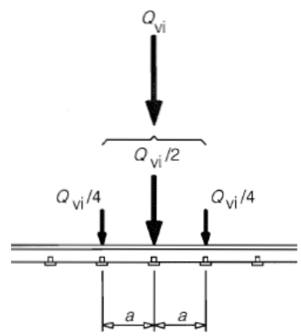

Figure 26 longitudinal distribution of load on sleepers

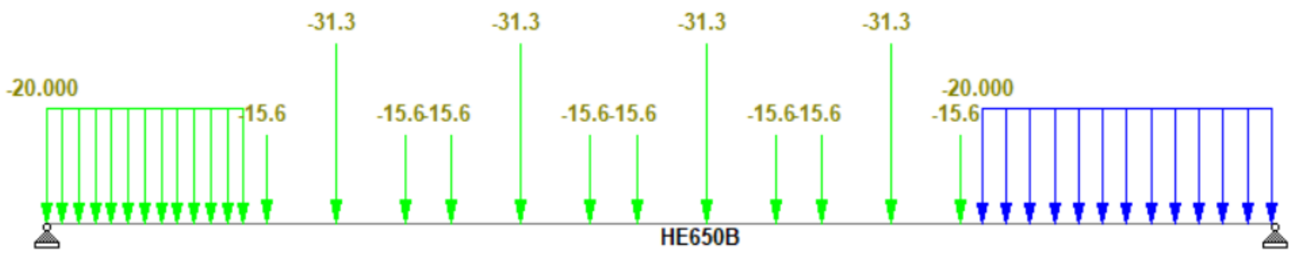

Figure 27Load position and magnitude of LM71 acting on HE650B beam

1.5.2.2 Assessment checks

For the above described load model, the bending moment and deflection are calculated for serviceability limit state using Staad Pro software. The reason for the use of this software is its availability at the moment. The values of maximum bending moment and deflections at x=5.7m $\left(\frac{L}{2}+0.4\right)m$ are obtained for LM71.

(1) Check for ultimate bending resistance

The figure 29 shows the resulting bending moment diagram acting on HE650B beam for the above described loads and their position.

Figure 28 Bending Moment Diagram for LM71

The maximum bending moment at x=5.7m:

$$BM_{max} = 507.305\ kNm$$

Design bending moment:

$$M_{Ed} = BM_{\max} * \alpha * \varphi * \gamma_{Q,1}$$

where:

$\alpha\ (load\ factor)$

= 1.21 [cl 6.3.2(3) EN1991-2-2003]

$\gamma_{Q,1}(Partial\ load\ factor)$

= 1.50 [TableA.1.2(B) NEN8701-2015]

$\varphi(dynamic\ factor)$

As per cl 6.4.5.2 (2a) EN1991-2-2003, for the carefully maintained track:

$$\Phi_2 = 1.44/(L_{\Phi}^{0.5} - 0.2) + 0.82 = 1.29; \quad 1 \leq \Phi_2 < 1.67$$

where L_Φ for simply supported girders is the span in the direction of the main girder

= 10.625m; Table6.2(5.1) EN1991-2-2003

Design bending moment:

$$M_{ed} = 507.305 * 1.21 * 1.29 * 1.5$$

$$= 1187.78\ kNm$$

Cross-sectional bending resistance:

$$W_y = 6.48E + 06\ mm^3\ (Table\ 3)$$

$$f_y = 235 \frac{N}{mm^2}$$

$$M_{Rd} = W_y f_y$$

$$= 6.48E + 06\ mm^3 * 235 \frac{N}{mm^2} = 1522.8\ kNm$$

Check:

$$UC_{bending} = \frac{M_{Ed}}{M_{Rd}} = \frac{1187.78}{1522.8} = 0.78 < 1\ (Ok)$$

(2) Check for serviceability (deflection)

Figure 29 shows the deflection plot for the HE650B beam due to the load described in figure 27. The maximum deflection is obtained at x=5.7m, the point of the maximum bending moment.

Figure 29 Resulting Deflection for LM71

Resulting deflection of HE650B girder:

$$\delta_{LM71} = 13.56mm\ (Figure\ 29)$$

$$\delta_{res} = \varphi * \delta_{LM71}$$

$$= 1.29 * 13.56$$

$$= 17.50mm$$

Limiting deflection:

$$\delta_{\lim} = \frac{L}{800} \quad \text{[cl A2.4.4.2.3(1) NA EN1991-2-2003]}$$

$$= \frac{10625}{800} = 13.30mm$$

Check:

$$\delta_{LM71} > \delta_{\lim}\ (Not\ Ok)$$

(3) Check for fatigue damage

Figure 30 describes the connection between the steel strip and top flange of the I-beam to hold the wooden block between the sleepers and the I-girders. The load will be directly transferred from the rail to the I-girders through this detail. Due to lack of well-informed drawing of this bridge, it can be assumed that this steel strip is connected to the I-beam flange through M16 bolt.

*Note: Damage for fatigue is calculated for the steel I girder beam for LM71 loading. Since the load is borne by the four I-girders directly from the rails through sleepers which is also evident through the relative stiffness of the HE650B beam and IPE450, the connections are not evaluated since there are minimal stresses. The purpose of the cross-beams is to prevent relative horizontal displacement between the girders/rails due to horizontal forces and prevent local buckling.

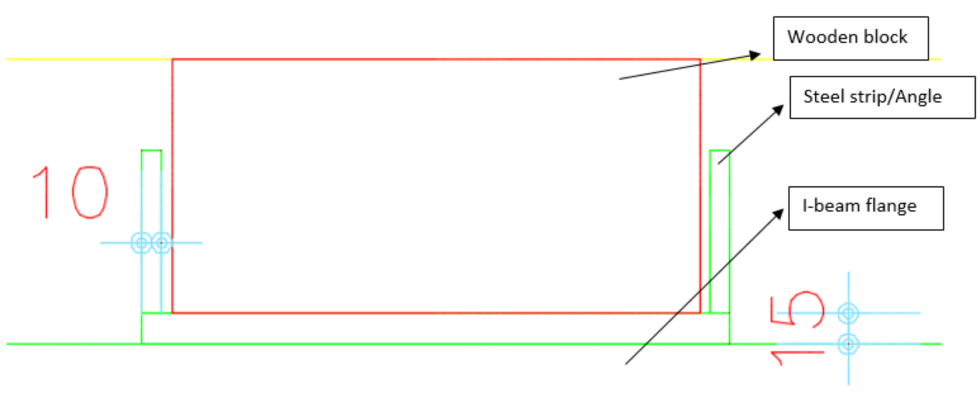

Figure 30 Local fatigue detail

The fatigue assessment is made according to the procedure described in section D.2 Annex D of EN1991-2-2003.This section recommends that the safety verification for details of steel bridges from fatigue should be done by satisfying the condition (2) D.2 EN1991-2-2003, which is formulated as:

$$\gamma_{Ff} * \lambda * \Phi_2 * \Delta\sigma_{71} \leq \frac{\Delta\sigma_c}{\gamma_{Mf}}$$

The terminologies included in the above condition are described below and the respective values for each of them are chosen.

γ_{Ff} is the partial safety factor for fatigue loading. The recommended value of γ_{Ff} is 1 as per the Note, (2) D.2 EN 1991-2-2003.

λ_{Mf} is the partial safety factor for fatigue strengths. Pro rail guidelines from section *12.2(3) OVS00030-6,* recommends the value of this factor to be 1.35.

Φ_2 is the dynamic factor as calculated in the (1) 1.5.2.2 for the check of ultimate bending resistance, which is 1.29.

$\Delta\sigma_c$ is the reference value for the fatigue strength. The top flange of the I-beam with holes can be treated as a structural element with holes subjected to bending and axial forces and checked for fatigue stresses against detail category 90 (Table 8.1, EN1993-1-9). Hence, $\Delta\sigma_c = 90\frac{N}{mm^2}$.

$\Delta\sigma_{71}$ is the stress range for the LM71 being placed at the most unfavorable position for the element under consideration. Hence, the stress range is calculated at x=5.7m which is the location for the maximum bending stresses on the top flange of I-girder under compression. This can be calculated as:

$$\frac{M_{Ed}}{I_{HE650B}} = \frac{\Delta\sigma_{71}}{y_{cg}}$$

$$\Delta\sigma_{71} = \frac{\left(507.305kNm * 1.29 * \left(\frac{650}{2}\right)mm\right)}{(2.11\ E + 09)mm^4} = 78.14\frac{N}{mm^2}$$

$\lambda\ is$ the damage equivalence factor for fatigue which takes account of the service traffic on the bridge and the span of the member. This damage equivalence factor is obtained from the equation 9.13, EN1993-2-2006.The equation described it as:

$$\lambda = \lambda_1 * \lambda_2 * \lambda_3 * \lambda_4 < \ \lambda_{\max}$$

Where λ_1 is the factor for the damage effect of traffic and depends on the length of the influence line;

λ_2 is the factor for the traffic volume;

λ_3 is the factor for the design life of the bridge;

λ_4 is the factor for the structural element is loaded by more than one track;

$\lambda_{\max}$ is the maximum λ value taking account of the fatigue limit;

λ_1 depends upon the influence length of the bridge and the rail traffic considered for the bridge. The critical length of the influence line for the simply supported length is taken as L according to (4) 9.5.3 EN1993-2-2006.The rail traffic to be considered as per (3) 6.3 NEN8701-2015 is 25*10^7 kN per year per track. Therefore, for L=10.625m span of the bridge and for standard rail traffic mix, the $\lambda_1$can be taken as 0.85 from table 9.4 of EN 1993-2-2006.This rail traffic mix is closely related to the historical rail traffic (preferred by NEN8701-2015), hence it is preferred.

λ_2 depends upon the traffic volume. For traffic volume of 25 E+06 ton per track, λ_2 can be extracted as 1 from table 9.5 of EN1993-2-2006.

λ_3 depends upon the design life of the railway bridge. According to (6),6.9 EN1991-2-2003, the fatigue assessment should be performed over the design life of 100 years. Hence, for the design life of 100 years, $\lambda_3 = 1$ from table 9.6 EN1993-2-2006.

For single track railway bridges, λ_4 is 1 from table 9.7 EN1993-2-2006.

The value of $\lambda_{\max}$ can be obtained from equation 9.15 of EN1993-2-2006, which states the value of 1.4.

Consequently,

$$\lambda = 0.85 * 1 * 1 * 1 = 0.85 < 1.4$$

Hence, the damage (D) observed in the detail in figure 26 can be calculated as:

$$D = \frac{\gamma_{Ff} * \lambda * \Phi_2 * \Delta\sigma_{71}}{\Delta\sigma_c / \gamma_{Mf}} = 1.31 \geq 1$$

1.5.2.3 Discussion

Overall, the structural integrity of the structure is doubtful as it is unable to satisfy SLS and FLS criteria per OVS 00030-06 and EN1991-2-2003 guidelines. For fatigue, the top flange of HEB650 is critical, which need to be looked upon and upgrading measures should be taken. A site inspection should be made to check the critical details for cracks and non-linear analysis of the structure should be made to verify the structural integrity of this structure. Though there are several solutions but as evident, the design of these old bridges did not consider serviceability and fatigue limit state as the important criteria. Thus, the steel railway bridges are critical and measures should be taken for improving their service life before a catastrophic event occurs. Table 4 below summarizes the results derived in the above sections.

Criteria	Requirement	Calculated resulting Values	Check	Unity Check
		LM71		
Strength (kNm)	*≥1522.8	1132.53	Ok	0.74
Deflection(mm)	≤13.28	16.67	Not Ok	
		Fatigue Check		
***Damage**	≤ 1	1.31	Not Ok	

Table 4 Assessment Results

* cross-sectional resistance

1.5.3 Environmental concern

With the continuous operation of these steel rail bridges in the environment, another point of concern is the environmental impact that these bridges have in the surrounding residential area. Noise especially structural borne in built environments is a primary issue in The Netherlands. As per TNO, the noise vibrations play cause huge environmental issues like sleep disorders, annoyance etc. in people due to the construction of homes close to rail routes in the country. This implies that a quitter rolling stock and rail infrastructure has to be developed to account for these emissions.

These old existing steel railway bridges are open sections without ballast. These sections are devoid of any noise absorbing elements in the structure. As per research was done in Cargovibes (European research project), these vibrations have a great impact on the sleep of the people residing near the rail infrastructure. Figure 27 shows the change in heartbeat rate for the people living near the railway lines during the passage of the train.

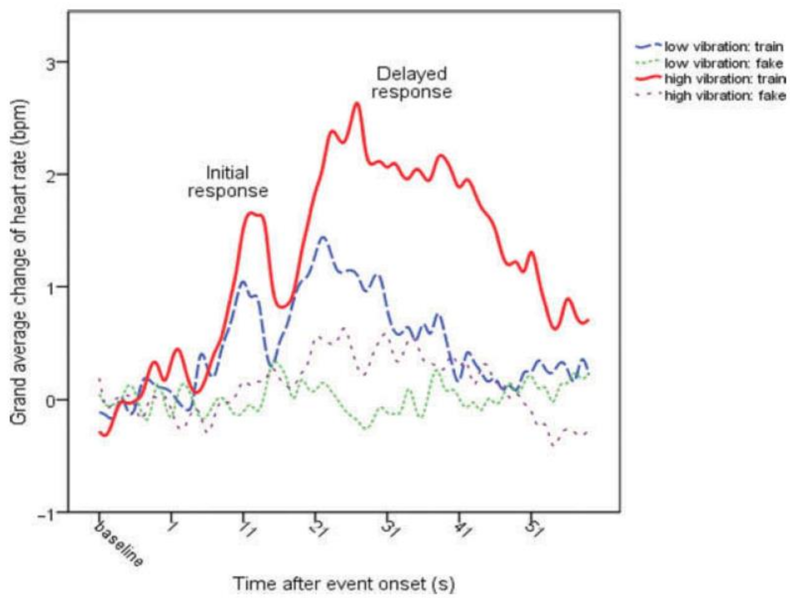

Figure 31 Averaged change in heart rate during sleep following freight train pass-bys of different vibration amplitudes (Cargovibes)

Hence, it is not only the structural assessment but also the environmental assessment that suggests that the future application of such bridges is detrimental for the Dutch society and immediate upgradation measures should be taken.

1.5.4 Possible solutions

After the assessment of the existing steel railway bridge, one can conclude that the bridge does not satisfy the EN1991-2-2003 and OVS00030-06 guidelines limiting values. This bridge is unable to meet checks for SLS and FLS. This means that not only the service life of the bridge must be improved but also the section stiffness should be increased.

The possible solutions to improve the existing scenario is retrofitting the existing bridge as discussed in section 2.2 or replace the existing steel rail bridge with a new steel bridge.

In addition, to meet OVS guidelines for regular repair and inspection of railway bridges and to handle situations like passenger exit in case of emergency, it is necessary that the additional geometrical clearance as per Appendix B should be provided.

If retrofitting is chosen as a possible solution to enhance the section properties, it is uncertain if it is possible to achieve it. The bridge is 44 years old and not much information is available on the corrosion of this structure. So, retrofitting is only possible after making a systematic inspection. The inspection would give an idea about the condition of the material of the structure if it is possible to re-use it after the existing level of corrosion. Subsequently, to add structural members for inspection path and emergency footpath would result in a new connection. For the steel bridge, the addition of a potential source of fatigue critical points would not be advisable when it already exceeds the fatigue damage. In addition, retrofitting is a costly process since it requires a high number of man-hours as it is a highly skilled process. Due to high track occupancy and intense rail traffic, as discussed in section 1.1&1.2, it may be costly to proceed with it. Nevertheless, it does not eliminate the possibility of using it but an economic analysis comparison between the retrofitting and replacement of the bridge would be encouraging to come to a cost-effective solution. Currently, this is beyond the scope of study for this thesis.

A common solution in The Netherlands is usually replacement with new steel bridge or concrete bridge.

Hence, it is suggested that replacement of steel bridge should be adopted since the new bridge will account for future high- speed rail dynamics and better fatigue strength.

1.5.5 State of the Art Bridge Design

In this section, a new conceptual design of the box-girder steel bridge is proposed. This study enables to compare the new and the old design due to the introduction of various structural and non-structural elements. These design elements incorporated in the recent Eurocodes for high speed rail are the result of mitigating noise vibrations, fatigue stresses and improving dynamic behavior to expect a full-service life. The figure 32 below shows the new conceptual design of the bridge based on limiting deflection criteria for comparison purposes. The bridge is designed according to EN1991-2-2003 for a span of 10.625m to fulfill deflection criteria of L/800 i.e. 13.3mm (cl A2.4.4.2.3(1) NA EN1991-2-2003). The height of the web is kept 800mm to ensure that the bridge rests on the existing foundation and no extra work (repair/upgradation) on the foundation is required.

New Steel rail bridge	
Centroid:y_{cg} (mm)	400mm from top flange
Moment of Inertia: I (mm^4)	1.3E+10
Top flange thickness:$t_{t,flange}$ (mm)	25
Bottom flange thickness:$t_{b,flange}$ (mm)	25
Web thickness and depth:t_{web} & h_{web}(mm)	20 & 800
Cross-beam	IPE 180, 600mm c/c
I-girders	HEB220, 3
Width of bridge	4m

Table 5 properties of new steel rail bridge

The bridge consists of the box-girder shape with dimensions of structural elements as defined in table 5. The passenger path and the repair/inspection path including cable ducts rest on IPE 180 cross-beam. This cross-beam is supported by HEB 220 I-shaped girder beams resting on the foundation. There is no connection between the cross beam and the box-girder to prevent any eccentric moments acting on the bridge.

1.5.5.1 Stiffness Calculations for Box-Girder section

Conceptual design for comparison of the weight of the existing old steel bridge and new bridge according to EN1991-2002 is made. The same load composition is considered as calculated for the existing steel rail bridge in section 1.5.2.1.

The deflection of a HE650B beam with $I_{yy,HE650B} = 2.11\mathrm{E}+9\ mm^4$ subjected to a load composition of one-fourth the magnitude of LM71 including the dynamic factor as calculated in (2) 1.5.2.2 is 17.5mm.

Hence, the stiffness requirement for a load composition as of LM71 (4 times load acting on single HE650B) including α and dynamic factor to restrain the deflection of HE650B to 13.28mm:

$$I_{yy,reqd} = I_{yy,HE650B} * 4 * \alpha * \frac{17.5}{13.28} = 1.34E + 10\ mm^4$$

$$E_{steel} = 2.1 * 10^5 MPa$$

Flexural stiffness required for box-girder bridge:

$$EI_{reqd} = E_{steel} * I_{yy,reqd} = 2.8E + 15\ mm^4$$

For the calculation of deflections at the moment only beam behavior is considered.

Assume a box girder section with top and bottom flange each 1520mm long and 40mm thick. The web of this section is 800mm deep and 20mm thick.

$$t_{flange} = 25mm\ and\ L_{flange} = 1520mm$$

$$t_{web} = 20mm\ and\ h_{web} = 800mm$$

$$I_{actual} = L_{flange} * \frac{t_{flange}^3}{12} * 2 + L_{flange} * t_{flange} * \frac{\left(h_{web} + \frac{t_{flange}}{2}\right)^2}{4} * 2 + \frac{h_{web}^3}{12} * t_{web} * 2 = 1.4 * 10^{10} mm^4$$

$$I_{actual} > I_{yy,reqd}$$

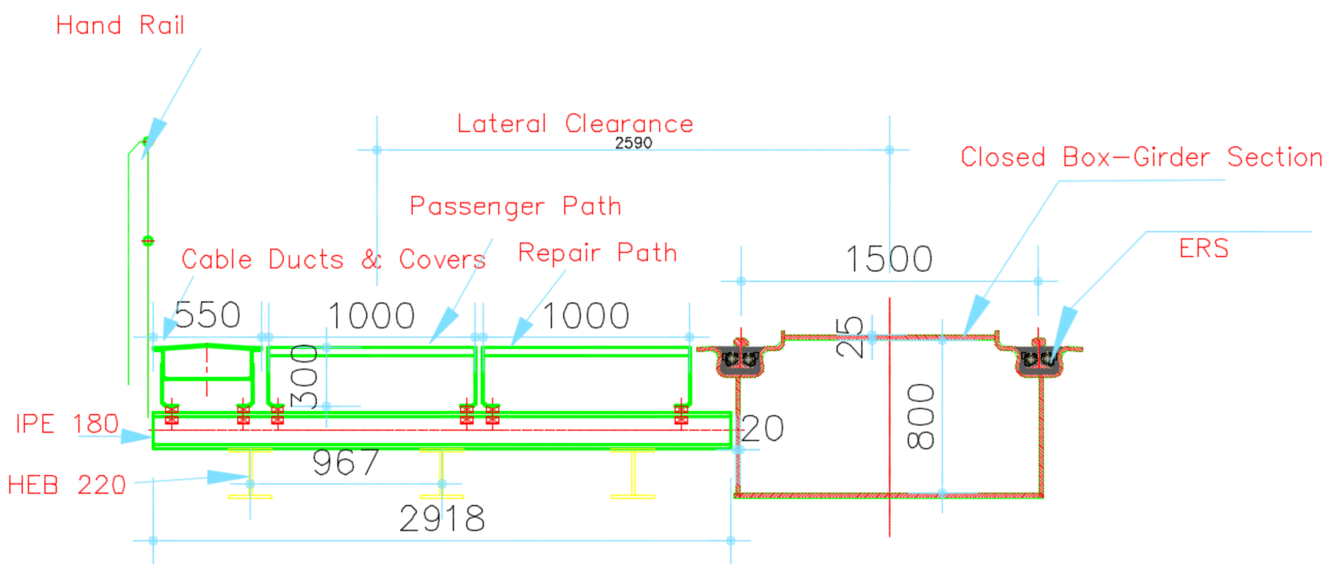

Figure 32 State of the art Box-Girder Steel Bridge

The salient features of this state of the bridge are described as follows:

1. Closed section and application of embedded rail track that reduces structural borne noise to the environment. Closed sections aid in restraining the propagation of sound waves (wheel-rail interaction) as compared to open sections.
2. The inclusion of passenger path for the emergency exit of a passenger in case of emergency and repair path for inspection of rail track and bridge structure regularly.
3. Design of bridge for high speed rail lines to account for intensifying rail traffic and serving the purpose of increased use of public transport indirectly.
4. Incorporation of design factors for amplified dynamic stresses comprehensively as suggested in EN1991-2-2003.
5. No connections on load bearing structural members to reduce the harsh impact of cyclic stresses in concentrated areas that lead to high local stresses in the structure.

1.5.6 Foundation issues

Foundations play an important role in the bridge structure as they support the bridge superstructure and absorb the loads from the superstructure. As it is established that most of the bridges have approached their service life, so has their foundations. As mentioned in section 1.5.1, the old steel railway bridge is laid on the masonry foundation, which is also around 43 years old. This question's the integrity of this foundation sub-structure. According to EN1997-1, the foundations should be checked for ULS and SLS design criteria. The main checks according to the code are: Bearing strength (ULS) and sliding (SLS). For both the checks, the vertical force acting on the foundations is the fundamental input parameter for analysis. This vertical force is dependent upon the dead weight of the structure, dead weight of functional elements on the bridge and traffic loads. As it can be seen that the new state of the art bridge has higher geometrical dimensions and more non-structural equipment's, which would increase the vertical reaction forces acting on the foundations. A comparison of the weight of the existing steel bridge and new steel bridge is carried below.

1.5.6.1 Weight on foundations

<u>The weight of existing bridge:</u>

The existing bridge section consists of 4 HE650B beam sections running throughout the span,17 IPE450 cross beam between HE650 and HE180B cross-beams spaced at 600mm respectively. Wherever possible, nominal weight of beams is considered.

The span of bridge:

$$L_s = 10625mm$$

The span of IPE450 beam:

$$L_{450} = 467mm$$

The span of HE180B beam:

$$L_{180} = 1053mm$$

$$Weight\ of\ HE650B = 225\frac{kg}{m} * L_s * 4 = 9562.50kg$$

$$Weight\ of\ IPE450\ beam = 77.6\frac{kg}{m} * L_{450} * 17 = 616kg$$

$$Weight\ of\ HE180B\ beam = 51.2\frac{kg}{m} * L_{180} * 17 = 916.53kg$$

$$Weight\ of\ bridge = 11.1\ ton\ or\ 1044\frac{kg}{m}$$

Weight of state of art steel Bridge

The new bridge consists of a box girder section as described in section 1.5.5.

$$L_{span} = 10625mm$$

$$t_{flange} = 25mm\ and\ t_{web} = 20mm$$

$$h_{web} = 800mm\ and\ l_{flange} = 1500mm$$

$$L_{IPE} = 2900mm$$

The weight of Box-girder section:

$$W_{struc,l} = \left(\left(l_{flange} * t_{flange} * 2\right) + \left(t_{web} * h_{web} * 2\right)\right) * l_s * \rho_{steel} = 8867.62kg\ or\ 8.8\ ton$$

The weight of non-structural section:

$$Weight\ of\ IPE\ 180\ cross\ beam = 19.2\ \frac{kg}{m} * L_{IPE} * 17 = 946.56kg$$

$$Weight\ of\ HEB\ 220\ beam = 3 * 71.5\frac{kg}{m} * L_{span} = 2279kg$$

$$Weight\ of\ cable\ ducts\ and\ covers = \frac{35kg}{m} * L_{span} = 371.85\ kg$$

$$Weight\ of\ pedestrian\ and\ inspection\ path\ steel\ gratings = 21.3\frac{kg}{m^2} * 2 * (10.625 * 1)m^2 = 452.62\ kg$$

$$Weight\ of\ handrail = 8.68\frac{kg}{m} * 10.625 = 92.2\ kg$$

Total Weight of new bridge: (Adding all the structural and non-structural weights)

$$W_{tot,new} = 13\ ton$$

So, from the above comparison one can see that the weight of the new steel bridge per structural elements is 20 percent lighter than the old bridge but including the functional requirements, it turns to be almost 33% heavier than the existing old steel railway bridge. This increased weight is due to repair/inspection and safety requirements recommended by Pro rail, which leads to an increment of vertical reaction forces on the foundation by 33%.

1.5.6.2 Settlement

The increase in the axial forces on the foundations due to the increased weight of the super-structures leads to an issue of settlement of foundations in the ground. The settlement of the foundation due to increase pressure on the soil can be much more depending on the soil conditions at the site of the bridge. Figure 33 shows the soil type in the Netherlands.

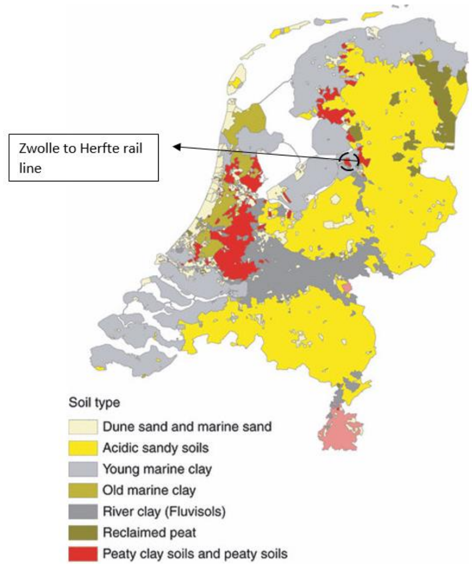

Figure 33 Soil types in Netherlands (Reijneveld, 2010)

From figure 26, it can be approximated that the soil type can be peatly clay soil or young marine clay. These clay soils have the low shear strength and can be an issue for settlement.

1.5.6.3 Degradation of Masonry Foundation

Other than the effect of loads, another issue with these masonry foundations is their material degradation with ageing. These masonry foundations are really old and some areas of these foundations are not easily approachable for inspection. This can lead to several issues like ageing of masonry material, dislocation of mortar joint, the growth of vegetation due to natural affects and traffic loads. Similar defects are shown in figure 34 below for masonry foundation of arch bridges.

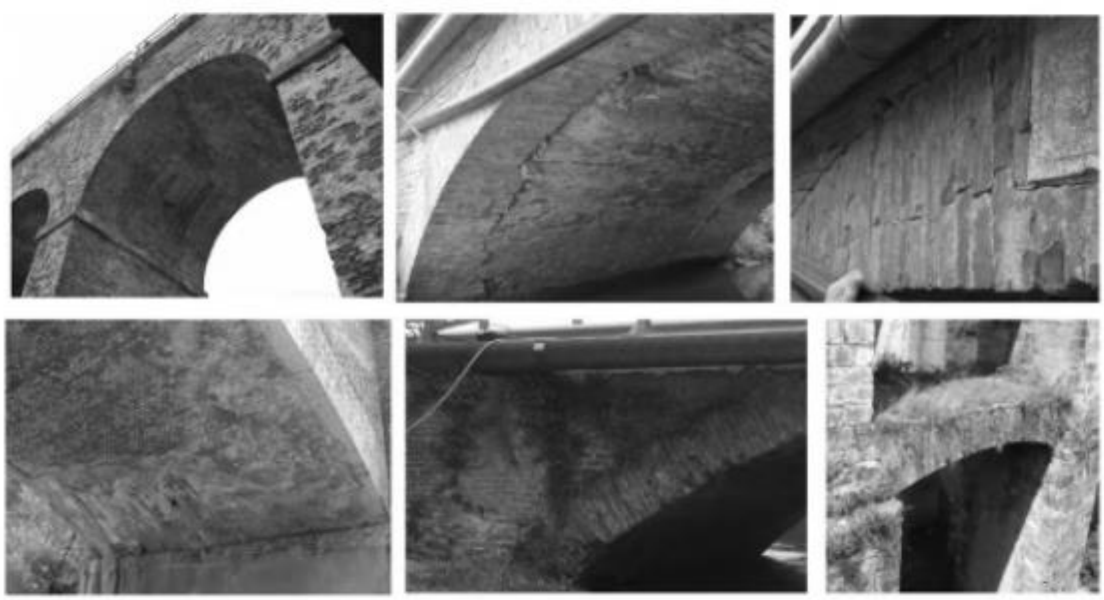

Figure 34 Defects in ageing masonry foundations: loss of brick units, longitudinal cracking, opening of joints, salt efflorescence in bricks, vegetation penetrating (Source: Dan Frangopol,2014)

The drawback of masonry foundation is their brittle nature, which can lead to collapse without showing any structural damage (Dan Frangopol,2014). To limit the settlement and material degradation renovation of existing masonry abutments would be required to carry out. This would add to the cost of replacing the old streel bridge with the new one and would be expensive.

1.5.7 Alternative solution

To counter the foundation issue, the alternative solution can be the application of light weight material known as fiber reinforced polymer. The density of this material is one-third the density of steel and much higher strength properties. The strength of this material is comparable to steel with achievable tensile strength between 100-400MPa. More details about this material are covered in section 2.2 of this report.

1.6 Problem Statement

Because of intensifying rail traffic, in combination with structural degradation or fatigue problems, simple steel bridges may reach the end of service life and need replacement. Common replacements are a heavier steel bridge or a concrete slab (also heavier). Due to the increased weight, the foundation may need upgrading as well, which is expensive and takes more time. Arcadis would like to investigate the possibility of composite rail bridges (relatively short span, simply supported single span bridges), in order be able to re-use the existing foundation and shorten the construction period. This statement has been provided by Arcadis, Netherlands to study for the master thesis student and check the feasibility in this regard.

1.7 Research question

Based on the provided problem statement, the main research question for this thesis is:

- To study the feasibility of FRP material railway bridge in replacing the existing old steel railway bridge such that the existing foundations can be reused.

1.8 Research objectives and structure

To answer the research question of the thesis, the main research question is divided into sub-questions which are answered in the upcoming chapters. The thesis has been structured into 7 parts which are covered in eight individual chapters. Each chapter describes the approach/research methodology used to achieve the stated objectives. The results of the objectives are used to answer these sub-questions which are part of the main research question.

The chapters defining the sub research questions and their respective objectives are as follows:

Chapter 2-Literature Study

- What is the behaviour and properties of FRP material while considering its application for high-speed railway bridge in The Netherlands?
  Objectives
  1. To study the Eurocode and OVS guidelines to determine the factors that govern the design of railway bridges.
  2. To study the state of the art FRP manufacturing techniques to choose the best possible manufacturing method for the rail bridge application.
  3. To study the influence of rail track system on the behaviour of the FRP bridge.
  4. To study the behaviour of FRP when subjected to static stresses, repeated cyclic stresses, and vibration. This is followed by determining the required parameters for the analysis.

Chapter 3-Conceptual study

- What structural shapes and the material combination can be used to achieve minimum flexural stiffness for LM71 load model?
  <u>Objectives</u>
  1. To study the Eurocode and OVS guidelines to determine the factors that govern the design of railway bridges. To study the state of the art FRP manufacturing techniques to choose the best possible manufacturing method for the rail bridge application.
  2. To study the influence of rail track system on the behaviour of the FRP bridge.
  3. To obtain possible various structural forms for ballast and ERS track system.

Chapter 4-Material properties

- Is it possible to design an FRP laminate for sufficient strength and Young's modulus?
  <u>Objectives:</u>
  1. To obtain a balanced symmetrical lay-up to reduce buckling loads, warping and twisting from residual stresses
  2. There is no shear extension coupling and bending extension coupling, which means orthotropic symmetrical laminate.

Chapter 5-Preliminary Design

- How do creep and functional requirements influence the design of FRP railway bridges?
  <u>Objectives:</u>
  1. To account for long term deflections along with short term deflections and check if they are within prescribed limits.
  2. To define the FRP orientation in the webs and faces.
  3. To optimise sections for reduced mass and increased stiffness.
  4. To check for local stresses that might affect the service life of the bridge.

Chapter 6-Static FEA

- How does the FRP railway bridge behave when subjected to ULS loadings and what failure modes can be expected?
  <u>Objectives:</u>
  1. To formulate finite element model for the desired FRP bridges in ABAQUS.
  2. Check the FRP bridge for expected failure modes and verify with hand-calculations.
  3. Obtain the final and feasible FRP bridge on the basis of weight and section depth.

Chapter 7-Fatigue analysis

- What is the behaviour and damage to FRP railway bridge/details when subjected to fatigue real train load models from EN1991-2003?
  <u>Objectives:</u>
  1. To find critical details for cyclic stresses in FRP railway bridge.

2. To plot the influence line diagrams for these details to obtain stress-history plots due to trains running across the bridge.
3. To obtain the plots of stress-histogram by performing rainfall counting method and calculate damage.
4. To compare the material utilisation for static and fatigue loadings.
5. To calculate the service life of the bridge.

1.9 Assumptions and limitations

To achieve the desired results that would aid in answering the specifics of the stated research sub-questions, it becomes necessary to make some assumptions and declare boundary conditions. These are as follows:

- The behaviour of FRP material is considered as a thick laminate material confirming to the geometric dimensions whereas micro-level behaviour has not been considered for the design of FRP structure is stiffness based.
- In the finite element model, the foam core is not modelled since Young's modulus and strength value is very low as compared to FRP laminate. Foam core is mostly used as a position holder for FRP laminates and restrains the influx of dirt, other external degrading factors.
- Influence of rail and ballast is not considered in Finite element model. Ballast has been considered as a load acting on the bridge deck structure.
- For static analysis, only vertical transverse loads according to EN1991-2 are dominant and analysed. Effect of horizontal and aerodynamic forces has been neglected.
- The scope of the research is confined to The Netherlands. Therefore, real load models for fatigue and transient analysis are considered according to OVS Dutch guidelines and Dutch rail scenario.
- Longitudinal distribution of a point force or wheel load on three different points is ignored.
- Variations in wheel loads resulting from track or vehicle irregularities are not considered.

2

Literature

In this chapter, several methods and state of the art is discussed, which is relevant to the aim of this research study. The aim of this chapter is to answer to study various Eurocodes and OVS guides that determine the governing criteria for the design of bridges for ULS loads and serviceability. The study about the application of different rail track systems and their impact on the bridge structure will be studied. The manufacturing details are compared for resulting strength and modulus parameters to choose the best fit. This will aid in determining the conceptual and detailed design by understanding the depth constraint required for the bridge to fit into the existing profile. The influence of plies stacking on the cyclic stresses will help to understand which component of FRP resist cyclic stresses and critical for fatigue analysis. The state of the art FRP bridge in the application are studied to understand the existing failure or issues in the application of FRP in bridges. This altogether will help in obtaining necessary information about FRP material and how this information can be used in the design to achieve for full service life of the bridge.

2.1 Assessment of old steel railway bridges

In the Netherlands, rail transportation mode is a significant part of the movement of passengers from one part to another due to its quick, reliable and safe character. Figure 35 shows the age distribution of small-span railway bridges spanning across the whole country.

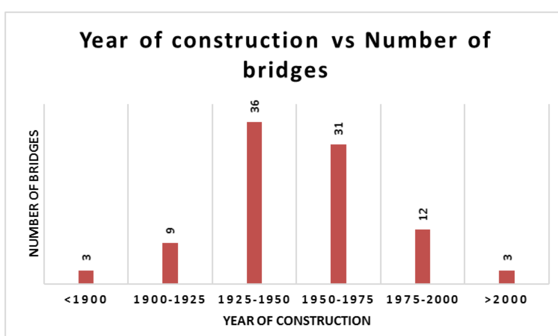

Figure 35 Age composition of Double Girder Bridges in The Netherlands (Archives: Arcadis, NL)

It can be observed from figure 35 that most of the infrastructure is old (>50 years) and designed according to old Eurocodes load combination. In the last few decades, the rail traffic has increased in terms of quantity and speed sustained by the continuous growth of European economy. This has led to increasing traffic loads at a substantial rate on this obsolete and aging infrastructure. This results in uncertainty against the reliability and durability of these bridge structures if they can sustain this heavy traffic beyond the extension of their service life without repair/maintenance.

2.1.1 Background from National Codes for Structural Assessment

To make sure that the existing bridge infrastructure in the country is functional and reliable during or beyond its extended service life, it becomes necessary to assess it according to the national guidelines.

The first requirement is to decide the safety format depending upon the importance of the network lines, economic consequences of failure, etc. In the Netherlands, this requirement can be obtained from the NEN 8701-2015 “Assessment of existing structures in case of reconstruction and disapproval -Actions”. There is another Dutch code NEN8700-2015, “Assessment of existing structures in case of reconstruction and disapproval -Basic rules” which lays the principles and rules to assess existing structures.

The clause 3.3 of NEN 8700-2015 recommends verifying the structure for static linear analysis, which includes ULS, serviceability and fatigue calculation according to NEN-EN 1990. Load models to be imposed on the bridge structure are to be refereed from NEN-EN-1991-2 as recommended by the clause 6 of NEN 8700-2015.

Ultimate Limit State Assessment: The clause 6.2 of NEN 8701-2015 recommends the load factors be applied to the existing railway bridges. The dynamic factor to be charged must be determined by Annex C of NEN-EN 1991-2. The dynamic factor for carefully maintained track must be applied.

Fatigue assessment: For the determination of the residual life, the standard traffic composition including dynamic magnification factor according to Annex D of NEN-EN 1991-2 must be applied. The volume of rail traffic to be considered is $25*10^7$ kN per year per track. If a more accurate calculation is required for determining the residual life, it is possible to deduct different taxes on the basis of actual measured train traffic, taking into account Annex D of NEN-EN 1990.

Serviceability assessment: For the comfort of the people, it is necessary to meet he SLS requirements for the current prevailing scenario as recommended in Eurocode1991-2. These limits recommended in Eurocode are superseded by National Annex Guidelines, which in turn is superseded by Pro-Rail OVS guidelines. The clause A2.4.2.3 of OVS00030-6 states that the maximum total vertical deflection should not exceed L/800, where L is the length of the span.

2.2 Strengthening of Steel railway structures

Strengthening of the existing structures is one of the most widely accepted practices for improving the service life of the existing structures. In particular, the research done for steel decks regarding the upgradation of the service life is discussed here.

1. Replacing the sleepers by ERS decks

   The figure 36 below shows the cross section before and after strengthening using silent bridge decks. In this type of upgradation, the old timber sleepers are replaced by ERS rail track system without any sleepers and ballast. This reduces the dead weight of the bridge and improves the flexural stiffness of the bridge section. It also enhances the acoustic properties of the bridge and reduces the noise emission because of wheel-rail interaction due to ERS concept. This eradicates the major social concern related to old steel bridges.

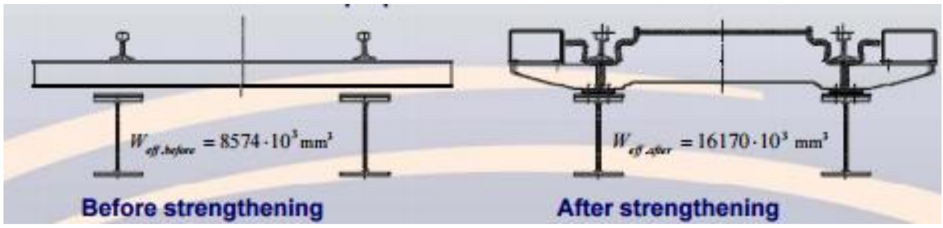

Figure 36 Silent Bridge Deck (Movares, 2010)

2. Strengthening of longitudinal girders by strengthening diagonals

   In bridges, where fatigue is a critical issue at connections of the main girder with the diagonals, this method aids in solving this critical issue. Here, diagonal members are strengthened to prevent local buckling near the ends. The compressive stresses at this location are really high. This is achieved by providing a support to the flange tips with circular hollow sections.

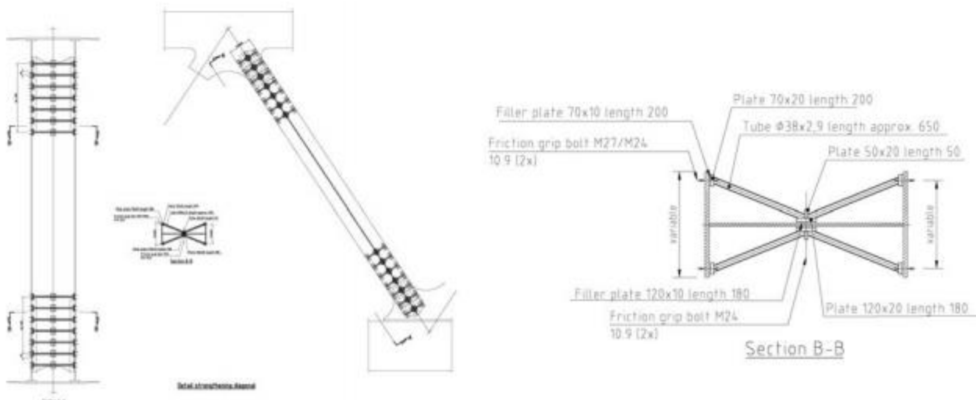

Figure 37 Strengthening of diagonals by preventing local buckling (SNIJDER, 2010)

3. Steel beams strengthened with bonded FRP composite materials

In situations where the stiffness of the existing bridge is an issue and at the same time the additional weight of the bridge worsens the existing situation materials play an important role. These materials are bonded externally to the steel members and improve the tensile strength and inertia of the composite structure. Due to its low eight and less labor-intensive application, this technique is efficient other than the standard techniques. Tests mentioned in SB,2007 prove that the strength of these composite structures is governed by the stress concentrations in the adhesive due to the difference in the properties of the material.

2.2 State of the art manufacturing process and bridge decks

An important factor in the successful application of the FRP material in the civil application is the fabrication process involved since it affects the cost, rate, and size of production and quality of the FRP product.

There are a variety of manufacturing techniques used for the civil industry like hand layup, Vacuum assisted resin transfer method(VARTM), pultrusion, filament etc. Table 6 shows the market share of such technologies used in the construction of FRP bridges in Europe.

Manufacturing Method	Number of Bridges

Pultrusion	56
VARTM	37
Hand Layup	18
Other	10
Total	121

Table 6 Manufacturing Methods of built bridges (O'Connor & Triandafilou 2009, p.7)

It can be observed that pultrusion and VARTM method are the most preferred method for the bridges as they are automated processes. Such processes provide a higher degree of control during production as well as compaction. In addition, they have higher in-service properties, strength and stiffness leading to a higher robustness against harsh environments as compared to manual methods.

Table 7 compares the mechanical properties obtained through Pultrusion and VARTM method (Hollaway,2010&Burnside,1997).

Manufacturing Method	Tensile Strength (MPa)	Tensile Modulus (GPa)	Flexural Strength (MPa)	Flexural Modulus (GPa)	Shear Modulus (GPa)
VARTM	138-193	10-40	100-400	10-40	1.5-8
Pultrusion	275-1240	21-41	200-500	21-41	1.35-2.24
Hand Layup	62-344	4-31	110-200	6-28	1-1.8

Table 7 Typical Mechanical Properties of GFRP manufactured

From the above table, one can observe that the mechanical properties of the hand layup are too low as compared to VARTM/Pultrusion method. Properties of VARTM and Pultrusion are comparable except shear modulus which is too low for Pultrusion method.

Table 8 displays the state of the art bridge deck commonly available in the market, which is manufactured using wide spread methods.

For the choice of materials and manufacturing method chosen in this thesis, refer chapter 4 for details.

2.3 Structural Behaviour of FRP beam sections

As compared to steel, FRP material has very low Young's modulus (Figure 38) but high strength. Therefore, the whole strength value of GFRP is never put in use. This leads to thicker sections in case of bridges as compared to steel, where deflection criteria (L/800) is decisive while designing (A2.4.2.3, OVS00030-6). Thus, the application of FRP on small span railway bridges leads to higher L/t ratio such that shear deformations need to be considered. Therefore, Timoshenko Beam model would represent the accurate behavior of FRP small span railway bridge. The importance of shear modulus comes into play and VARTM method is therefore preferred.

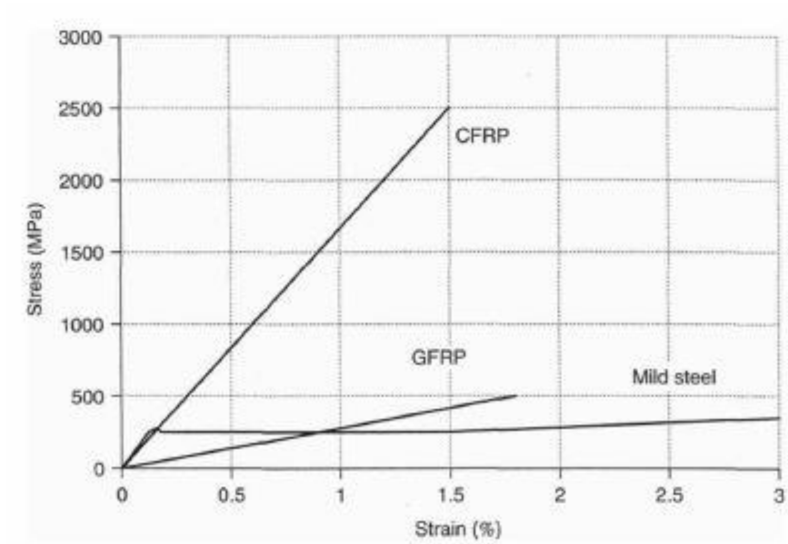

Figure 38 Stress-Strain curve of materials

Table 8 State of the Art FRP Bridge Decks

Deck System	Manufacturing Method	Deck Thickness (mm)	Deck Weight kN/m²	Connection between deck and slab	Configuration
Hardcore (USA)	VARTM	Various	Various	Glued	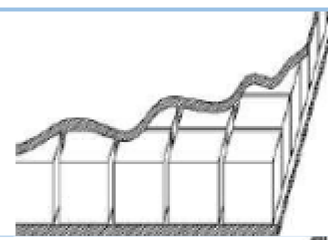
Kansas (USA)	Hand Lay up	Various	Various	Glued	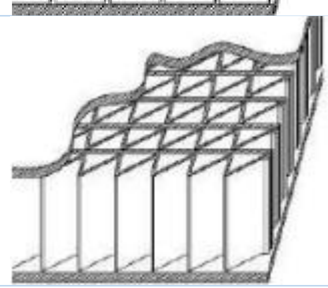

ACCS (UK)	Pultrusion	Various	-	Glued/ Mechanical	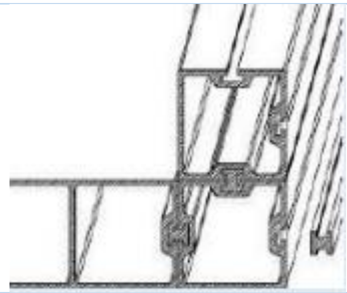
ASSET (Denmark)	Pultrusion	225	0.93	Glued	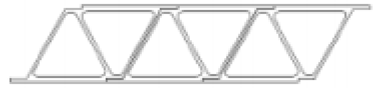
Delta Deck (Korea)	Pultrusion	200	-	Glued	
DuraSpan (USA)	Pultrusion	195	1.05	Glued/ Mechanical	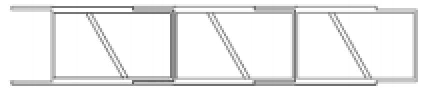
EZ-Span Deck (USA)	Pultrusion	216	0.96	Glued	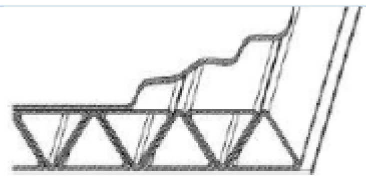
Strongwell (USA)	Pultrusion	170	-	Glued/ Mechanical	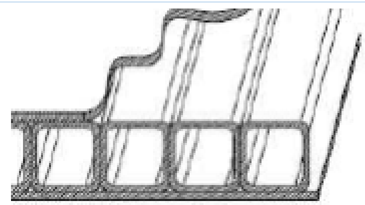
Superdeck (USA)	Pultrusion	203	1	Glued	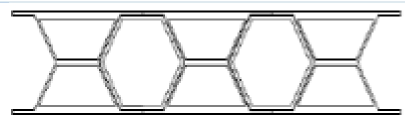

2.4 Design of FRP laminate and Fiber Architecture

The design of fiber architecture depends upon the application of FRP material. CUR 96 suggests that the design of the FRP laminate should be strain based. Some of the important and critical recommendations from (Mallick, 2007) are summarized here as follows:

- The unidirectional fiber reinforced ply is assumed at transversely isotropic, such that its elastic constants are reduced to as below:

$$E_1; E_2 = E_3; \nu_{12} = \nu_{13}; G_{12} = G_{13}; G_{23} = \frac{E_2}{2(1+\nu_{23})}$$

  - The first step is to obtain then critical bridge loading for the bridge to calculate the magnitude and direction of critical stresses resulting in the structure.
  - The second step is to align the UD fibers in the direction of critical stresses per strain theory mentioned in CUR,96. It is also recommended in CUR,96 that the minimum of 15% of fibers should be present in each principal direction.
  - To account for unexpected loads from any direction, it is suggested to add plies in ±45° angle.
  - For unexpected transverse loads, a minimum number of 90° plies as suggested above should be introduced.

- To limit the effect of surface deterioration due to scratches or by the impact of ballast at the time of passage of high speed trains, it is suggested to not use 0° plies on unprotected surfaces.
- Use repeated sub laminates rather than thick plies which are more susceptible to cracking.
- Use symmetric (balanced) laminates to reduce buckling loads, warping, twisting from residual stresses.
- Avoid too large jumps in fiber orientation angles between different plies to minimize the interlaminar shear stresses.
- Laminate has sufficient shear and bending stiffness.
- There is no shear extension coupling and bending extension coupling, which means orthotropic symmetrical laminate

2.5 Rail Track system

The rail track system plays an important role in the transfer of loads from the axle of bogies to the ground with the aid of sleepers, fasteners, ballast or slab track. In civil application, there are 2 types of rail track system: Ballast -rail track system and Embedded Rail track system

2.5.1 Ballast-Rail Track System

The ballasted rail track system consists of a rail laid on timber/concrete sleepers, which are supported on a bed of ballast. Figure 39 shows an example of a rail track system with ballast and supported on the asphalt layer.

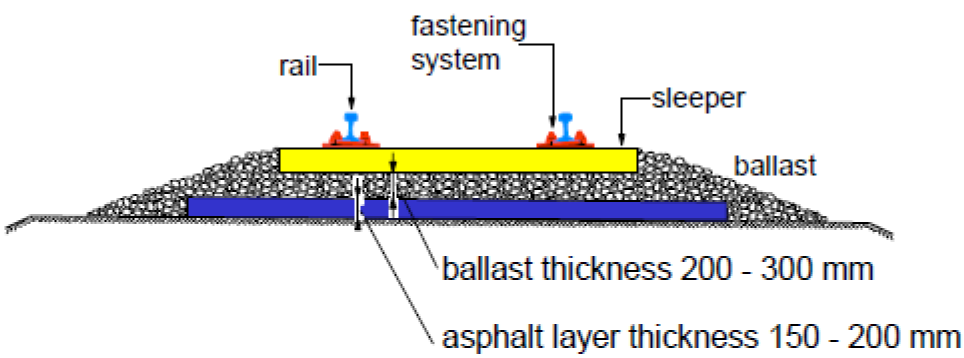

Figure 39 Ballasted rail-track system

The main advantages of this system are its economic viability, easy to maintain and repair and provide higher elasticity to the rail-bridge section. However, it does possess some disadvantages like limited lateral restraint, high mass of ballast can cause damage to rails and wheels due to the churning of ballast.

2.5.2 Embedded Rail Track System

To counter all the disadvantages mentioned in the ballast rail track system, a new concept known as embedded rail track system is adopted. This system varies in the form of a fastening system which in this case is continuous and is laid as a recess in the base of this structure which is filled with an embedding material.

The general cross-sectional arrangement of the fastening system can be seen in Figure 40. Its most important elements are:

1. longitudinal recess created in the base structure,

2. elastic embedding material,

3. elastic base strip,

4. space filling elements

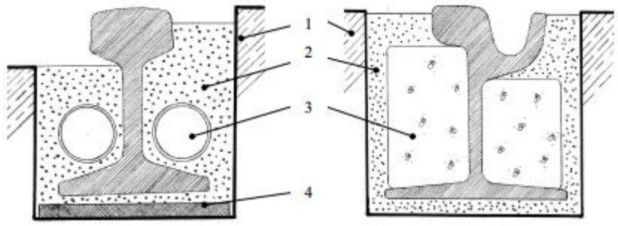

Figure 40 Continuously Embedded Rail Systems (LUDVIGH, 2001)

The material of the recess can be reinforced concrete or steel, depending on the track structure. To enhance the vertical elasticity of this system, a rubber or cork strip is placed under the rail base.

The benefits of ERS system can be reaped the most when the depth of the bridge cross section is a constraint. This system also provides an aesthetic appearance, ensures more lateral stiffness, and low emission of acoustic waves.

(K.H. Oostermeijer, 2000) compared the dynamic behavior of conventional ballasted structure and embedded rail structure developed by Dutch railways, which is grooved on a concrete slab. Figure 41 shows the damping of embedded rail structure overall high as compared to the ballasted structure. The main frequency range for noise vibrations is generally between 500-1500 Hz. The damping of ERS is mostly higher than ballasted structure between 200-1000 Hz, hence this leads to low noise while usage of ERS.

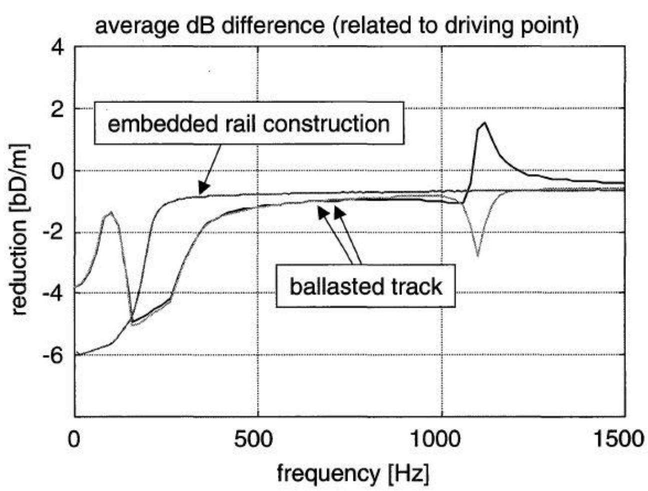

Figure 41 Distance damping ballasted track and embedded rail structure

2.6 Fatigue

Fatigue is a physical process that leads to deterioration of any material due to repeated cyclic stress. Many structures in the civil application are exposed to this phenomenon like moving loads on the bridges, vibrations from wind, waves on the hydraulic structures etc. Many structures suffer premature failure due to fatigue as these alternate loads can result into failure at stress levels lower than the ultimate stresses.

The phenomena of fatigue in FRP composites is well known and established in the aerospace industry. However, this information cannot be applied for civil application due to nature of loads experienced.

The fatigue life process can be seen in Figure 42 shown below.

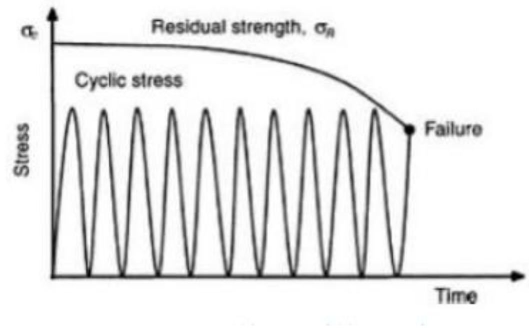

Figure 42 Fatigue life process (cholsta, 2012)

The best design procedure is to determine the fatigue strength of an FRP composite from the tests (J C., 1996)).

The factors that determine the fatigue strength of FRP are the static ultimate strength of the composite material and the mean stress level. There is little impact of notches on the fatigue performance of FRP composites as compared to steel. The reason can be attributed to the inhomogeneous and imperfection material characteristics of FRP. The growth of these imperfections is slow due to the fibers that act as barriers.

2.6.1 Influence of laminates stacking on S-N curves:

The influence of the stacking of plies at different angles can be studied on strain basis. Generally, UD plies govern the S-N plot.

Figure 43, shows the comparison of fatigue strength between unidirectional and +/- 45° glass-polyester laminates. From the plot, it can be observed that the fatigue strength of +/- 45° glass-polyester laminates is better represented by the unidirectional laminate.

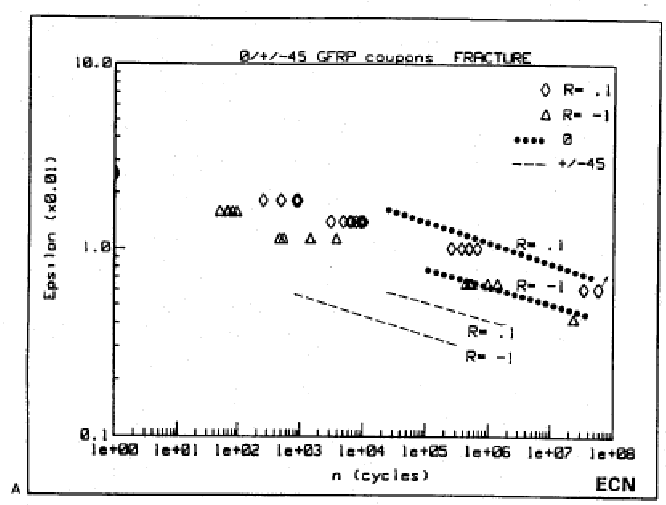

Figure 43 Fatigue results (log-log) of the GFRP coupon specimens.

Similar results are obtained on a normalized stress basis, in which the fatigue results of the+/- 45° glass-polyester laminates are close to the fatigue data of unidirectional laminate (Figure 44).

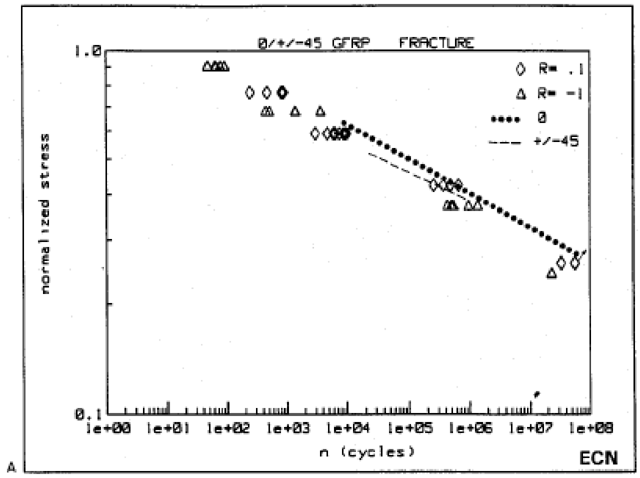

Figure 44 Comparison of 0°, +/-45°, and 0°/ +/-45° GFRP coupon results.

So, both on a strain and normalized stress basis the fatigue behavior is dictated by the unidirectional layers.

2.6.2 Fatigue relation:

For constant amplitude fatigue loading, S-N curve at an R-ratio of -1 is used as it covers both tension and compression and seems to fit most logically in the Constant Life Diagram. The CLD is directly based on static tensile strength and static compressive strength. Basically, two possibilities are applied for the relation between stresses and the number of cycles (Delft, 1997):

$$\log(N_f) = a_1 + b_1 * \sigma_{amp}$$

(36)

$$\log(N_f) = a_2 + b_2 * \log(\sigma_{amp)}$$

(37)

The constant b_i in the above equations is referred to as the slope of the S-N curve.

To obtain the number of cycles to failure for other R- values, Goodman type relations can be applied.

To obtain the number of cycles to failure for other R-values, Goodman type relations can be applied. Using the below equations fatigue formulation can be summed as: (Delft, 1997)

$$\sigma_{mean} \geq 0: N_f = (\sigma_{amp)} /UTS \left(1 - \frac{\sigma_{mean}}{UTS}\right))^{-10}$$

(38)

$$\sigma_{mean} \leq 0: N_f = (\sigma_{amp)} /UTS \left(1 - \frac{\sigma_{mean}}{UCS}\right))^{-10}$$

(39)

Where UTS = Ultimate tensile strength; UCS= Ultimate compressive strength; σ_{amp} = stress amplitude of a cycle; N_f= No of cycles to failure

2.6.3 Background of Concerned Codes for fatigue

Section 11.7.6 JRC,2016 suggests the values of the essential material parameters that can be used for the fatigue analysis of FRP material structures. For the relationships mentioned above, the value of the regression parameters a and b can be obtained from the table 11.6 of JRC 2016. The table 9 below describes the related parameters which are dependent upon the R ratios.

UD non-crimp fabric	Glass/epoxy U fabric	Glass/polyester U fabric	Carbon/epoxy U fabric
	a,b	a,b	a,b
R=-1	-10, 600*(V_f/0.55)	-9, 700*(V_f/0.55)	-15, 900*(V_f/0.55)
R=0.1	-10, 1100*(V_f/0.55)	-7, 1300*(V_f/0.55)	-30, 1200*(V_f/0.55)
R=10	-10, 750*(V_f/0.55)	-	-

Table 9 Reference Values for regression Parameters a and b for UD laminate

The above mentioned parametric values are valid for laminates with $35\% \leq V_f \leq 65\%$ for laminates to determine the S-N line for fatigue analysis in the direction of fiber with fiber reinforcement content of more than 12.5%.

JRC,2016 even provides a reference S-N curve for different material parameters using these regression parameter values as shown in figure 45 below.

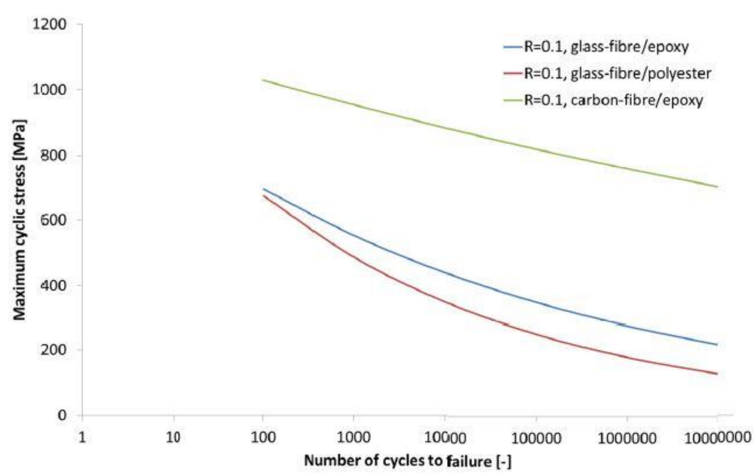

Figure 45 S-N curve for GFRP, R=0.1 (JRC,2016)

2.6.4 Fatigue Calculations for Railway Bridges:

Fatigue load models defined in Annex D.3 of EN 1991-2-2003 are "equivalent amplitude load models" which are derived from the variable amplitude stress ranges generated by real traffic loads acting on the bridges. These load models are used to estimate the fatigue damage of bridge structure and connections due to fatigue.

In principle, the procedure used to derive the fatigue load models in Eurocode is as follow:

1. Selection of critical points, where the bending, normal or shear stresses are maximum or there is a peak.
2. Using local fatigue load models for the type of traffic mix, obtain the influence line diagram for the respective critical stresses.
3. Employ an appropriate scheme to transform the stress history obtained into stress histogram with a number of constant amplitude stress ranges.
4. Apply miners damage accumulation rule to obtain an equivalent stress range $\Delta\sigma_E$, causing the same damage factor as the stress histogram generated in traffic simulation.

2.7 Serviceability

To avoid the effect of damage from deformation, deflection and vibration and to provide comfort to the users, it is important to set limiting values.

As per SLS analysis, the deflection of the bridge is an important criterion to meet. For FRP structures, this check becomes more relevant when the stiffness of such material is low and their real-life behavior is modelled by Timoshenko beam.

2.7.1 Deflection from Bending and Shear

The following equations represent the equation for bending and shear deflections of isotropic, homogeneous beams which can be used for composite materials (J, 1996):

$$\text{Deflection (bending)} = \frac{k_1 F_v L^3}{EI}$$

Where: k_1 (Table 10) is a factor that takes into account the end conditions and loading type of the beam, F_v is defined as the total vertical load applied on the beam, L is span length of the beam and EI is the appropriate flexural stiffness of the full section of the beam

$$\text{Deflection (shear)} = \frac{\mathrm{K_2 F_v L}}{\mathrm{A_v G_{xy}}}$$

Where: k_2 (Table 10) is a factor that takes into account the end conditions and loading type of the beam, F_v is the total vertical load applied on the beam, A_v is the area of the web and G_{xy} is defined as the web in-plane shear modulus

Table 10 values of k_1 and k_2

End Conditions	Loading Type	k_1	k_2
Cantilever	Point load at end	1/3	1
Cantilever	Uniformly Distributed	1/8	1/2
Supported at ends	Point load at center	1/48	1/4
Supported at ends	Uniformly Distributed	5/384	1/8
Fixed at ends	Uniformly Distributed	1/384	1/24

2.7.2 Dynamic Analysis

2.7.2.1 Background from Eurocodes

Currently, the design requirements related to the dynamics of railway bridges can be found in two different Eurocodes. EN1991-2 contains requirements related to loading and dynamic analyses, while EN1990, Annex A2 contains bridge performance criteria.

Because FRP material offers low damping as compared to conventional bridge and low weight of FRP material, dynamic analysis is important to verify the traffic safety criteria for FRP railway bridges (Woraphot Prachasaree, 2015).

A dynamic analysis can be performed looking from two different perspectives. The first perspective looks at the structural integrity of the bridge, with criteria related to **traffic safety** (fulfilling these eventual ballast instability and loss of wheel/rail contact). The other perspective is related to the perception of the passengers travelling on the train, with criteria related to **passenger comfort**.

In this thesis, the study will focus on traffic safety of the bridge.

- **Traffic Safety:** NEN 1990-2002 lays the criteria for traffic safety in an A2.2.2.2 section of its guidelines which are as follows:
  1. A limit on vertical acceleration of the bridge deck of γ_{bt} =3.5 m/s^2 (ballast) or γ_{df} =5 m/s^2 (no ballast). The frequency of acceleration must be considered to be maximum of 30Hz,5n_0 or n_3.
  2. A limit on vertical deflection of the bridge deck of L/800.
  3. Further criteria related to vertical deformation of the deck, twist of the deck, transverse rotation of the ends of each deck, longitudinal displacement of the end of the deck, horizontal transverse deflection, horizontal rotation of a deck and limits on the first natural frequency of lateral vibration.

2.7.2.2 Dynamic Theory

As mentioned above, the problem of the dynamic response of the FRP bridge is interesting due to its low weight. In this section, one will discuss the dynamic model that would be appropriately used in this feasibility study.

Vehicle load model:

In reality, the moving train load can be modelled via different ways as shown in figure 46.

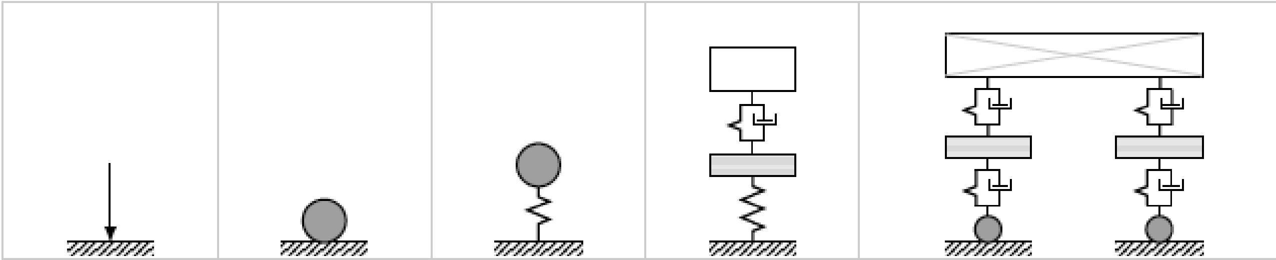

Figure 46 Train bogie modelled as moving load, unsprung mass, 1 DOF sprung mass, 2 DOF sprung mass (B.Komen,2015)

The simplest vehicle model out of these models is the moving force model. In this, a moving vehicle across the length of the bridge is modelled as moving force, while inertia effects are neglected. This approximation is valid when the inertia of the vehicle is low as compared to the dead weight of the vehicle itself and the mass of the bridge. The 1 DOF sprung mass model is a more complicated train model which is used when the mass-inertia of the vehicle is significant and the span of the bridge is considerably large than the spacing between the axles of the bogies of the train.

In case of a rail vehicle moving with constant velocity along a straight rail path, the effects of the mass inertia forces are mainly caused by vehicle-bridge interaction and bridge surface irregularities. Factors that affect the vehicle inertia are high vehicle speed, flexible bridge structure, heavier vehicle, lighter bridge structure and stiff suspension system of the bogies.

The main objective of the dynamic analysis is to study the dynamic response of the bridge, while the response of the vehicle itself is ignored. In this case, application of complicated load models is unnecessary ((Bjorklund, 2004). Hence, the use of moving force model is justified in this thesis project.

Modelling of the vehicle-bridge system:
In the simplest way, the railway bridge is considered as Timoshenko beam with moving load 'F' passing across the bridge with velocity 'v'

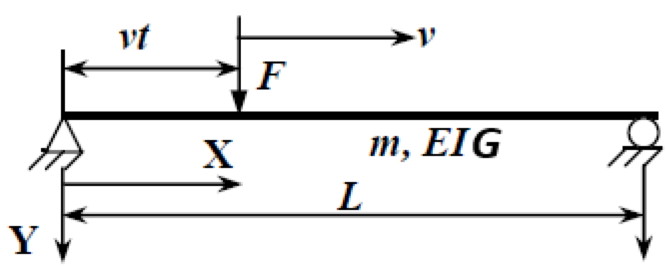

Figure 47 The constant force through the simply supported bridge with constant speed

Considering vibrations of a simply supported Timoshenko beam of finite length 'L", subjected to a moving force 'F', the equation of motion of this system can be written as follow:

$$-\frac{GA}{\kappa}\frac{\partial^2 w(x,t)}{\partial x^2}+\frac{GA}{\kappa}\frac{\partial \phi(x,t)}{\partial x}+A\rho\frac{\partial^2 w(x,t)}{\partial t^2}=F\delta(x-vt)$$

$$EI\frac{\partial^2 \phi(x,t)}{\partial x^2}+\frac{GA}{\kappa}\frac{\partial w(x,t)}{\partial x}-\frac{GA}{\kappa}\phi(x,t)-I\rho\frac{\partial^2 \phi(x,t)}{\partial t^2}=0$$

Where A and I denote the cross-section area and moment of inertia respectively, E and G are the Young modulus and shear modulus respectively, κ is the shear coefficient, ρ is the density and δ (-) is the Dirac delta.

For finite, simply supported beam the boundary conditions can be expressed as:

$$w(0,t) = w(L,t) = 0$$

$$\frac{\partial \phi(0,t)}{\partial x} = \frac{\partial \phi(L,t)}{\partial x} = 0$$

2.7.2.3 Dynamic Behaviour of high speed railway bridges

The risk that resonance frequencies are excited in railway bridges is increased when the velocity of the trains that pass the bridge exceeds 200km/kr. This phenomenon appears when the frequency of the train loads or a multiple of the frequency matches a natural frequency of the bridge. The vibrations amplitudes in the bridge caused by the load from train axles are strongly built up when resonance effect appears and it is important that the bridge is constructed to withstand this phenomenon.

The load frequency of a train is dependent on the distance between equally spaced train axles and the velocity of the train, according to:

$$f = \frac{v}{D}$$

Where v is the velocity of train and D is the characteristic length between the axles.

2.7.2.4 Damping coefficient of FRP bridges:

There is not much research available about the dynamic parameters of the FRP bridges to define the value of damping coefficient of FRP bridges. Though there are few experimental tests that can be referred for this thesis study. Experiments were conducted in West Virginia university in 2012 to study the dynamic response of two FRP highway bridges as shown in figure 48 below.

Figure 48 Market street bridge and katy truss bridge(GangaRao,2012)

Market street bridge on the left in figure 23 is a bridge with a span of 177 feet and 56 feet wide. The FRP deck is connected to steel plate girders using shear studs and concrete grout.

Katy truss bridge is an another FRP bridge with FRP deck connected to girder using mechanical connectors and adhesive bounding. This bridge is 90 feet long and 14 feet wide.

Dynamic tests from GangaRao,2012 confirm that the damping ratio for Katy Truss bridge is 0.5% and Market street bridge is 1.97%.

2.7.2.5 Train load model:

For the assessment of the dynamic behaviour of bridges, selection of train load model is very important. The article 4, A2.4.4.3.3 of EN1991-2-2003 states that real trains must be considered for dynamic analysis of bridges. Therefore, to get an idea about the real trains in The Netherlands and what type of real train is chosen for analysis, a detail description is provided in section C.6 of Appendix C.

2.8: State of the art FRP bridges

2.8.1 GFRP Pultruded Road bridge

The first full FRP composite bridge of Europe is the West Mille bridge reconstructed in 2002.The span of the bridge is 10m and the width of 7m. The bridge consists of a GFRP pultruded deck supported on 4 rectangular Glass FRP beams. These beams are additionally coated with a thin layer of CFRP to increase the flexural strength of the beam.

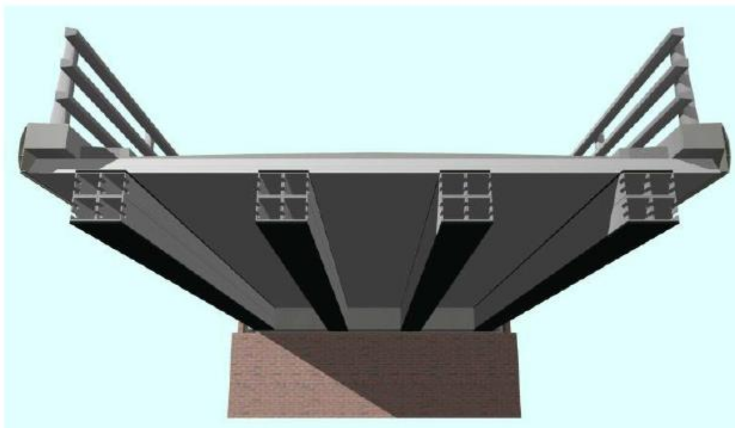

Figure 49View of the cross-section of the West Mill Bridge (MARA, 2015)

The beams are manufactured by assembling four rectangular longitudinal sections and bonding them together using an epoxy adhesive which can be seen in Figure 50.

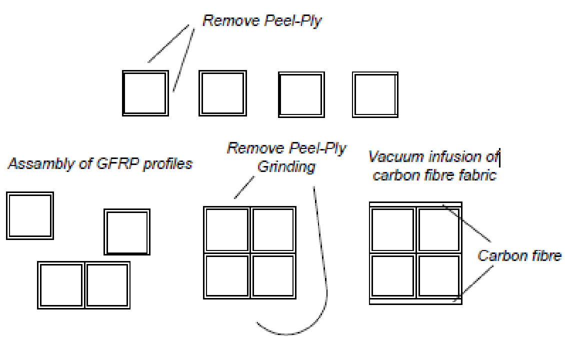

Figure 50 Manufacture process of the beam used for the West Mill Bridge (MARA, 2015)

The edge of the beams was constructed using polymer concrete which was connected to the beams using steel bolts which can be seen in Figure 51.

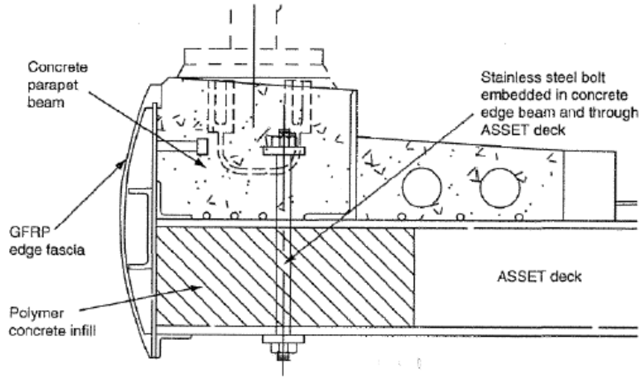

Figure 51 Connection details of the West Mill Bridge (MARA, 2015)

A series of load tests were performed on the West Mill Bridge during a period of 8 years. The results of the test concluded that the GFRP beams and deck have sufficient performance. The adhesive bond between the structural components and the bolted connection had reasonable medium- term durability. The only defect observed was cracking of the polymer concrete at the edge beam.

2.8.2 Hybrid carbon-glass fiber motorway bridge

The M111 bridge is another FRP bridge constructed of a mixture of carbon and glass fibers to obtain economy using hand lay-up technique in Madrid. The bridge is a continuous bridge with a span of 10m, 14m and 10m each supported on two concrete columns as seen in figure 52.

Figure 52 M111 Bridge (MARA, 2015)

This type of manufacturing had some problem with an exothermic chemical reaction due to heat released from material thickness in the curing process. This was solved with the application of another resin which was low exothermic.

A series of test were conducted to retrieve information about ULS, SLS and shear behavior of the bridge. It was observed that the bridge has an elastic behaviour as evident through figure 54. Shear buckling and tensile failure on the bottom side of the beam at the mid span were also reported in the results which took place at a load corresponding to approximately 1.76 times the ULS load.

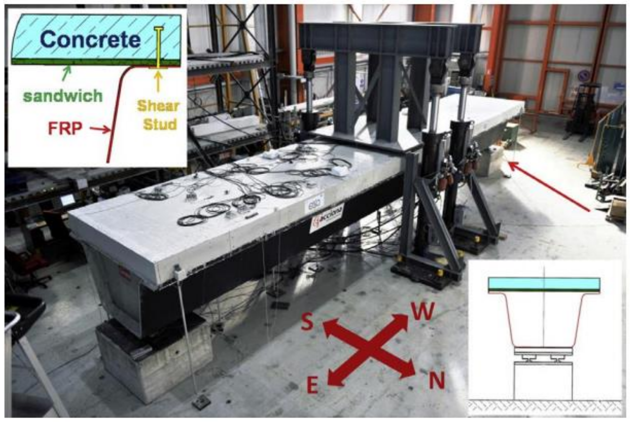

Figure 53 Set Up of testing (MARA, 2015)

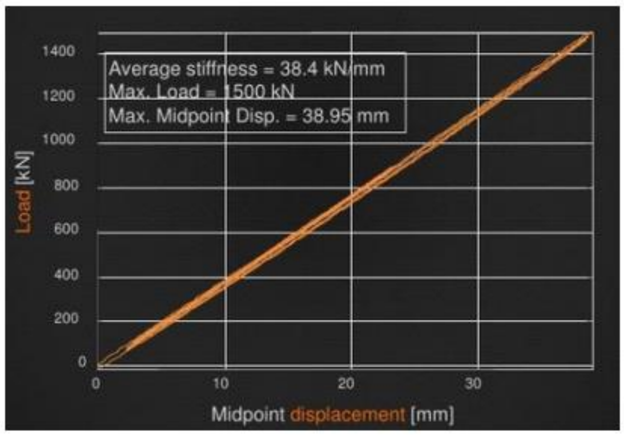

Figure 54 Load-Displacement curve (MARA, 2015)

Figure 55 Shear buckling failure of beam (MARA, 2015)

2.8.3 FRP-Steel Mill Creek Bridge

Bentley creek bridge is a rehabilitated steel-FRP highway bridge. The bridge is a through truss steel structure which consists of two parallel trusses with no overhead bracing and a floor beam stringer system. The deck of this truss bridge was made of concrete. Figure 56 shows the elevations and the roadway section of the bridge.

Figure 56 Elevation and Roadway section of the bridge (WILLIAM F. ALBERS, 2007)

After the steel truss members were repaired, the FRP Hardcore patented panel was used to replace the deteriorated concrete slab. The main advantage of the application of these FRP panels was the drastic reduction in the dead weight of the bridge.

This FRP panel were connected to the steel girders. Due to the varying height of the section, the connection of bolts or rods was not easy. Therefore, holes were drilled through the lower face panel and core so as to attach the deck to the steel girder. Figure 57 (a) shows the deck clamped to the steel girder and figure 57 (b) shows the detail of bolt connected to the steel girder though the upper face panel.

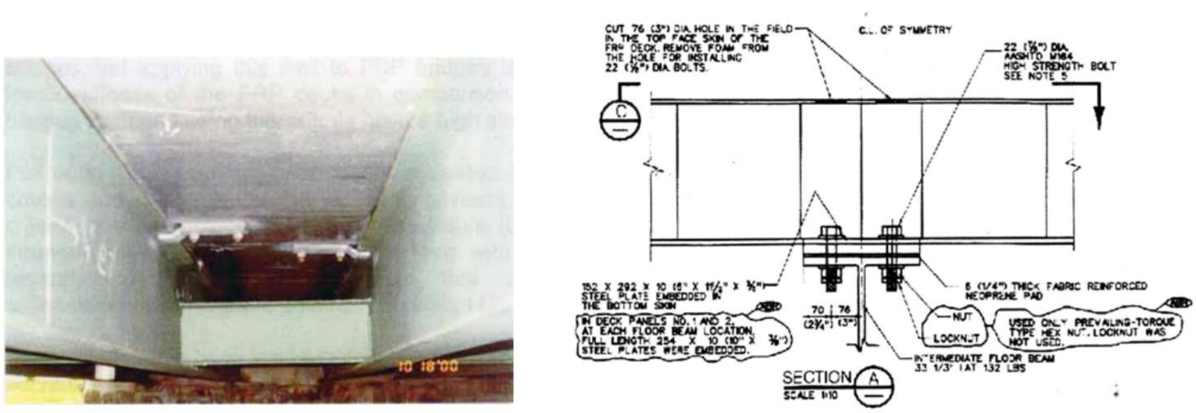

Figure 57 (a) Hardcore FRP deck clamped to steel girder (b)bolted connection between lower deck panel and steel girder (GÜRTLER, 2004)

2.8.4 Hybrid FRP-concrete bridge deck

A hybrid application of FRP-concrete material is made for a road bridge known as Kings stormwater channel bridge. The bridge is 13m wide and 10m long two-way span super-structure (figure 58). This bridge utilizes prefabricated carbon thin shells (figure 59) which are produced by filament winding. These carbon shells are filled with light weight concrete on-site. The lightweight concrete provides compression force transfer and prevents the thin-walled CFRP tubes from buckling. The lightweight nature of this bridge is additionally fulfilled by using GFRP

DURASPAN panels shown in figure 60. These structural elements are connected to each other using carbon shell connection technique which is illustrated in figure 61.

The carbon-shell joining technique consists of holes drilled in the carbon shell which is filled with concrete. In this filled concrete dowels are inserted to make a connection between FRP panel and carbon shell to transfer forces.

Figure 58 Kings stomwater channel bridge (Aref, 2007)

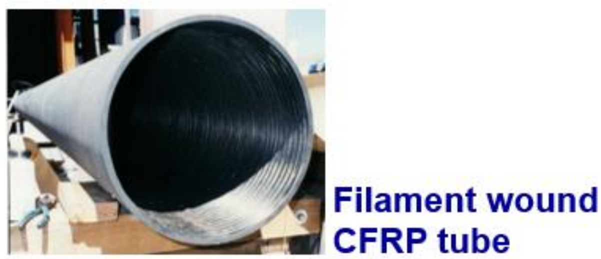

Figure 59 CFRP tube (Aref, 2007)

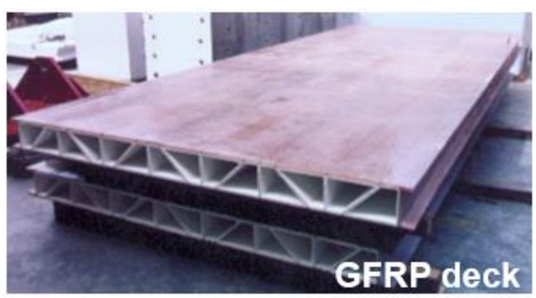

Figure 60 DURASPAN GFRP deck panel (Aref, 2007)

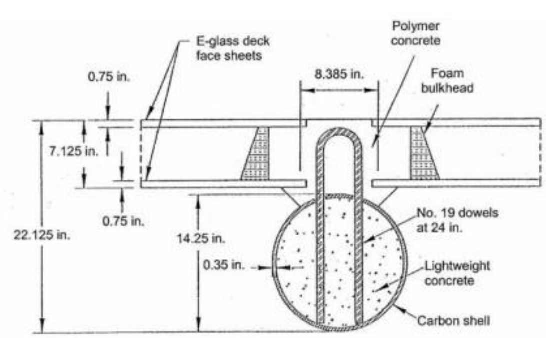

Figure 61 Carbon-shell connection scheme (GÜRTLER, 2004)

3

Conceptual Design

The main objective of this chapter is to attain the possible conceptual design shapes for the bridge using FRP and FRP-steel combinations such that they could provide sufficient stiffness to limit deflection resulting from LM71 load model to L/800. Then, an evaluation of several structural designs on the basis of the presence of connections and depth required will be made to indicate which structural design forms will be dealt in detail for preliminary design.

3.1Design requirements

FRP structural elements are known for their high strength, fatigue resistant, lightweight, corrosion resistant and quick installation property. The following flow chart briefly explains the design process involved:

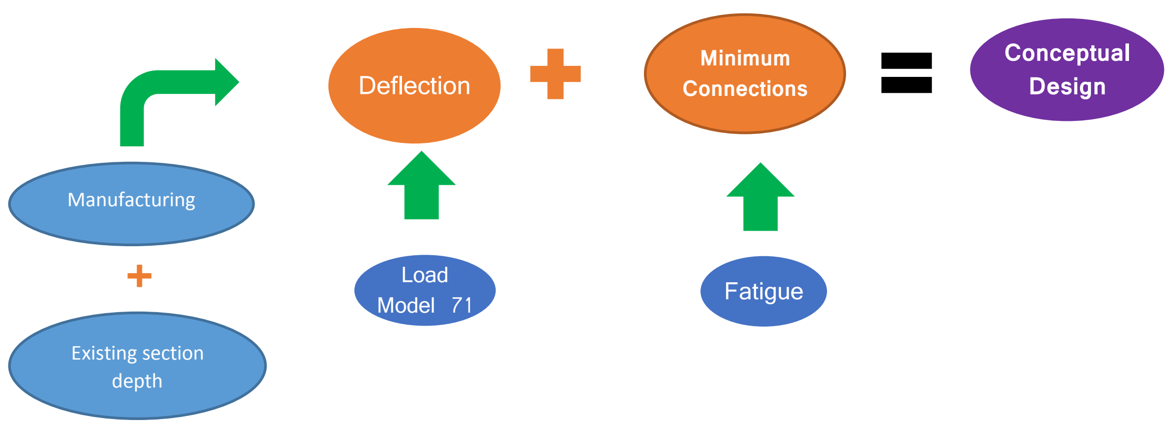

Figure 62 Design Philosophy Flow Chart

The flow chart in figure gives an idea about the key criteria considered for the conceptual design of the FRP bridges. From the assessment of the old steel bridge in section 1.5.2, it can be observed that deflection and fatigue have been the limiting factors to attain full service life of the bridge. These criteria are discussed below in detail as below:

1. Deflection: According to cl A.2.4.4.2.3 (1) NEN-EN-1990+A1+A1/C2/NB (2011), the deflection should be within L/800, where L is the span of the bridge.

2. Manufacturing technique: VARTM has been preferred since the properties of the FRP panel can be customized according to the design needs but also high shear stiffness values can also be achieved. This preference becomes important due to resulting high shear stains from LM71. For more detail into this behaviour, one can refer section 2.3 of the literature study.

3. Service life: The recommended service life of the bridge according to NA EN1991-2-2003 should be 100 years.

4. Existing depth of section: The depth of the new rail bridge section should within 973mm including rails and bearing. This allows the re-use of the existing foundations.

5. Vertical acceleration of the deck: For the traffic safety, the maximum vertical acceleration of the bridge deck for high speed trains running at or greater than 200 km/hr should not exceed 3.5 m/s^2 (ballast) or 5 m/s^2 (no ballast).

6. Geometrical allowances: To ensure that the geometrical allowances asked by ProRail in their OVS guidelines are followed, a bridge drawing with lateral allowances for passenger path and repair/inspection path for reference is described in Appendix B.

To make sure that all the above design requirements are met, FRP and combination of FRP-steel are considered and design forms are proposed. In this study, only the design of structural elements is considered for the mean time.

3.2 Design Concepts

Based on the above-mentioned design philosophy, the proposed structural design forms of bridges using FRP and FRP-steel combination are investigated. For the basic calculations related to FRP material, properties(E=33.8GPa) of Unidirectional E-Glass fiber ply with the volume fraction of 45% from JRC,2016 have been used. At present, the influence of secondary deformations is ignored while making calculations but their influence is considerable which will be covered in the next chapter.

3.2.1 Form selection criteria

According to the norms defined in the design philosophy section, the study will try to find various forms that can be suited for the bridge design within the bridge depth section requirements. The form selection is based on the following factors and is discussed as follows:

1. Type of materials considered: For the conceptual design, both steel and FRP materials are considered for bridge structural material. Therefore, both of the pure FRP section and composite FRP-steel will be considered for the bridge structure material.
2. Rail track: Another factor that influences the bridge shape is the rail-track structure considered for the design. ERS system allows more structural depth due to the absence of ballast when the depth of the section is a constraint. In the ballast-track system, around 350mm of the depth is occupied by ballast alone, which reduces the depth of the structural element.

3.3 Form I

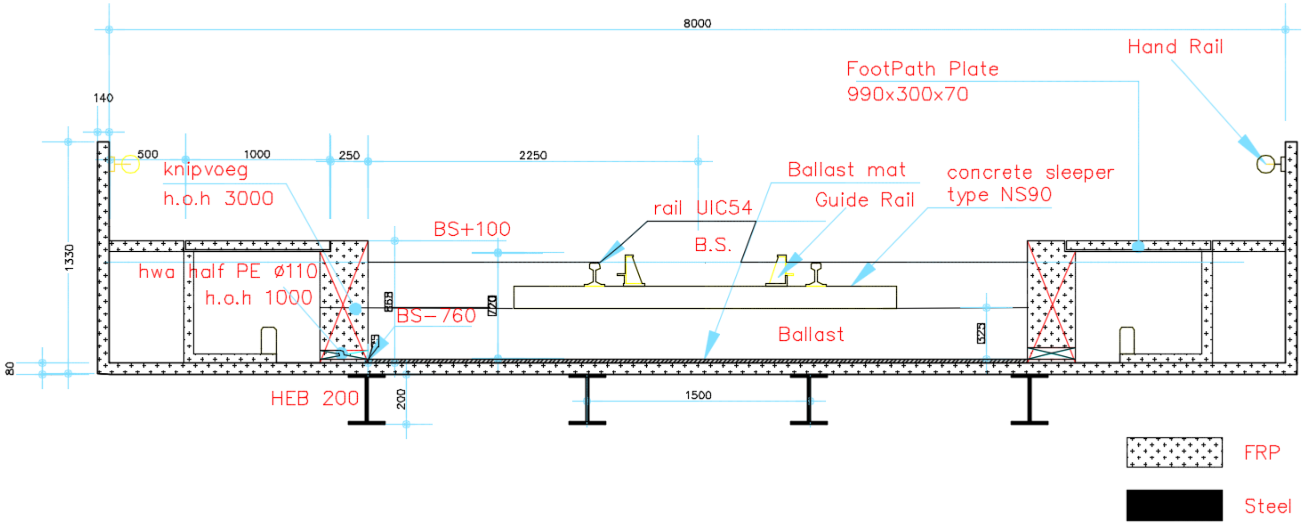

Figure 63 FRP-Steel composite bridge with Ballast rail track system

Form I consist of FRP-steel composite interaction with ballast laid on the railway bridge. U-shaped FRP profile is considered in combination with HEB200 beams to attain required flexural stiffness through its side walls when ballast and sectional depth constraint limits it. The idea of this section is to show that FRP-steel sections are also possible for a replacement. The FRP profile will be connected to the steel flanges through general bolts or bonded connections. The FRP profile for this form is considered as a glass fiber sandwich panel as described below in 3.3.1. According to OVS00030-1, the passenger path and inspection path should be on at least one of the sides of the track. To maintain symmetry such that there is no eccentric moments, passenger paths and inspection widths area provided at both the sides. This will also result in more safe and reliable section since some trains have doors only on one side for the exit of passengers. The non-structural elements will also be fabricated of FRP material. A guide rail is provided on the rail system to prevent the derailment of the train such that it does not bump into the passenger path and damages the FRP non-structural elements.

3.3.1 Section Properties

To calculate the section properties of this hybrid section, the Form 1 section is divided into 3 sub-sections which are vertical panel section, horizontal panel section and HEB200 beams section.

<u>Vertical panel section</u>

The vertical panel section comprises of 2 vertical FRP sandwich panels with face of 1250mm long and 40mm thick. There are 10 webs are 10mm thick and 60mm deep, spaced at a distance of 100mm. This sandwich panel (figure 64) can be modelled as an I beam with the thickness of flange as the thickness of the faces which is 40mm and width of the flange equal to the length of the face which is 1250mm. The webs of the I beam is 100mm (thickness of web * number of webs) and depth of 60mm.The schematic model of I beam for this vertical panel is shown below in figure 65.

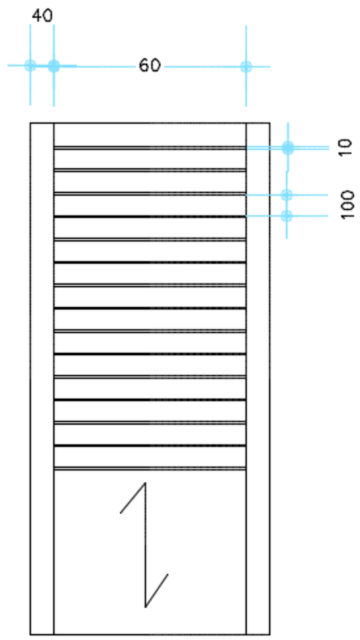

Figure 64 Vertical panel of Form I

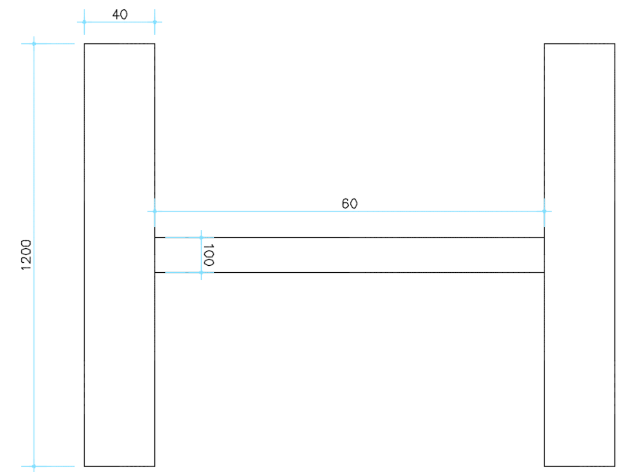

Figure 65 I-beam model of vertical panel (Form I)

<u>Dimensions of I beam model:</u>

$t_{flange,v} = 40mm$

$h_{flange,v} = 1200mm$

$t_{web,v} = 100mm$

$h_{web,v} = 60mm$

$N_{webs,v} = 10$

$$Area\ of\ vertical\ panels\ (A_v) = \left(\left(t_{flange,v} * h_{flange,v} * 2\right) + \left(t_{web,v} * h_{web,v}\right)\right) * 2 = 204000mm^2$$

$$Moment\ of\ inertia\ of\ vertical\ panels\ (I_v) = \frac{2 * t_{flange,v} * h_{flange,v}^3 + h_{web,v} * t_{web,v}^3}{12} * 2$$

$$= 2.3E + 10\ mm^4$$

$$centroid\ of\ vertical\ panels\ (y_v) = -600mm$$

The reference axis for calculation of centroid and moment of inertia is the edge of the top face of FRP horizontal panel.

<u>Horizontal panel</u>

The horizontal panel section comprises of a FRP sandwich panels with the face of 8000mm long and 20mm thick. There are 72 webs are 10mm thick and 40mm deep, spaced at a distance of 100mm. This sandwich panel (figure 66) can be modelled as an I beam with the thickness of flange as the thickness of the faces which is 20mm and width of the flange equal to the length of the face which is 8000mm. The webs of the I beam is 720 mm (thickness of web * number of webs) and depth of 40mm. The schematic model of I beam for this horizontal panel is shown below in figure 67.

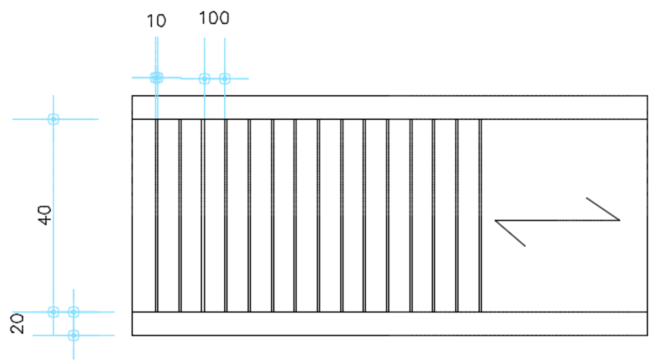

Figure 66 Horizontal Panel of Form I

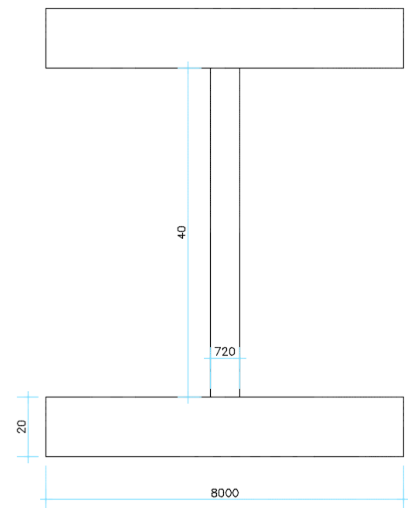

Figure 67 I- beam model of horizontal panel (Form I)

$t_{flange,h} = 20mm$

$l_{flange,h} = 8000mm$

$t_{web,h} = 720mm$

$h_{web,h} = 40mm$

$N_{webs,h} = 72$

$$Area\ of\ horizontal\ panels\ (A_h) = \left(\left(t_{flange,h} * l_{flange,h} * 2\right) + \left(t_{web,h} * h_{web,h}\right)\right) = 348800mm^2$$

$$Moment\ of\ inertia\ of\ horizontal\ panel\ (I_h) = \frac{l_{flange,h} * \left(h_{web,h} + 2 * t_{flange,h}\right)^3 - h_{web,h}^3 * \left(l_{flange,h} - t_{web,h}\right)}{12}$$

$$= 14506666.67\ mm^4$$

$$centroid\ of\ horizontal\ panel\ (y_h) = -40mm\ from\ reference\ axis$$

<u>Steel HEB200 beams section</u>

Steel section consists of 4 HEB200 beams. It is to be transformed into an equivalent homogenous section to calculate cross-section properties.

Modular ratio:

$$n = \frac{E_s}{E_{FRP}} = 6.36$$

Transformed steel beam section:

$$b_{transformed} = b * n = 1272.72mm$$

$$t_{w,transformed} = t_w * n = 57.27mm$$

$$y_{beams} = 180mm\, from\, reference\, axis$$

$$Area_{beams} = \left(t_{w,transformed} * h_w + \left(2 * t_f * b_{transformed}\right)\right) * 4 = \ 191670mm^2$$

$$I_{beams} = \frac{b_{transformed} * h^3 - \left(h - 2t_f\right)^3 * \left(b_{transformed} - t_w\right)}{12} * 4 = 3254953550 \text{ mm}^4$$

HE200B			
Geometry		Section properties	
h = 200 mm	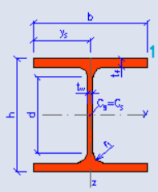	Axis y	Axis z
b = 200 mm		I_y = 5.70E+7 mm^4	I_z = 2.00E+7 mm^4
t_f = 15 mm		W_{y1} = 5.70E+5 mm^3	W_{z1} = 2.00E+5 mm^3
t_w = 9 mm		$W_{y,pl}$ = 6.42E+5 mm^3	$W_{z,pl}$ = 3.04E+5 mm^3
r_1 = 18 mm		i_y = 85.40 mm	i_z = 50.70 mm
y_s = 100 mm		S_y = 3.21E+5 mm^3	S_z = 1.52E+5 mm^3
d = 134 mm		Warping and buckling	
A = 7810 mm^2		I_w = 1.71E+11 mm^6	I_t = 5.96E+5 mm^4
A_L = 1.15 m^2.m^{-1}	G = 61.3 kg.m^{-1}	i_w = 47.10 mm	i_{pc} = 99.30 mm

<u>bridge section</u>

The combination of vertical, horizontal and steel beams section comprises the hybrid section.

Centroid of transformed bridge section:

$$y_{cg} = (A_v * y_v + A_h * y_h + Area_{beams} * y_{beams})/(A_v + A_h + Area_{beams}) = -136.81mm$$

The distance between the centroid of vertical FRP section and centroid of bridge section:

$$a_1 = y_{cg} - y_v = 463.18mm$$

The distance between the centroid of horizontal FRP section and centroid of bridge section:

$$a_2 = y_{cg} - y_h = 176.81mm$$

The distance between the centroid of steel beams section and centroid of bridge section:

$$a_3 = y_{cg} - y_{beams} = 316.81mm$$

$$Flexural\, stiffness\, of\, bridge\, section = E_v * I_v + E_v * A_v * a_1^2 + E_h * A_h * a_2^2 + E_{steel,trans} * A_{beams} * a_3^2$$
$$= 3.2E + 15\; Nmm^2$$

$$* E_v = E_h = E_{steel,trans} = 33000 \ Nmm^2$$

Table 11 shows the properties of Form I.

Properties of transformed section	
Centroid (y_{cg})	136.8mm from top edge of top face of horizontal panel
Flexural stiffness (Nmm^2)	3.2E+15
Rail-track system	Ballast track system
Width of bridge (mm)	8280
Steel girder	HEB 200

Table 11 Properties of Form I

3.4 Form II

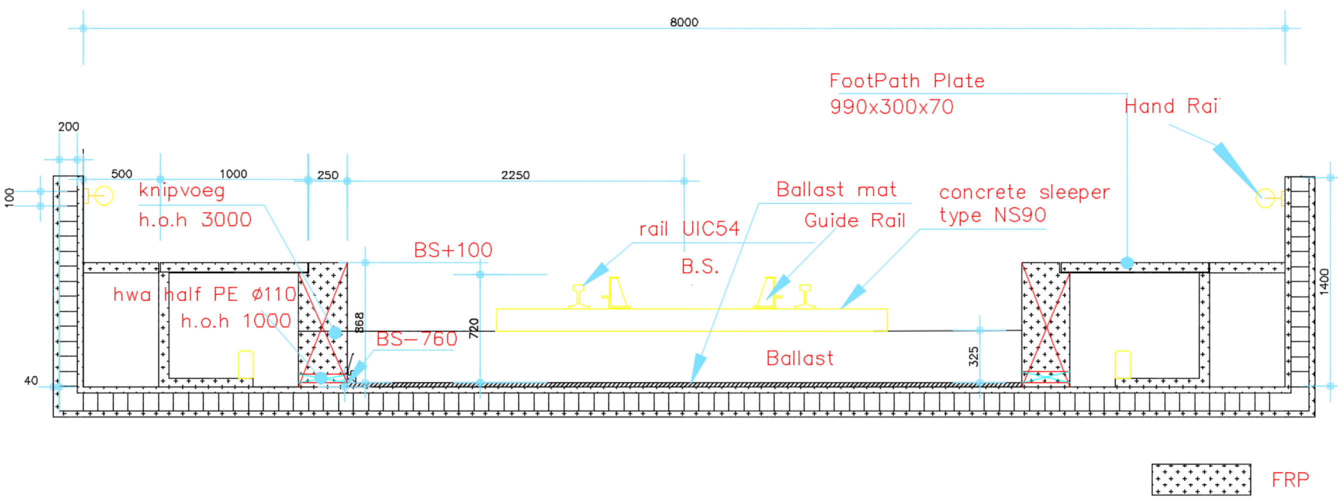

Figure 68 FRP bridge with ballast-track system

Form II consists of only FRP railway bridge with ballast laid on it. As it can be observed that in Form I, a possibility of FRP steel interaction is also possible. But the U-shaped form gives the advantage of increasing the depth of side walls and achieving required flexural stiffness. In this concept, the possibility of only FRP material is considered along with ballast track system. Since FRP is lighter than the steel, the advantage of this form of the Form I will be light weight. The face has a thickness of 40mm and webs are 10mm thick with c/c distance of 100mm. The space between the webs is filled with 110S PMI rigid foam material which holds the webs in its assigned position while manufacturing. Non-structural elements are also made of FRP material and the guide rail is provided to prevent the derailment and further damage.

3.4.1 Section Properties

To calculate the section properties of this hybrid section, the Form II section is divided into 2 sub-sections which are vertical panel section and horizontal panel section.

<u>Vertical panel section</u>

The vertical panel section comprises of 2 vertical FRP sandwich panels with the face of 1400mm long and 40mm thick. There are 10 webs are 10mm thick and 200mm deep, spaced at a distance of 100mm. This sandwich panel can be modelled as an I beam with the thickness of flange as the thickness of the faces which is 40mm and width of the flange equal to the length of the face which is 1400mm. The webs of the I beam is 200mm (thickness of web * number of webs) and depth of 200mm. The schematic model of I beam for this vertical panel is shown below in figure 69.

$t_{flange,v} = 40mm$

$h_{flange,v} = 1400mm$

$t_{web,v} = 200mm$

$h_{web,v} = 200mm$

$N_{webs,v} = 10$

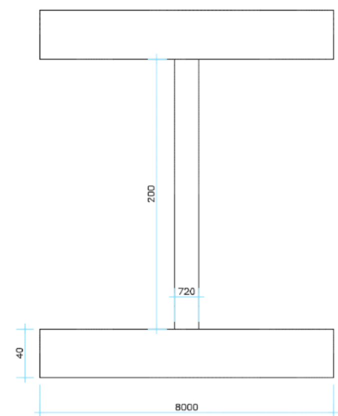

Figure 69 I-beam model of vertical panel (Form II)

$$Area\ of\ vertical\ panels\ (A_v) = \left(\left(t_{flange,v} * h_{flange,v} * 2\right) + \left(t_{web,v} * h_{web,v}\right)\right) * 2 = 304000mm^2$$

$$Moment\ of\ inertia\ of\ vertical\ panels\ (I_v) = \frac{2 * t_{flange,v} * h_{flange,v}^3 + h_{web,v} * t_{web,v}^3}{12} * 2$$

$$= 1.84E + 10\ mm^4$$

$$centroid\ of\ vertical\ panels\ (y_v) = 700mm$$

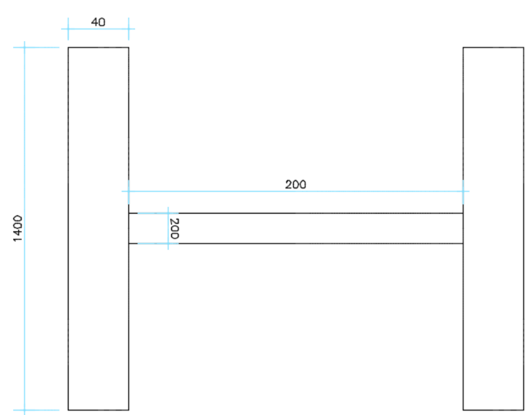

The reference axis for calculation of centroid and moment of inertia is the edge of the top face of horizontal FRP panel.

<u>Horizontal panel section</u>

The horizontal panel section comprises of a FRP sandwich panels with the face of 8000mm long and 40mm thick. There are 72 webs are 10mm thick and 200mm deep, spaced at a distance of 100mm. This sandwich panel can be modelled as an I beam with the thickness of flange as the thickness of the faces which is 40mm and width of the flange equal to the length of the face which is 8000mm. The webs of the I beam is 720 mm (thickness of web * number of webs) and depth of 200mm. The schematic model of I beam for this horizontal panel is shown below in figure 70.

$t_{flange,h} = 40mm$

$l_{flange,h} = 8000mm$

$t_{web,h} = 720mm$

$h_{web,h} = 200mm$

$N_{webs,h} = 72$

Figure 70 I-beam model of horizontal panel (Form II)

$$Area\ of\ horizontal\ panel\ (A_h) = \left(\left(t_{flange,h} * l_{flange,h} * 2\right) + \left(t_{web,h} * h_{web,h}\right)\right) = 784000mm^2$$

$$Moment\ of\ inertia\ of\ horizontal\ panel\ (I_h) = \frac{l_{flange,h}*\left(h_{web,h}+2*t_{flange,h}\right)^3 - h_{web,h}^3*\left(l_{flange,h}-t_{web,h}\right)}{12}$$

$$= 565333333.33\ mm^4$$

$$centroid\ of\ horizontal\ panel\ (y_h) = 140mm$$

<u>FRP bridge section</u>

Centroid of bridge section:

$$y_{cg} = (A_v * y_v + A_h * y_h/(A_v + A_h) = 296.47mm$$

The distance between the centroid of vertical FRP section and centroid of bridge section:

$$a_1 = y_{cg} - y_v = 403.5mm$$

The distance between the centroid of horizontal FRP section and centroid of bridge section:

$$a_2 = y_{cg} - y_h = 156.48mm$$

$$Flexural\ stiffness\ of\ bridge\ section = E_v * I_v + E_v * A_v * a_1^2 + E_h * A_h * a_2^2$$

$$= 2.89E + 15\ Nmm^2$$

Table 12 sums up the cross-sectional and geometric properties of Form II.

Properties	
Centroid (y_{cg})	296.47 from top face of horizontal panel
Flexural stiffness (Nmm^2)	2.89E+15
Rail-track system	Ballast track system
Width of bridge (mm)	8280

Table 12 Properties of Form II

3.6 Form III

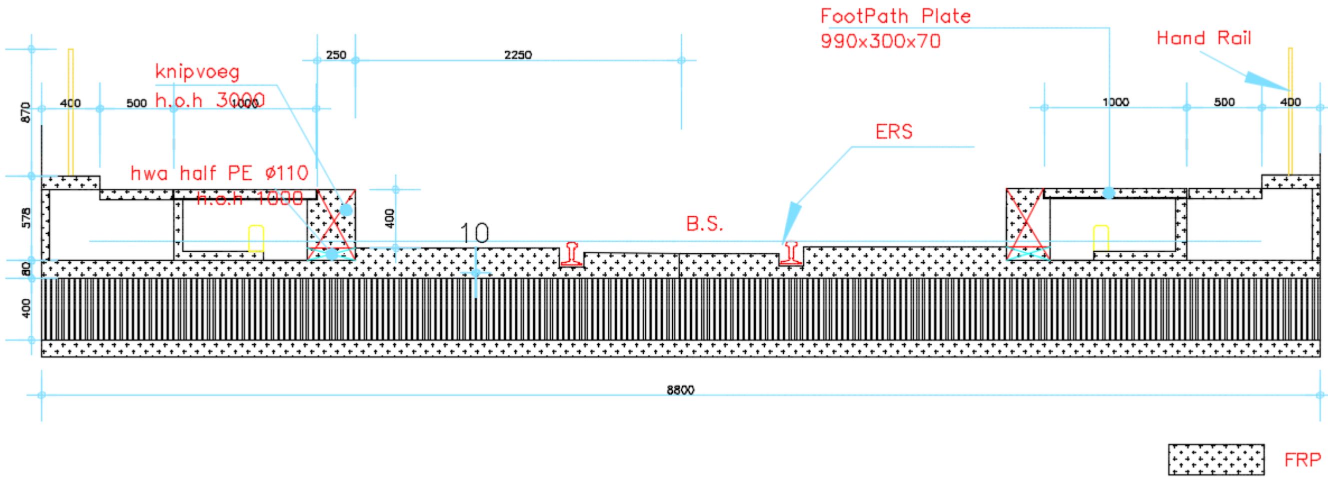

Figure 71 FRP bridge with ERS

Form III is made up of only FRP material with the embedded rail system. This form only uses the the FRP material as a sandwich panel with faces and webs. The non-structural elements are fabricated with the FRP material. The face is 80mm thick and webs 10mm thick spaced at 50mm c/c distance. This section would be lighter than the Form III since no steel is used. The space between the webs is filled with 110S PMI rigid foam to withhold the webs intact in their own position while manufacturing.

3.6.1 Section Properties

The horizontal panel section comprises of a FRP sandwich panels with the face of 8800mm long and 80mm thick. There are 146 webs are 10mm thick and 400mm deep, spaced at a distance of 50mm. This sandwich panel can be modelled as an I beam with the thickness of flange as the thickness of the faces which is 80mm and width of the flange equal to the length of the face which is 8800mm. The webs of the I beam is 1460 mm (thickness of web * a number of webs) and depth of 400mm.

$$t_{flange,h} = 80mm$$

$$l_{flange,h} = 8800mm$$

$$t_{web,h} = 1460mm$$

$$h_{web,h} = 400mm$$

$$N_{webs,h} = 146$$

$$Area\ of\ horizontal\ panel\ (A_h) = \left(\left(t_{flange,h} * l_{flange,h} * 2\right) + \left(t_{web,h} * h_{web,h}\right)\right) * 2 = 1992000mm^2$$

$$Moment\ of\ inertia\ of\ FRP\ panel\ (I) = \frac{l_{flange,h} * \left(h_{web,h} + 2 * t_{flange,h}\right)^3 - h_{web,h}^3 * \left(l_{flange,h} - t_{web,h}\right)}{12}$$

$$= 8.96\ E + 10\ mm^4$$

$$flexural\ stiffness = EI = 2.95E + 15\ Nmm^2$$

$$centroid\ of\ vertical\ panels\ (y_h) = 280mm$$

Table 14 sums up the cross-sectional and geometrical properties of Form III.

Properties	
Centroid (y_{cg})	240 from the bottom edge of the bottom face of panel
Flexural stiffness (Nmm^2)	2.95E+15
Rail-track system	Embedded rail track system
Width of bridge (mm)	8800

Table 13 Properties of Form III

3.7 Comparison of Structural Forms

Table 15 compares the above described structural forms based on the design philosophy explained.

Design Form	Connections	Calculated flexural stiffness	Required flexural stiffness	Bridge Rail system
Form I	**Yes**	**3.2E+15**	$2.8 * 10^{15} N * mm^2$	Ballast system
Form II	**No**	**2.89E+15**		Ballast System
Form III	**No**	**2.95E+15**		Embedded Rail system

Table 14 Comparison of Conceptual Design Forms

From table 15, it can be observed that despite satisfying flexural criteria, Form I have connections, which in general are a potential source of fatigue. So, their application is not advised for the railway bridge where fatigue is already a concern as in the case of old steel railway bridge.

4

Material Properties

4.1 Introduction

In this chapter material properties for the FRP laminate will be discussed. The main aim of formulating a customized ply is to achieve a Young's and shear modulus as higher as possible by making sure that the ply requirements from CUR,96 are met and less material is utilized to fulfill stiffness criteria and low weight requirements. FRP ply is a composite material made of a fiber and resin in appropriate ratios. In addition, the manufacturing process will be determined that is chosen for the bridge structural form fabrication.

The material properties of the fibers and resin in the FRP composite can be obtained from JRC,2016. The most common glass fiber/ resin used in the industry is E-Glass/Polyester which will be used in this research project as well. Table 16 shows the material properties of this fiber and resin obtained from JRC 2016.

4.2 Manufacturing Method

As discussed in section 2.2 of the report, manufacturing method plays an important role in determining the material properties of the resulting laminate. For the design of FRP bridge, serviceability criteria are an important factor. Therefore, to meet the deflection criteria as prescribed in section 2.6, it is important to ensure that the chosen laminate has high Young's and Shear modulus. Another criterion to think upon is the local crushing of the FRP ply. Due to high concentrated axle loads on bridges, this can be a critical issue. Therefore, it becomes essential that the laminate has sufficient compressive strength in a direction perpendicular to its main longitudinal axis. As a result of the comparison made in Table 7 of this report, it can be concluded that VARTM method would be a wise choice to fabricate the FRP panels.

4.3 Material Properties

In this section, the study will discuss the properties of the fundamental materials chosen for the laminate and the resulting material properties of the ply lay-up (laminate) considered. Table 16 below shows the material properties of all the proposed FRP elements.

4.3.1 Choice of Fiber

For the application of FRP in the civil industry, two types are fibers are commonly available; glass and carbon. Carbon Fiber is much lighter and has relatively higher (2-3 times) Young 'modulus than Glass fiber. But the cost of carbon fiber is roughly 5-6 times of Glass fiber (Kok, 2013), which makes it highly uneconomical. Therefore, E-Glass fiber is considered as a fundamental material choice for the ply.

		E Glass
Density (kg/m^3)		2570
Tension in Fiber Direction	Poisson's ratio ν_f	0.238
	Youngs Modulus E_{f1} (MPa)	73100
	Strain limit $\in_{f1}$ (%)	3.8
	Strength σ_{f1} (MPa)	2750
Tension in perpendicular to fiber direction	Poisson's ratio ν_f	0.238
	Youngs Modulus E_{f2} (MPa)	73100
	Strain limit $\in_{f2}$ (%)	2.4
	Strength σ_{f2} (MPa)	1750
Compression in fiber direction	Strain limit $\in_{f1}$ (%)	2.4
	Strength σ_{f1} (MPa)	1750
Shear	Modulus G_f (MPa)	3000
	Strain limit γ_{f12} (%)	5.6
	Strength τ_{f12} (MPa)	1700
		Polyester Resin
Density (kg/m^3)		1.2
Poisson's ratio $\nu_{12,\ resin}$		0.38
Tensile or compression strength (MPa)		55
Young modulus in tension (MPa**)**		3550
Strain limit in tension or compression (%)		1.8
In-plane shear modulus (MPa)		1350
Shear strength (MPa)		50
Shear strain limit (%)		3.8
Tg (°C)		60
		110S PMI rigid Foam
Gross Density	kg/m^3	110
Compressive Strength	MPa	2.97
Compressive Modulus	MPa	130
Tensile Strength	MPa	3.27
Tensile Modulus	MPa	157
Shear Strength	MPa	5,47
Shear Modulus	MPa	138

Table 15 Characteristic Properties (JRC,2016 and Eurocomp)

4.3.2 Choice of Resin

There is a number of resins available in the market. There is not much difference in the contribution of the resins in the stiffness of FRP panel as it is too low when compared with fibers, though elongation of resins is generally considered a deciding factor. But in this stiffness based design strain criterion is not dominating. Therefore, polyester resin is chosen as a fundamental matrix for binding the Glass fibers since it is the most economically fabricated resin available in the market (Kok, 2013).

4.3.3 Choice of Foam

Generally, the foam cores are used to provide stability and strength to sandwich panels but in our scenario, the foam cores are used to support the webs and orient the FRP plies according to the geometric layout during the fabrication process. The shear forces and normal forces will be restrained by the plies in the webs in the longitudinal section of the bridge. In the transverse section of the bridge, where no webs are placed and transverse shear forces can be encountered a foam core of sufficient shear rigidity would be preferred. Therefore, to make the production of the bridge panel as uniform,110S PMI rigid foam is proposed throughout the bridge structure in the hollow space between the webs and the skin/faces.

4.4 Design of FRP Laminate

FRP laminate considered in this thesis project is a superset of numerous plies composed of E- glass fiber with Polyester Resin as binding matrix. This section deals with the design of FRP laminate which follows the recommendations laid in section 2.4.

4.4.1 Design of Ply and laminate lay-up

In this section, the design calculations of FRP ply will be presented.

The density of E-Glass fiber:

$$\rho_{glass} = 2570\frac{kg}{m^3}$$

Eq 1

$$Aerial\ Weight = 1200\frac{gm}{m^2}$$

Eq 2

The density of Polyester Matrix:

$$\rho_{matrix} = 1200\frac{kg}{m^3}$$

Eq 3

The volume fraction of fibers in the ply:

$$V_f = 0.6$$

Eq 4

The density of ply:

$$\rho_{ply} = \rho_{glass} * V_f + \rho_{matrix} * (1 - V_f) = 2022\frac{kg}{m^3}$$

Eq 5

The thickness of ply:

$$t_{ply} = \frac{Aerial\ Weight}{V_f * \rho_{glass}} = 0.8mm$$

Eq 6

Ply lay-up: [90/+-45/0_3/+-45/0_3/+-45/90/+-45/90/+-45/0_3/+-45/0_3/+-45/90]

Number of plies in lay-up:

$$N_P = 23$$

Laminate Thickness:

$$t_{lam} = N_p * t_{ply} = 18.4mm$$

Eq 7

4.5 CLT Analysis of Laminate

Laminate analysis using Classical Laminate Theory for mechanical properties has been carried out using a tool known as Composite Star 2.0 from Etamax Engineering, Australia.

4.5.1 Input Parameters

As described in Table 16, similar input parameters for FRP elements are used in this tool as shown in figure 72. Figure 74 shows the thickness and density calculated by the tool, which is same as the result obtained in section 4.4.1.

Fiber		E [GPa]		G [GPa]		Nu	
ID	Name	1	2	12	23	12	23
1	new fiber 1	73,1	73,1	3	3	0,238	0,238

Figure 72 Input for Fiber

Matrix		E [GPa]	G [GPa]	Nu
ID	Name			
1	new matrix 1	3,55	1,35	0,38

Figure 73Input for matrix

Ply		Micromec	Fiber		Matrix		Fraction		Thickness [mm]	Density [kg/m3]
ID	Name		Fiber ID	Fiber name	Matrix ID	Matrix name	type	amount [%]		
1	new ply 1	yes	1	new fiber 1	1	new matrix 1	fiber volume	60	0,8	2,022

Figure 74 Ply Properties

#	Ply		Angle [°]	Thickness [mm]
	ID	Name		
1	1	new ply 1	90	0,8
2	1	new ply 1	45	0,4
3	1	new ply 1	-45	0,4
4	1	new ply 1	0	0,8
5	1	new ply 1	0	0,8
6	1	new ply 1	0	0,8
7	1	new ply 1	45	0,4
8	1	new ply 1	-45	0,4
9	1	new ply 1	0	0,8
10	1	new ply 1	0	0,8
11	1	new ply 1	0	0,8
12	1	new ply 1	45	0,4
13	1	new ply 1	-45	0,4
14	1	new ply 1	90	0,8
15	1	new ply 1	45	0,4
16	1	new ply 1	-45	0,4
17	1	new ply 1	90	0,8
18	1	new ply 1	45	0,4
19	1	new ply 1	-45	0,4
20	1	new ply 1	0	0,8
21	1	new ply 1	0	0,8
22	1	new ply 1	0	0,8
23	1	new ply 1	45	0,4
24	1	new ply 1	-45	0,4
25	1	new ply 1	0	0,8
26	1	new ply 1	0	0,8
27	1	new ply 1	0	0,8
28	1	new ply 1	45	0,4
29	1	new ply 1	-45	0,4
30	1	new ply 1	90	0,8

Figure 75 Ply Lay-up Input

4.5.2 Laminate Properties

Figure 76 shows the properties of the laminate calculated using the tool by CLT theory and Table 17 shows the matrices of the resulting laminate required for the civil application as FRP bridge.

E in-plane [GPa]		G in-plane [GPa]	Nu in-plane		Eta in-plane				E flexural [GPa]		G flexural [GPa]	Nu flexural		Eta flexural				Nu out-of-plane		G out-of-plane [GPa]	
x	y	xy	xy	yx	xy_x	xy_y	x_xy	y_xy	x	y	xy	xy	yx	xy_x	xy_y	x_xy	y_xy	xz	yz	xz	yz
30,055	19,589	5,605	0,345	0,225	0	0	0	0	29,016	21,681	5,31	0,303	0,226	0	0	0	0	0,669	1,32	2,352	2,352

Figure 76 Laminate Properties:

$A := \begin{pmatrix} 5.79\,10^{8} & 8.08\,10^{7} & 0 \\ 8.08\,10^{7} & 3.25\,10^{8} & 0 \\ 0 & 0 & 6.12\,10^{7} \end{pmatrix} \frac{N}{m}$	(No shear-extension coupling)
$B := \begin{pmatrix} 0 & 0 & 0 \\ 0 & 0 & 0 \\ 0 & 0 & 0 \end{pmatrix} N$	(No bending-extension coupling)

$D := \begin{pmatrix} 1.48\cdot10^{4} & 2.25\cdot10^{3} & 0 \\ 2.25\cdot10^{3} & 9.17\cdot10^{3} & 0 \\ 0 & 0 & 1.774\cdot10^{3} \end{pmatrix} N\cdot m$	(Bending Matrix)

Table 16 Material Stiffness Matrices

From the above table, it can be concluded that the recommendations mentioned in section 2.2.4 have been followed as the coupling elements of the above matrices is zero and it results in no coupling between bending-torsion at the micro level. The above matrices system also concludes that the resulting ply lay-up is orthotropic symmetric laminate.

Flexural Strength of laminate in the longitudinal direction of ply:

$$\sigma_1 = E_{fx} * \varepsilon_{normal} = 348.192\ MPa$$

Eq 8

The strength of laminate in the transverse direction of ply:

$$\sigma_2 = E_y * \varepsilon_{normal} = 235.172\ MPa$$

Eq 9

Shear Strength of ply:

$$\tau_{xy} = G_{fxy} * \varepsilon_{shear} = 40.512\ MPa$$

Eq 10

4.5.3 Validation of tool

In this section, validation of the results obtained from the used tool will be made with the known result. As a benchmark study, material values for a Bi-directional (0/90) ply composed of E-gLass fiber(V_f=55%) and polyester resin are calculated and compared with the mechanical values given in JRC,2016 for UD ply with V_f=55%.

Figure 77 shows the input parameters for E-Glass fiber and Polyester resin matrix in the tool. Figure 78 shows the laminate composition and Figure 79 shows the mechanical values of the resulting ply.

Fiber		E [GPa]		G [GPa]		Nu	
ID	Name	1	2	12	23	12	23
1	E-Glass	73,1	73,1	3	3	0,238	0,238

Figure 77Input Parameters for UD E-Glass

Matrix		Density [kg/m3]
ID	Name	
1	Polyester	1.200

Figure 78 Input Parameters for Polyester resin

Stacking sequence of laminate: Bi-directional ply

#	Ply		Angle [°]	Thickness [mm]
	ID	Name		
1	1	UD ply	0	0,4
2	1	UD ply	90	0,4

Figure 79Bi-Directional Ply Lay-up

Ply		Micromec	Fiber		Matrix		Fraction		Thickness [mm]	Density [kg/m3]
ID	Name		Fiber ID	Fiber name	Matrix ID	Matrix name	type	amount [%]		
1	UD ply	yes	1	E-Glass	1	Polyester	fiber volume	55	0,8	1.953,5

Figure 80 Input Paramters for Bi-Directional Ply

E in-plane [GPa]		G in-plane [GPa]	Nu in-plane		Eta in-plane				E flexural [GPa]		G flexural [GPa]
x	y	xy	xy	yx	xy_x	xy_y	x_xy	y_xy	x	y	xy
27,152	27,152	3,557	0,135	0,135	0	0	0	0	27,152	27,152	3,557

Figure 81 Mechanical Properties of Bi-Directional Ply using Composite Star

V_f	E_1 [GPa]	E_2 [GPa]	G_{12} [GPa]	ν_{12}
25 %	12.8	12.8	1.9	0.21
30 %	14.7	14.7	2.1	0.20
35 %	16.8	16.8	2.4	0.20
40 %	18.9	18.9	2.6	0.19
45 %	21.0	21.0	2.9	0.19
50 %	23.3	23.3	3.3	0.19
55 %	25.6	25.6	3.7	0.18

Figure 82 Indicative Values for Bi-Directional Ply from JRC,2016

From the above figures, it can be observed that the results of the tool in figure 81 match the value of JRC, 2016 in figure 82 for $V_f = 55\%$.Hence the analysis results of this tool are authentic and reliable. The results vary by just 6%, which is within allowable variation. In addition, it is to keep in mind that the values given in JRC,2016 are indicative too.

4.5.4 Ply stacking and orientation

Based on above recommendation, the ply lay up for the laminate is composed of [90/+-45/0_3/+-45/0_3/+-45/90/+-45/90/+-45/0_3/+-45/0_3/+-45/90], where the thickness of laminate proposed is about 20 mm for the skin and 10mm for the webs. Each ply is 0.8mm thick.

1-> in the direction of the fibres orientation
2-> in the direction perpendicular to the orientation of fibres

Figure 83 below shows the orientation of the fibres and its axis

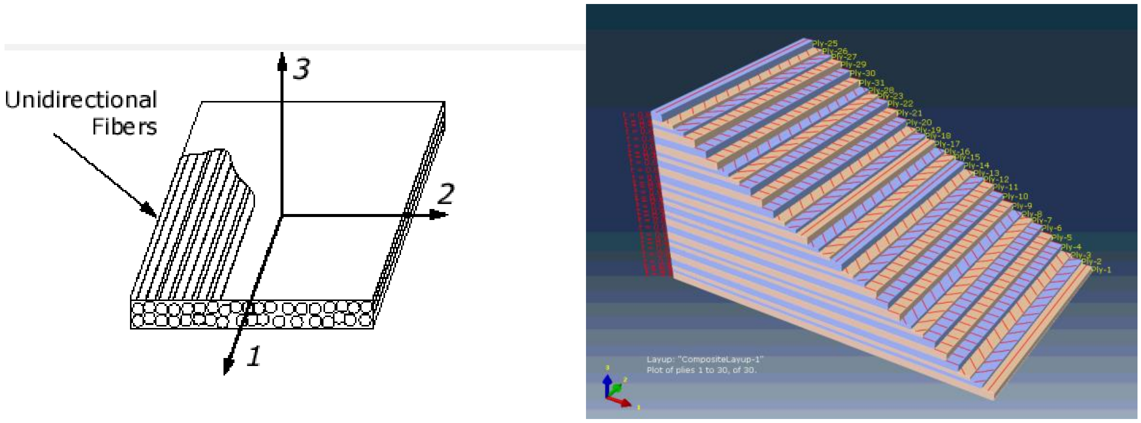

Figure 83 Orientation of Fibers and Stacking of Plies

5

Preliminary Design

The aim of this chapter is to see if it is possible to design the FRP bridge with ballast and ERS for both short and long- term deflections, such that the depth of the cross-section is within the allowable existing depth requirement. At the same time to minimize the weight of the bridge and reduce material utilization, the shape optimisation has been made wherever possible.

5.1 Introduction

In this chapter, emphasis will be paid to understanding the creep behaviour of the FRP material and how it influences the design of FRP material bridge structures. To understand this scenario in addition to the existing design constraints, this creep factor is added to the preliminary design philosophy and then analysed for the resulting total deflections if that they are within prescribed limits. To do such, exact material properties defined for the bridge structure will be utilised and this inclusion will help in determining the exact realistic deflections for the structure.

In the preliminary stage, the structural design form II and III will be analysed using accurate material properties obtained in chapter 4 for the combination of short and long-term deflections. The geometry layout of the bridges is inspired by the lateral allowances for the non-structural elements or functional requirements. The part of the study will also be including these functional requirements and how do they influence/incorporate in the bridge design concept. A variant study will be carried out on Form II for analysing the webs orientation for reduced mass but attaining limiting deflection within the available existing depth. As mentioned earlier, creep will also be considered for preliminary design. Figure 84 demonstrates the summary of the preliminary study.

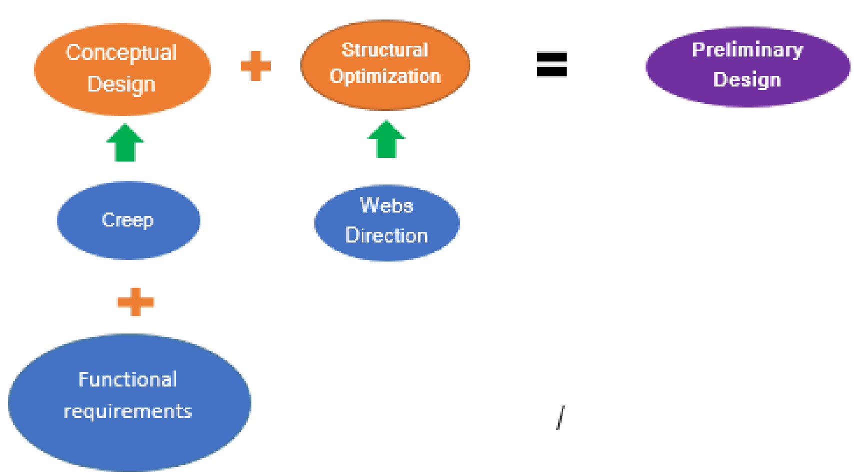

Figure 84 Flow Chart for Preliminary Design

5.2 Influence of creep

The effect of creep is generally dominated by the resin rather than the fiber or interfacial properties. The resin being resin is a viscoelastic material and thereby exhibits time dependent and therefore results in time dependent modulus of the FRP laminate. Under-cured resins are affected by creep significantly which results in crack initiation during early stages of application of FRP laminates. This affect is further aggravated by the influence of moisture and environment temperature exposure.

For the design of bridge superstructures, creep is introduced through environmental temperature to which the structure is exposed to the presence of dead loads. This leads to additional long term deflections. This creep affect is further worsened by heat generated by the frictional forces due to the passage of trains. The FRP material in contact with the rails will experience much higher temperature and would result in drastic creep effects. Only UD fibers are considered to provide stiffness for resisting resulting deflections. Hence, the influence of creep is considered for analysis by considering it through long term deflections.

5.3 Fiber architecture

In this section, the orientation of fibers in the FRP bridge and how do they align with the geometry will be described. Figure 85 shows the plies and their orientation in the face of the FRP panels when running in the longitudinal direction of the bridge. The thickness of plies in the faces is 0.8mm each. The colored hatches are defined for each type of ply for visualization and the labels have been made in figure 85.

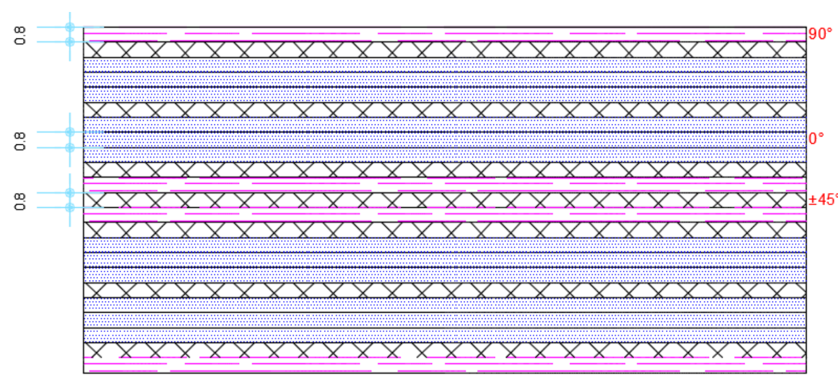

Figure 85 Orientation of plies in longitudinal running faces

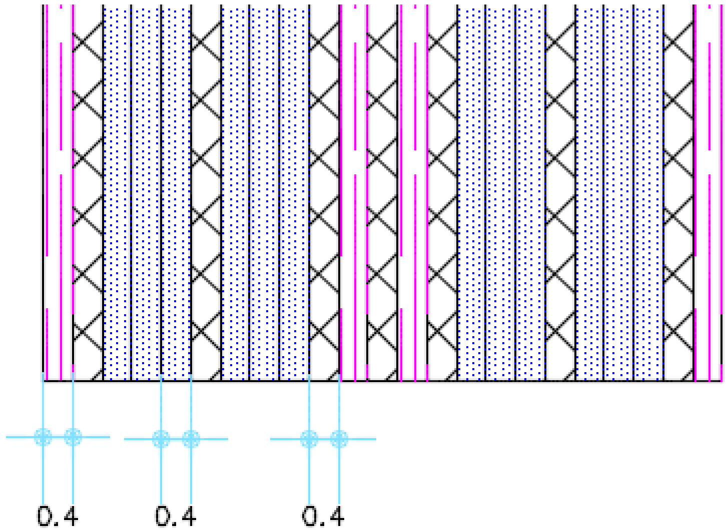

Figure 86 Orientation of plies in longitudinal running webs

Figure 86 illustrates the orientation of fibers in the webs running in the longitudinal direction of the bridge. With similar hatching patterns and labels, once can visualize the clear orientation of the plies in the webs in figure 86. The thickness of the plies in the webs is 0.4mm.

5.4 Form II bridge with ballast

Figure 87 shows the preliminary design of the bridge, which is governed by deflection by LM71 and creep. The thickness of the faces in the horizontal panel is 60mm and the webs are 450mm long. The vertical FRP panels are inclined by 10 degrees for the ease of fabrication when the three moulds would be used in the fabrication facility. The vertical panel has faces of 40mm thick and webs of 330mm deep. The intersection of vertical panel and horizontal panel is smooth like a curve of radius 80mm and 120mm at the top faces and bottom faces respectively. The passenger and inspection paths are provided on both sides as discussed in conceptual design section 3.4.

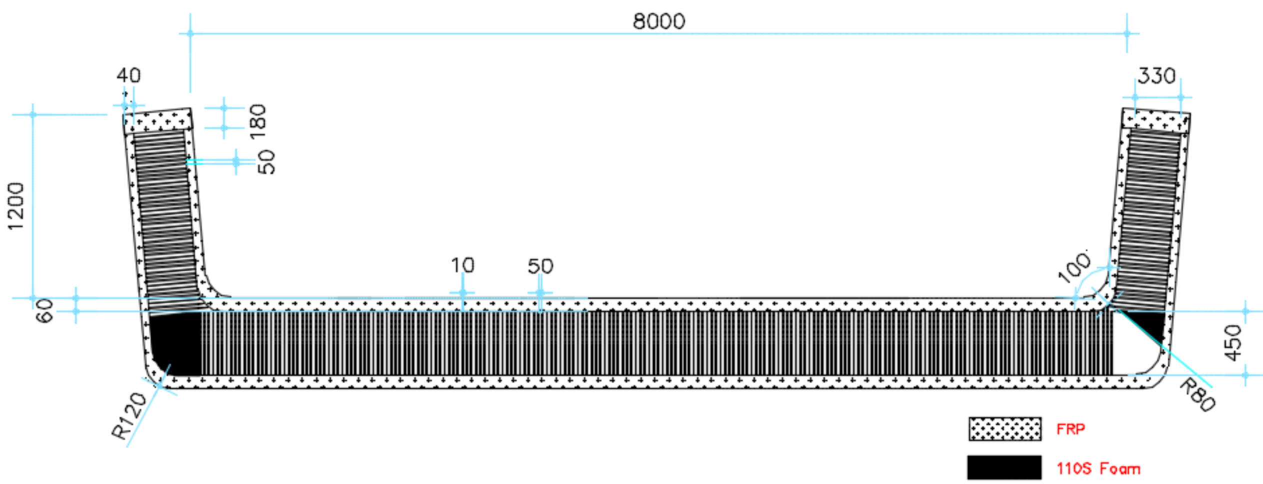

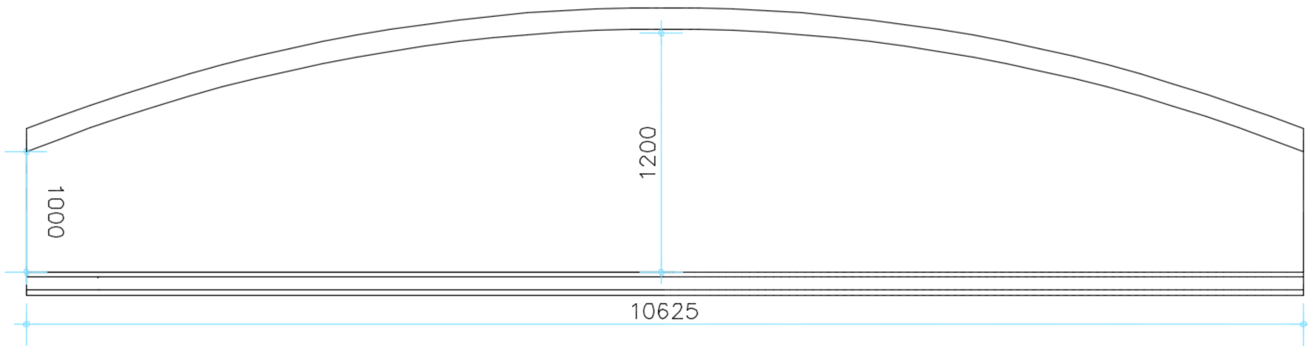

Figure 87 Preliminary Design of Form II

Figure 87 shows the elevation view of the bridge. The bridge shape is optimized for reduced material consumption. A similar elevation profile just like the bending moment shape of the bridge under bending due to LM71 plus creep loads is provided. Therefore, the peak of the elevation is at a span distance of 5.4m from the left support. At the supports, an initial elevation of 1m is given to support the emergency exit of passengers such that the depth of the vertical panel is at the same level as of passenger path.

5.4.1.1 Functional requirements

A ballast mat of 25mm thick is provided on the deck surface to prevent the damage from the vibrations of ballast and damage of top face from the moisture and external environmental conditions. It also reduces ground or structure-borne vibrations. Ground-borne vibrations that might otherwise enter the foundations of neighboring buildings, travel through its structure and causing walls, floors and ceilings to pulsate, recreating noise known as 'Secondary Noise', noise that cannot be reduced by closing curtains etc.

The foot path and walk path plate are made of FRP gratings from Strongwell company to support pedestrian loads as shown in figure 88. The approximate weight of the FRP panel grating of 1m*4m*25mm is 12.69kg/m^2.

Figure 88 FRP walkway gratings

The platform near the tracks that supports FRP gratings is 125mm and 900mm long. Another L-shaped support to the FRP pathways can be provided of a sandwich panel of 125mm thick. These vertical support platforms are considered as sandwich panels from Fiberline company (compositeadvantage).The sandwich panel from this company can withstand a concentrated load of 18kN which is sufficient to withstand vertical support force acting from crowd loading of 5kN.The weight of these sandwich panels is 0.45kN/m^2 (compositeadvantage).

This vertical sandwich panel supports will be connected to the FRP horizontal deck through adhesive bonding. The reason being, the crowd load acting on the grating will be directly transferred to the FRP horizontal panel through supports. Another load that can be considered is the aerodynamic action from the passing train. The distance between the center of rail track to this platform is 2.25m. Since the minimum distance for this load to be included is 2.3m from the center of rail track is 2.3 meter, therefore an aerodynamic action load for the speed of 200kmph from 6.6.2 EN1991-2-2003 will be 0.65kN/m^2.This load will be acting on the vertical platform will be of magnitude 0.585kN (0.65*0.9kN/m). To counter this load, these non-structural elements will be bonded to the top face of FRP horizontal panel which will transfer this shear force to the bridge superstructure. The shear force that would be acting would be roughly 0.292kN. Considering the base of this vertical platform of 250mm and choosing adhesive glue KFL 156 with a shear strength of 29MPa from 5M corporation, the thickness required for this glue would be:

$$t_{glue} = \frac{\frac{0.292kN}{125mm}}{\frac{29N}{mm^2}} = 0.08mm \sim 0.1mm$$

A round handrail is considered for the support of passengers on the time of accidental evacuation. Figure 89 shows the protytpe of handrail used by Strongwell company.The density of this handrail is 1.7g/cc.

Figure 89 FRP handrail (Strongwell)

5.5 Form III with ERS

Form III consists of an embedded rail system FRP railway bridge. In the preliminary analysis, creep deformations are also taken into account.The preliminary design of design form III is presented below in figure 90.With similar input parameters as done for Form II, FE analysis is performed for calculation of deflection.

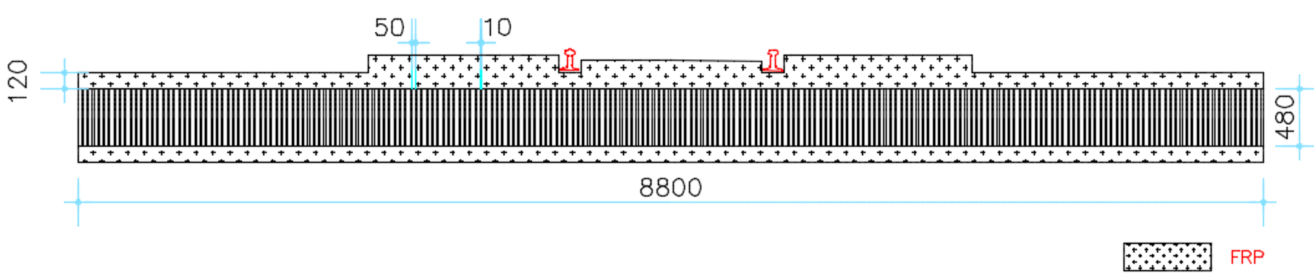

Figure 90 Preliminary Design of Form III

The application and design of non-structural elements are similar as described for Form II in section 5.4.1.1

5.4.2.1 Functional requirements

Most of the functional requirements of this form are same as that of Form II with a slight difference. The only detail that is considered here separately is the webs directly under the rails. To prevent under-cut from the direct application of rail loading from the rail to the FRP face, it is suggested that the rails are supported by steel plate of 140mm length and 10mm thick. the webs directly under the rail would be thickened to 60mm so that the vertical stresses are directly taken by that web and don't spread out. This would prevent the cut on the FRP face due to highly concentrated load. Though there will be stresses due to a temperature difference in the materials, the influence of these stresses has not been studied in the thesis study. Figure 91 shows the detail drawing of the interface of the rail-face and webs.

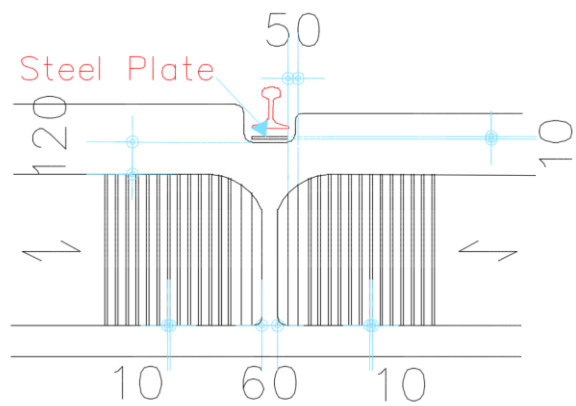

Figure 91 Web details under the rail

6

Static FE Analysis

6.1 Introduction

In this chapter, it is expected to answer the feasibility of FRP bridge section as per ULS limit state requirements of EN1991-2-2003 for railway loadings and see if the expected failure modes are critical for the structural function or not. The finally chosen bridge system Form II with ballast and Form III using embedded rail system are analysed in detail using FEA software ABAQUS. Possible failure modes are determined from FEA and validated against hand calculations. Loads and load combinations considered for analysis are discussed in detail in Appendix C.

It is important to note that Form I is not considered in this study since the emphasis is paid on the feasibility of full FRP material bridge sections and the presence of connections between steel and FRP is detrimental for fatigue and durability of these bridges.

For finite element analysis, it is required to make sure that the model developed is a perfect fit to reality so as to obtain accurate results. There is a number of aspects that influence the FE results. These aspects of the material model, mesh size, element type selected, analysis type chosen etc are discussed in detail to understand the modelling technique adopted. For this, the important input parameters like load models and boundary conditions that define the conditions and the expected results should be known. These models are discussed below in detail to get a clear picture about FE modelling.

6.1.1 Material Model

In order to perform any type of analysis, it is essential to have a material model that governs the behaviour of the stresses and strains obtained in the analysis. For our analysis, the FRP material is modelled as a homogenous elastic material with type engineering constants. Table 18 shows the material properties assigned:

Parameters	
E_1	29016 Nmm^2
E_2	21681 Nmm^2
E_3	21681 Nmm^2
G_{13}	5321 Nmm^2
G_{23}	2352 Nmm^2
Nu_{13}	0.34
Nu_{23}	0.31

Table 17 Material model parameters

Where 1 is the direction of the longitudinal direction of laminate,2 is the direction of the transverse direction of the laminate and 3 is the direction perpendicular to the plane of the laminate.

6.1.2 Mesh size

Mesh size is an important criterion to be selected for finite element analysis. Meshes are required to calculate the results at the nodes created to get accurate results. Fine meshes are better but they are computationally expensive and coarse meshes may not give accurate results. Therefore, a mesh size should be chosen judiciously to account for accurate results but save time as well.

For Form II and IV mesh size of 125 and 150 is chosen respectively as shown in figure 92.

A structured meshing technique is chosen for the mesh which produces a uniform grid. These grid points are distributed uniformly along the structure giving a well graded and uniform constructed grid.

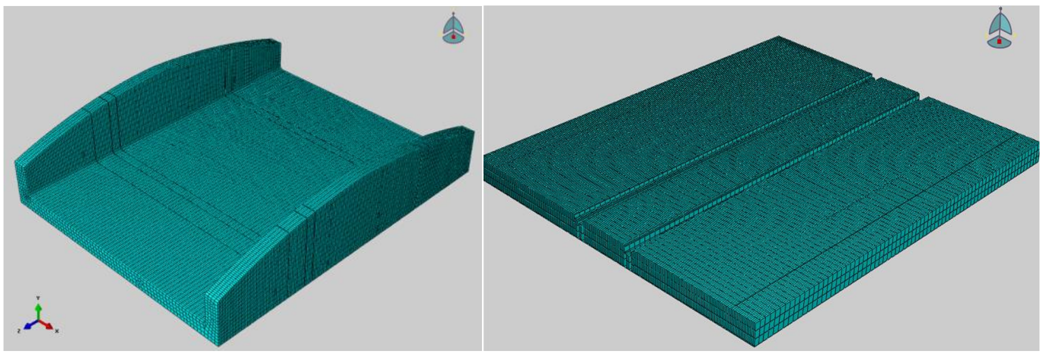

Figure 92 Mesh pattern for FE models

6.1.3 Element type

The selection of element type is an important criterion for an accurate selection of an element type with a degree of freedoms representing the real degree of freedom of the structure should be done. The finite element model consists of an assembly of small elements connected to each other through nodes. Depending upon the geometrical thickness to span ratio of faces of 0.01, the behaviour of the real structure would be represented by shell elements. In this model, S4R shell element is assigned for the whole model. Conventional shell elements are elements that are used to model geometries with the thickness is smaller than the length dimension with displacement and rotational degrees of freedom. S4R is a 4-node general-purpose shell, reduced integration with hourglass control, finite membrane strain. The thickness of this shell element can be defined in the property definition. Since the expected results are related to deflections and stresses at the top, bottom and mid-point of the section, this element would be an easy fit for the analysis of both the forms.

Figure 93 S4R Dof

6.1.4 Load models

After all the model input parameters are assigned, the next step is to define the load models against which the failure models will be evaluated. For this loads calculated in Appendix C are modelled here. The modelling procedure will be discussed here in detail to throw light on the nature of load considered in finite element analysis and their position.

6.1.4.1 Load models for Form II

- LM 71 Load: LM 71 load model is applied on the top face of the horizontal panel. It is assumed that the load is distributed by the rails through the ballast on the top face of the horizontal panel. The length of the surface equals the length of the UDL load of 1.71 m and 2.5 m from both supports. The concentrated load is assumed to be spread on the horizontal panel at an angle of 1:4 from the sleepers in the longitudinal direction and 1:4 from the end of sleepers in the transverse direction. The dimensions of NS90 sleeper are 2520mm*300mm*232.9mm. The depth of the ballast considered is 350mm.Therefore the surface on which the concentrated loads will be distributed is 2695mm in transverse direction $(2520 + (\frac{350}{2}))$ and 475mm $(300 + \left(\frac{350}{2}\right))$in the longitudinal direction. Hence, the concentrated load is applied as a pressure load of 0.19MPa and Both the loads are applied as surface loads of 0.04N/mm^2 and 0.15N/mm^2.The UDL load is distributed along the length of 1.71m and 2.5m from either end. With similar transverse distribution as for concentrated loads, these are modelled as a pressure load of 0.029MPa

Figure 94LM71model for Form II

- Dead Load: To account for long term service life of the FRP bridge, the influence of creep is considered on the FRP bridge material. This influence is considered through a dead load of the bridge structure which is the dead weight of the bridge, rails and functional elements of the bridge. This dead load corresponds to the quasi-permanent load acting on the bridge for the period of 100 years. The load is applied on the whole surface of the horizontal panel as a pressure load of 0.013MPa (105kN/m/8m) (dead weight of bridge/width of bridge). For a detailed calculation of dead load please refer Appendix C, section C.2.1.

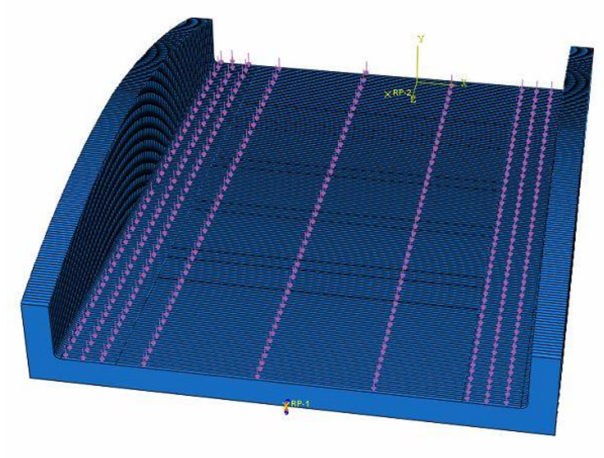

Figure 95 Creep Load for FEM of Form II

- Crushing Load: To check for the local crushing of webs, the most critical load position is assumed when the train just enters the bridge and the first vertical concentrated axle load is distributed to the webs at the ends of the entrance resulting in highest vertical stresses on the webs and supports. Load distribution is same as of LM 71 model, a pressure load of 0.15N/mm^2.

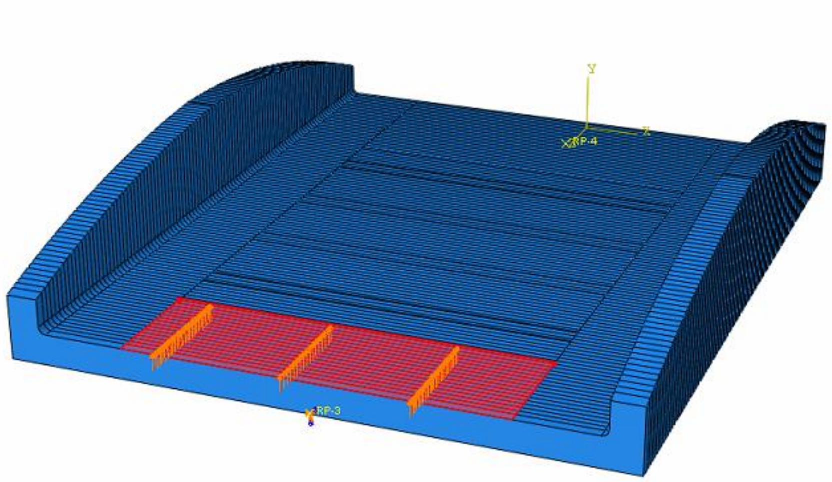

Figure 96 Axle Load model for FEM of Form II

- Accidental Load: A jacking load is introduced at the sides of the railway bridge to lift the train from the track in case of any accidental situation. A load of 500kN is distributed on a jacking plate of (0.7*1.6) m^2(6.7.5, OVS00030-06). This load is modelled as a surface load of 0.44 N/mm^2.

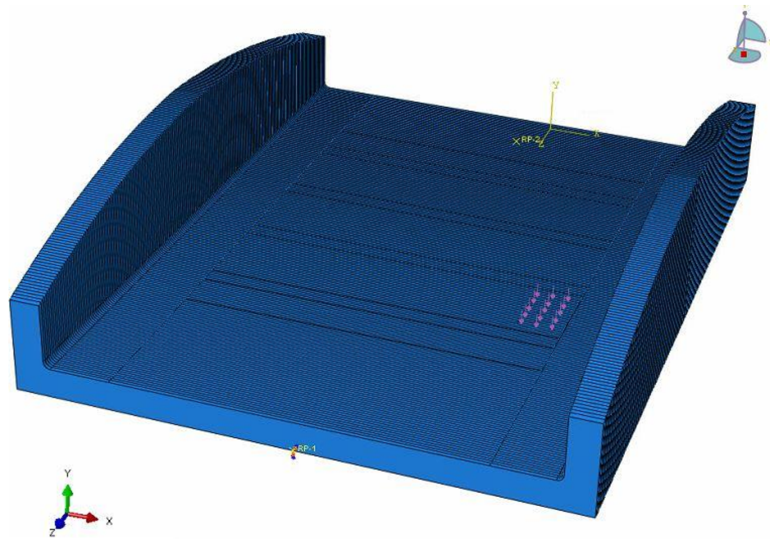

Figure 97 Jacket Load for FEM of Form II

.6.1.4.2 Load Model for Form III

- LM 71 Load: LM 71 load model is applied on the trough of the embedded rail system. It is assumed that the load is distributed by the rails on the bridge. The concentrated load of LM71 is distributed as a pressure load on the surface of (140*320) mm^2 (foot of rail) and the line load is distributed as a pressure load on the surface of bridge distributed on the foot of rail (180mm). The magnitude of the pressure loads modelled is 2.79N/mm^2 and 0.22 N/mm^2 respectively.

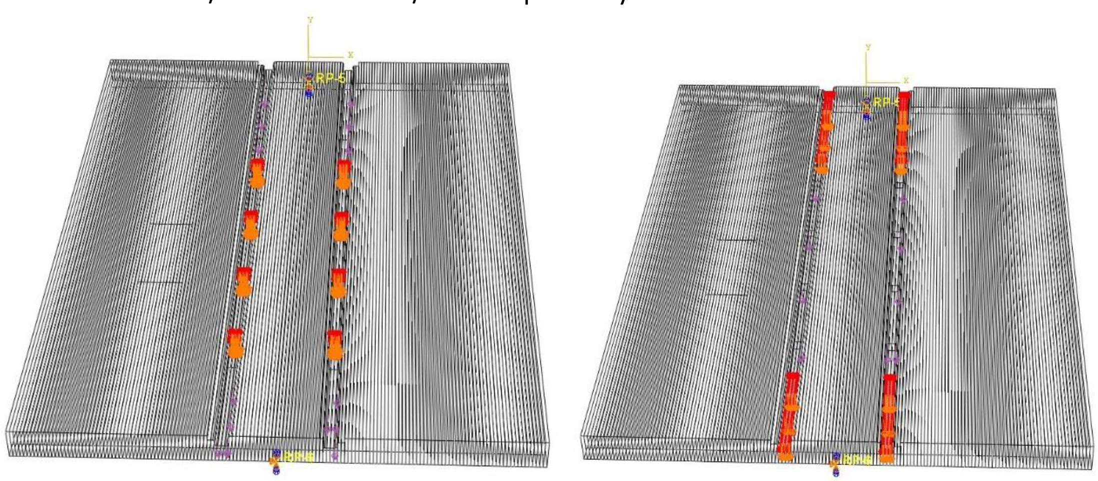

Figure 98 LM71 for FEM of Form III

- Dead Load: To account for long term service life of the FRP bridge, the influence of creep is considered on the FRP bridge material. This influence is considered through a dead load of the bridge structure which is the dead weight of the bridge, rails and functional elements of the bridge. This dead load corresponds to the quasi-permanent load acting on the bridge for the period of 100 years. The load is applied on the whole surface of the horizontal panel as a pressure load of 0.006MPa (total dead load/width of bridge). For a detailed calculation of dead load please refer Appendix C, section C.2.1.

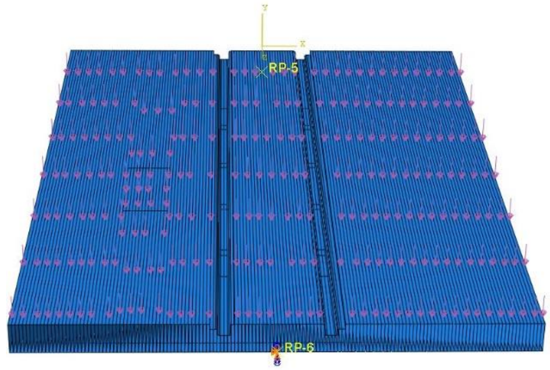

Figure 99 Creep load for FEM of Form III

- Crushing Load: To check for the local crushing of webs, the most critical load position is assumed when the train just enters the bridge and the first vertical concentrated axle load is distributed to the webs at the ends of the entrance resulting in highest vertical stresses on the webs and supports. Load distribution is same as of LM 71 model, a pressure load of 3.85N/mm^2 on a surface of (140*320)mm^2.

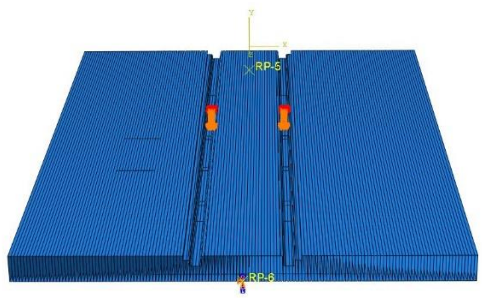

Figure 100 Axle Load for FEM of Form III

- Accidental Jacket Load: A jacking load is introduced at the sides of the railway bridge to lift the train from the track in case of any accidental situation. A load of 500kN is distributed on a jacking plate of (0.7*1.6) m^2 (6.7.5, OVS00030-06). This load is modelled as a surface load of 0.44 N/mm^2.

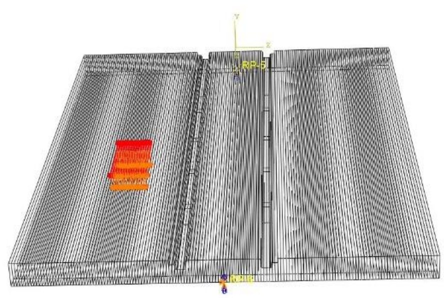

Figure 101 Jacket Load for FEM of Form III

6.1.5 Boundary conditions

When applying boundary conditions to the finite element model, it is necessary to consider that the model simulates the real-world scenario. As mentioned in the problem statement, the feasibility of simply supported bridge is considered. Therefore, simply supported conditions are assumed for the bridge models. The boundary conditions replicate the surface of the bearing in the real world to the FE model. Before applying boundary conditions, the first step to consider is the type of bearing to be selected.

6.1.5.1 Bearing selection

For the selection of bearing, a bearing from Mageba Switzerland company is chosen for analysis. A calculation program is available on their website for preliminary choice of type of bearings. In this study, the choice is made for Type C type of Natural/Chloroprene rubber (NR/CR) in their calculation program. Figure 107 shows the input given for the calculation of width and thickness of the bearing for the maximum vertical force of 1566kN at the supports. The figure below shows the configuration of the Type C rectangular bearing.

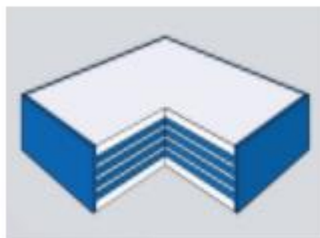

Type C

General Data

Type of bearing:		Type C
Shape of bearing:		Rectangular
Connection of bearing:		Other
Material of bearing:		NR/CR

ULS-Loads:

Maximum vertical force	NSd,max:	3924 [kN]

Figure 102 Input for bearing choice (Source:http://tools.mageba.ch:8011/WebFormElastomerlagerEN1337.aspx)

The resulting width and thickness of the bearing from the calculation suggest a width of 350mm in the longitudinal direction, length of 450mm in transverse direction and thickness of 80mm.

6.1.5.2 Modelling of bearing surface

To simulate this real bearing in ABAQUS, a surface is created for the above dimensions at both ends of the supports. A reference point is created in the middle of the support edges as shown in figure 104. This reference point is given boundary conditions of u1=u2=u3=ur2=ur3=0 to simulate simple support behavior.

Modelling technique:

ABAQUS provides surfaced based coupling restraint between a reference node and a group of nodes called as coupling codes. There are two types of surfaced based coupling restraints: kinematic and distributing constraints. In this thesis, kinematic coupling restraints are used to apply boundary conditions to the model. Such constraints are useful when a group of coupling nodes is constrained to the rigid body motion of a single refence point node. The kinematic coupling constraint prescribes the twisting motion to the model without constraining the radial motion.

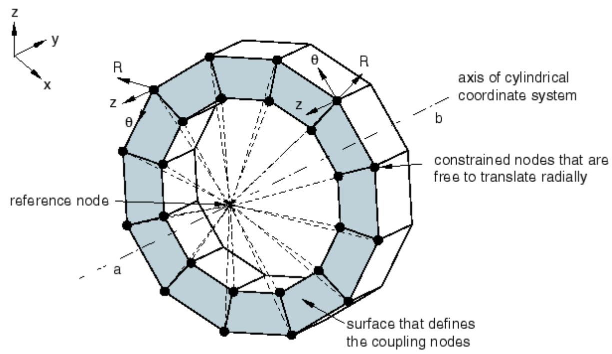

Figure 103 Kinematic Surface Coupling Constraint

In this thesis work, the boundary conditions for both the bridge Forms II and IV are modelled using this concept. In figure 104, the reference nodes (RP1 and RP2) which are defined at the edge of Form II are shown and the bearing surface is constrained using the kinematic coupling constrain. Simply supported environment is achieved by assigning reference points to the nodes at the mid of the edges of supports and coupled with the bearing surface through coupling constraint in ABAQUS. This ensures that the bending of the bearing surface is coupled and uniform with the bridge structure.

Simply supported boundary conditions are modelled on the 250mm wide surface of the bottom face the FRP panel. This surface acts as a surface for the bearing of the bridge on which the bridge rests.

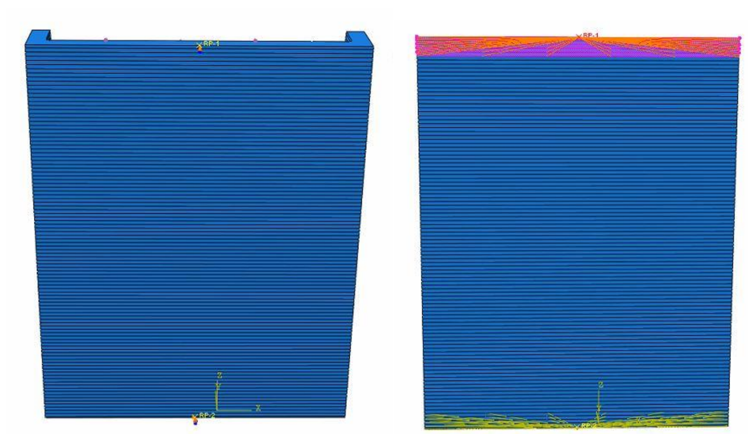

Figure 104 Reference Node and BC for Form II

Similarly, for form III boundary condition are prescribed as shown in figure 105.

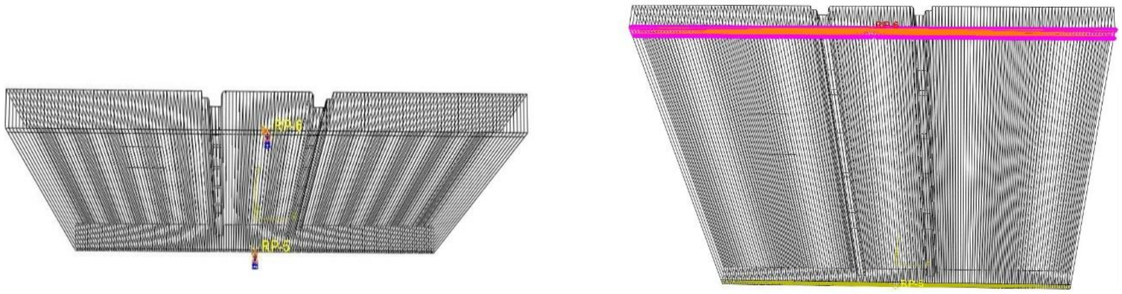

Figure 105 Reference Node and BC for Form III

6.1.6 Type of FE analysis

The type of analysis used for calculating stresses and deflections for the static ULS loading is Static General analysis. For buckling analysis, linear perturbation step is selected.

6.2 Material and Conversion Factors

For the detailed design of FRP structures, conversion factors and material factors are used to calculate the reduced parameters for a design that can be the result of varied fabrication processes method involved. The limit state analysis parameters are derived from JRC,2016 for vacuum infused sandwich panels. For different limit state conditions, different partial safety and conversion factors are considered in JRC 2016 as shown in figure 106 below.

	Aspect being verified						
Influencing factor	Strength (ULS)	Stability (ULS)	Fatigue (ULS)	Creep (SLS)	Momentary deformation (SLS)	Comfort (vibrations) (SLS)	Damage (SLS)
η_{ct}	√	√	√	√	√	√	√
η_{cm}	√	√	√	√	√	√	√
η_{cv}	√	√		√			√
η_{cf}		√		√	√	√	√

Figure 106 Account of conversion factors

6.2.1 Ultimate limit state

Material factors for FRP material:

For the resistance of cross-section,

$\gamma_{m1} = 1.35$ (values of material properties are derived from input parameters available from literature)

$\gamma_{m2,uls} = 1.35$ (for the strength of the cross section)

$\gamma_{m2,loc} = 1.5$ (Stability ULS local)

$\gamma_{m2,global} = 1.35$ (Stability ULS global)

The total partial safety factor:

cross-section resistance in ULS

$$\gamma_{m,uls} = \gamma_{m1} * \gamma_{m2,uls} = 1.82$$

Local Stability:

$$\gamma_{m,loc} = \gamma_{m1} * \gamma_{m2,loc} = 2.03$$

Global Stability:

$$\gamma_{m,glob} = \gamma_{m1} * \gamma_{m2,glob} = 1.82$$

Conversion factors

Thermal influence:

$$\eta_{ct,strength} = 0.9 \text{ (strength of the cross section)}$$

Thermal influence for stability (ULS) and deflection(SLS) depends on the relation between the service temperature and the glass transition temperature (T_g). For this study, it is assumed that the service temperature is above 20 °C and for the Polyester resin T_g = 60 °C, the condition T_g – 40 °C <T_d < T_g – 20°C is satisfied.

$$\eta_{ct,stability} = 0.9$$

Influence of humidity:
The influence of humidity is similar for both strength and stability of cross-section.

$$\eta_{cm} = 0.9 \ (Media\ class\ II\ and\ cured)$$

Influence of creep:
The influence of creep is assessed regarding the duration of the load. This creep factor considered is same for strength and stability ULS. The creep factor for a sandwich panel with GFRP skins and PU rigid foam core, $V_f = 50\%$, is defined by (Ma´rio Garrido, 2013) as:

$$\chi(t) = \frac{1}{(1 + 0.11 * t^{0.25})}$$

where 't' is a time in years. This model can approximately give creep factor for this study model of $V_f = 60\%$ and GFRP faces with rigid foam core.

For t=100 years, this can be calculated as:

$$\eta_{cv,L} = 0.75$$

Influence of fatigue:

The fatigue conversion factor is only considered for stability-ULS. As per JRC,2016, it is

$$\eta_{cf} = 0.9$$

Total conversion factors:

Strength (ULS)
Fatigue is not considered in the calculation of cross section strength. Therefore, the total conversion factors for the strength of the cross section are:

$$\eta_{uls} = \eta_{ct,strength} * \eta_{cm} * \eta_{cv,L} = 0.67$$

Stability (ULS)
The total conversion factor for the stability ULS in the longitudinal direction of the laminate are:

$$\eta_{stab} = \eta_{ct,stab} * \eta_{cm} * \eta_{cv,L} * \eta_{cf} = 0.6$$

6.2.2 Serviceability limit state

The partial safety factors are not taken into account for SLS whereas the conversion factors are considered. The influence of the humidity, thermal and fatigue conversion factors are the same as in the case of stability ULS.

As per EN1990 for frequent load combination which corresponds to short term deflections, the influence of creep is not considered. Therefore, the total conversion factor for short-term SLS verification is:

$$\eta_{ser,short} = \eta_{ct,stab} * \eta_{cm} * \eta_{cf} = 0.73$$

Long term conditions correspond to the quasi-permanent load combination. The influence of creep is considered for the design life of the FRP bridge, which is 100 years. This factor is same for the ULS situation. The total conversion factor for long term SLS-verification is:

$$\eta_{ser,long} = \eta_{ct,stab} * \eta_{cm} * \eta_{cv,L} * \eta_{cf} = 0.54$$

6.2.3 Influence of Fatigue

The partial safety factors taken into account are similar values as calculated for ULS. The conversion factors considered are due to influence of humidity and temperature conditions only calculated in the ULS section. The total conversion factor for FLS verification is:

$$\eta_{fat} = \eta_{ct,strength} * \eta_{cm} = 0.81$$

6.3 ULS analysis and check for failure modes

In this section, verification about the ultimate limit loads of EN1991-2-2003 for possible failure modes of the FRP bridge sections per JRC,2016 will be made.

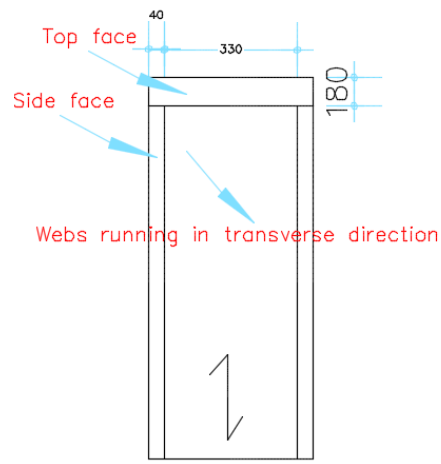

6.3.1 Form II limit state analysis

This section of study will deal with limit state analysis of Form II bridge regarding strength, stability and deflections.

6.3.1.1 Cross-section dimensions and geometrical properties

The span of bridge:
$L_b = 10625mm$

The width of Bridge:
$B_P = 8000mm$

Thickness of top face from vertical panel: (Figure 107)

$t_{face,v} = 180mm$

The thickness of side face from the vertical panel:
$t_{face,s} = 40mm$

Thickness of face from horizontal panel: (Figure 108)
$t_{face,h} = 60mm$

The depth of web from the horizontal panel:

$h_{core,h} = 450mm$

The depth of web from the horizontal panel:

$h_{core,v} = 330mm$

Height of vertical panel at mid-span:

Figure 107 Vertical Panel details (Form II)

$h_v = 1200mm$

The thickness of webs in both horizontal and vertical panel:

$t_{core} = 10mm$

The spacing between webs in both horizontal and vertical panel:

$s_w = 100mm$

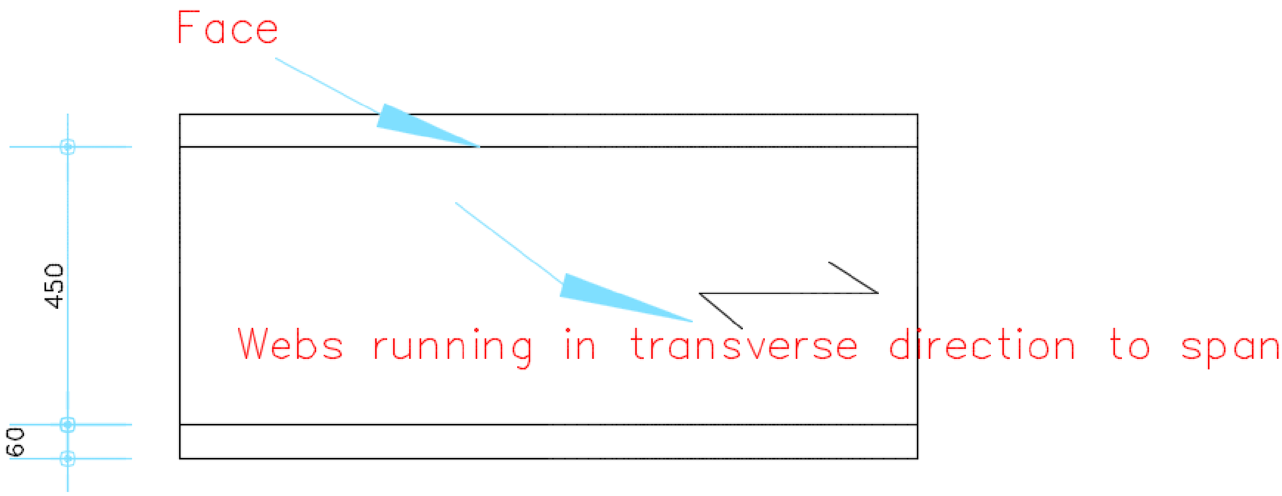

Figure 108 Horizontal Panel details (Form II)

The fibers in the webs of both the horizontal and vertical panels orient towards the transverse direction of the bridge. Hence, the young's modulus of webs in the longitudinal direction is 22GPa.

Area of the cross-section:

Area of faces of horizontal and vertical panel obtained from Autocad (Figure 109):

$$Area\ of\ faces = 1.39m^2$$

Area of webs in the horizontal panel:

$$A_{webs,h} = h_{core,h} * t_{core} * \frac{B_P}{s_w} = 0.36m^2$$

Area of webs in the vertical panel:

$$A_{webs,v} = h_{core,v} * t_{core} * \frac{h_v}{s_w} * 2 = 0.07m^2$$

The total area of the cross-section:

$$Area_{FORMII} = Area\ of\ faces + A_{webs,h} + A_{webs,v} = 1.82m^2$$

Moment of inertia from Autocad (Figure 109):
(Considering the bending is restrained by the faces of the FRP panels only at the mid-span)

$$I_{FORMII} = 0.5m^4$$

The weight of Form II bridge:

Weight

$$Weight_{FormII} = Area_{FORMII} * \rho_{ply} = 3.69\frac{ton}{m}$$

```
Command: _QSAVE
Command: MASSPROP

Window Lasso - Press Spacebar to cycle options2 found

Select objects:
 ----------------   REGIONS   ----------------

Area:                     1397473.5961
Perimeter:                48115.7865
Bounding box:          X: -43988.8121  --  -35162.0252
                       Y: -18832.6050  --  -16841.9645
Centroid:              X: -39578.6834
                       Y: -18247.0002
Moments of inertia:    X: 4.6580E+14
                       Y: 2202031977421608
Product of inertia:   XY: -1.0092E+15
Radii of gyration:     X: 18256.9260
                       Y: 39695.3838
Principal moments and X-Y directions about centroid:
                       I: 5.0628E+11 along [1.0000 -0.0023]
                       J: 1.2929E+13 along [0.0023 1.0000]
```

Figure 109 Cross-section properties from Autocad

6.3.1.2 Serviceability limit state verification (Deflections)

For the verification of serviceability limit state of the bridge, only the check for deflections is considered in this study for Form II. This is done to ensure that they are within the limiting value of L/800.The deflections considered here are short term deflection due to LM71 and long-term deflections due to quasi-static dead loads of structure. Only SLS verification is performed for this form

(a) Short Term Deflections

The deflection of a FRP bridge comprises of bending and shear deformations. For short term deflections, deflection due to LM71 load is considered.

<u>Bending Deformations</u>

<u>Deformation in longitudinal direction:</u>

The bending deformations for a beam with E=29GPa and I= 0.5m^4 are calculated using matrixframe software package. Similar loads and load positions are given as input as of section.

The resulting bending deformations from the LM71 is:

$$\delta_{b,L} = 1.4mm$$

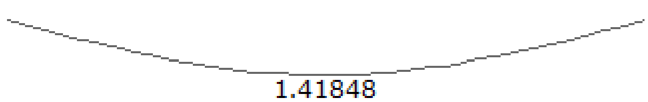

Figure 110 Bending deformation from LM71

<u>Deformation in transverse direction:</u>

For the calculation of transverse deformations, it is assumed that the concentrated load of 250kN is supported by horizontal panels for the length of 1600mm (distance between the axle loads) at the mid-span.

Transverse span:

$$L_t = 8m$$

The inertia of faces of horizontal panel resisting deformation:

$$I_t = 2 * t_{face,h} * 1600mm * \frac{(t_{core,h} + t_{face,h})^2}{4} = 0.012m^4$$

For the transverse span of the bridge and E=29GPa, I=0.012m⁴, a calculation is made in the matrixframe software where the load of 250kN at mid-span is subjected to a beam of length equal to the transverse span of the bridge.The axle load is modelled as a uniformly distributed load spread over the length of 2520mm, which is the length of the sleepers. The resulting UDL load would be 99.2 kNm

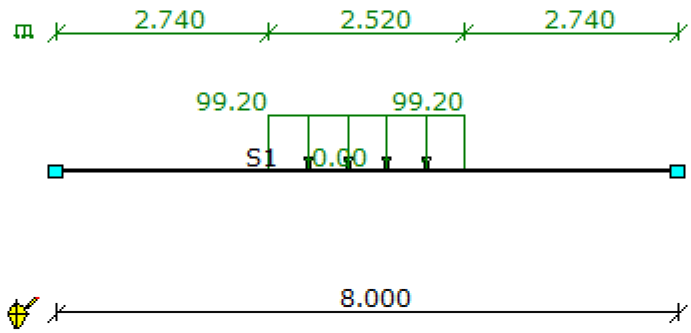

Figure 111 Load model for transverse deflections

The resulting transverse deformations obtained from the above calculation are shown in figure112 below:

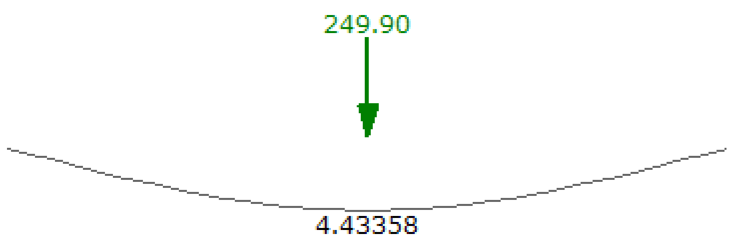

Figure 112 transverse deflection

$$\delta_{b,T} = 4.43mm$$

<u>Shear Deformations</u>

Due to Concentrated Load:

$$\delta_{s1}(a,b) = \frac{P * a * b}{5 * L_s}$$

Due to Uniformly Distributed Load:

$$\delta_{s2}(a,b) = w * a * \frac{(L_s + b)}{2}$$

Where a and b are distances from either end of the supports to the position of the loads acting on the bridge.

For P=250kN and w=80kN/m at at a distance of 2.2m,3.8m,5.4m and 7m from one end of the support

$$\delta_s = \frac{\delta_{s2}(2.2,8.4) + \delta_{s1}(3.8,6.8) + \delta_{s1}(5.4,5.2) + \delta_{s1}(7,3.6) + 2 * \delta_{s2}(2.5,8.1)}{G_{xy} * A * k_{tim}} = 0.4mm$$

For rectangular sections,

$$k_{tim} = 0.83$$

<u>Total short-term deflections</u>

$$\delta_t = \left(\delta_{b,L} + \delta_{b,T} + \delta_s\right) * \alpha * \frac{\varphi}{\eta_{ser,short}} = 13.23\ mm < \frac{L}{800}$$

(b) Long Term Deflections

Long term deflections generally comprise of creep deflections due to dead load on the structure. The dead load acting on the bridge is:

$$W_{dead} = \frac{105kN}{m}$$

This load is modelled on a a beam of 10.625m E=29GPa, I=0.019m^4, a calculation is made in the matrixframe software as shown in figure 113.

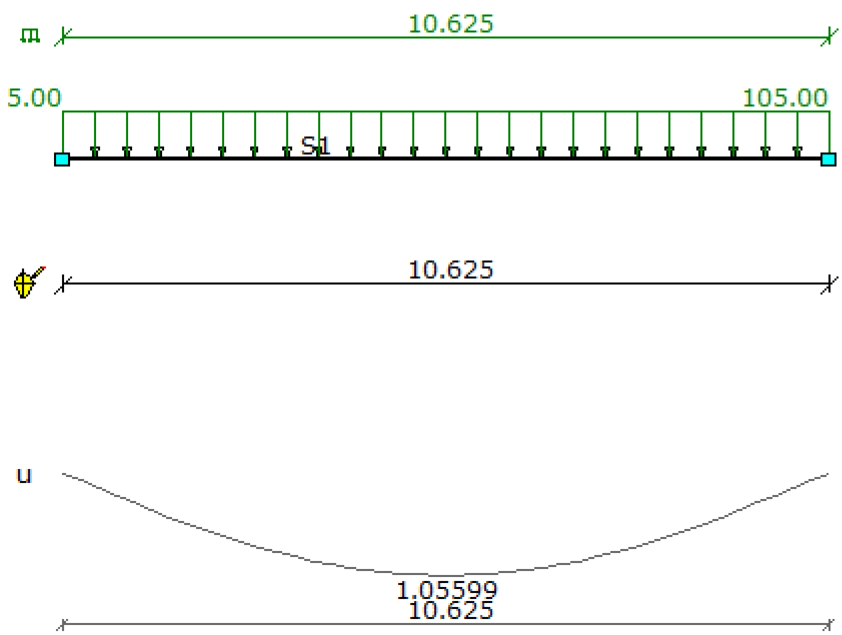

Figure 113 long term deflections calculation

$$\delta_{creep,b} = 1.05mm$$

Deflection Due to Shear:

$$\delta_{creep,s} = \frac{W_{dead} * L_s^2}{8 * G_{xy} * k_{tim} * A} = 0.18mm$$

<u>Total long-term deflections:</u>

$$\delta_{creep,net} = \frac{\delta_{creep,b} + \delta_{creep,s}}{\eta_{ser,long}} = 2.3mm$$

These long-term deflections can be restrained by providing a camber to the bridge structure.

Comparison with FEA

Figure 114 shows the resulting short-term deflections obtained from LM71 and figure 115 shows the resulting long-term deflections due to dead load of the bridge structure.

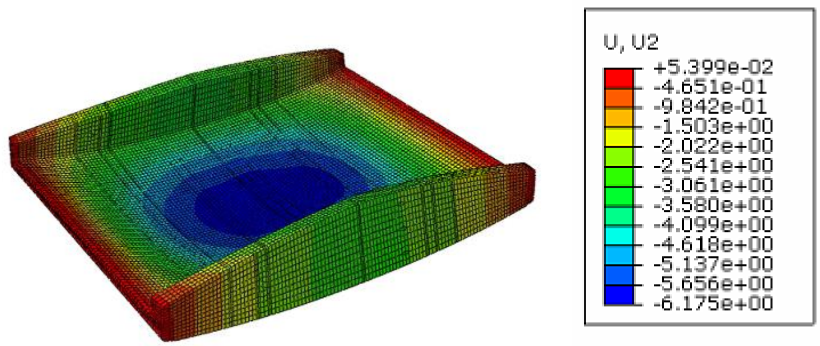

Figure 114 Short term deflection (Form II)

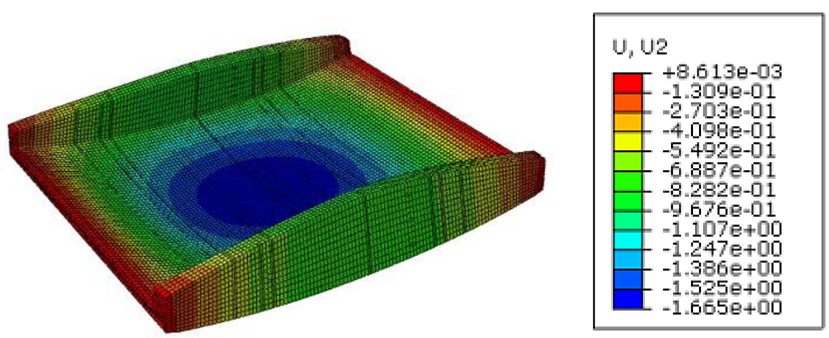

Figure 115 Long term deflection (Form II)

Maximum deflections at the center

$$\delta_{short,max,fea} = 6.175\ mm$$

Total short- term deflections:

$$\delta_{short,total,FEA} = \delta_{short} * \alpha * \frac{\varphi}{\eta_{ser,short}} = 13.2mm < 13.28mm\ (\frac{L}{800})$$

Total long-term deflections:

Long- term deflection at the mid-span around the edge, where transverse deflections are zero:

$$\delta_{long,total,FEA,edge} = \frac{1.1}{\eta_{ser,long}} = 2.2\ mm$$

Maximum long-term deflections in the mid-span of the bridge:

$$\delta_{long,total,FEA,max} = \frac{1.6}{\eta_{ser,long}} = 3.2\ mm$$

$$\eta_{ser,s} = 0.73,\ \eta_{ser,l} = 0.53, \alpha = 1.21\ \&\ \varphi = 1.29$$

Therefore, serviceability criterion is fulfilled.

6.3.2 Form III limit state analysis

This section of study will deal with limit state analysis of Form III bridge regarding strength, stability and deflections.

Cross-section properties and geometrical dimensions

The span of bridge:

$$L_b = 10.625m$$

The width of Bridge:

$$B_P = 8.8m$$

Area of bridge cross-section:

$$t_{face} = 120mm$$

$$t_{core} = 480mm$$

$$t_{web} = 10mm$$

$$s_{web} = 50mm$$

Number of webs:

$$N_{web} = \frac{B_P}{s_{web}} = 176$$

$$Area_{formIV} = \left(t_{face} * B_P * 2\right) + \left(t_{web} * 146 * t_{core}\right) = 2.81m^2$$

$$y_{cg} = \frac{2 * t_{face} + t_{core}}{2} = 360mm\ from\ bottom\ of\ the\ panel$$

$$EI_{yy} = E_f * B_P * \frac{t_{face}^3}{6} + E_f * B_P * \frac{t_{core}^3}{12} + E_f * B_P * t_{face} * \frac{\left(2 * t_{face} + t_{core}\right)^2}{2} = 8.26 * 10^{15} N * mm^2$$

$$I_{yy} = \frac{EI_{yy}}{E_f} = 0.285m^4$$

The weight of Form III bridge:

$$W_{FormIII} = Area_{formIV} * \rho_{ply} = 5.681\ ton/m$$

6.3.2.1 Serviceability limit state verification

In this section, verification for deflections of the bridge will be made to ensure that they are within the limiting value of L/800.The deflections considered here are short term deflection due to LM71 and long-term deflections due to quasi-static dead loads of structure.

(a) Short Term Deflections

As explained earlier for Form II, the same procedure is followed in this section.

The resulting bending deformations from the LM71 calculated from matrixframe software package are shown in figure 116.

$$\delta_b = 2.5mm$$

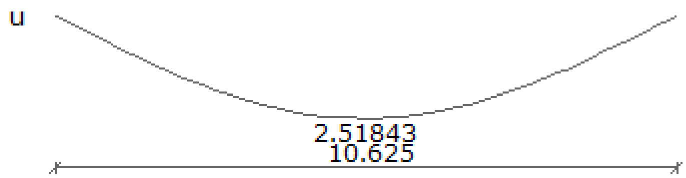

Figure 116 LM71 deflections for Form III

The resulting shear deformation from LM71

$$\delta_s = 0.2mm$$

<u>Total short-term deflections</u>

$$\delta_t = (\delta_b + \delta_s) * \alpha * \frac{\varphi}{\eta_{ser,short}} = 5.7\ mm$$

(b) Long Term Deflections

Long term deflections generally comprise of creep deflections due to dead load on the structure. The dead load acting on the bridge is:

$$W_{dead} = 57.6\frac{kN}{m}$$

This load is modelled on a a beam of 10.625m E=29GPa, I=0.285m^4, a calculation is made in the matrixframe software as shown in figure 117.

Deflection Due to Bending:

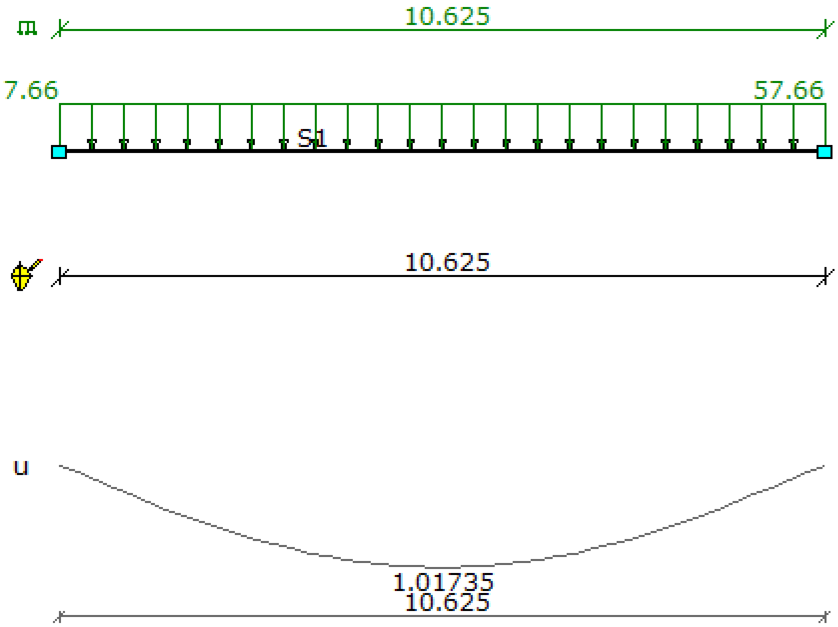

Figure 117 Deflections due to long term loads

$$\delta_{creep,b} = 1.01mm$$

Deflection Due to Shear:

$$\delta_{creep,s} = \frac{W_{dead} * L_s^2}{8 * G_{xy} * A * k_{tim}} = 0.06mm$$
$$k_{tim} = 0.83$$

<u>Total long-term deflections:</u>

$$\delta_{creep,net} = \frac{\delta_{creep,b} + \delta_{creep,s}}{\eta_{ser,long}} = 2.14mm$$

<u>Comparison with FEA</u>

Figure 118 shows the resulting short-term deflections obtained from LM71 and figure 119 shows the resulting long-term deflections due to dead load of the bridge structure.

Therefore, serviceability criterion is fulfilled.

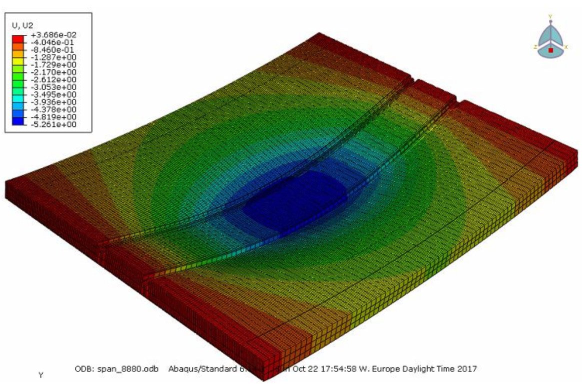

Figure 118 Short Term Deflection

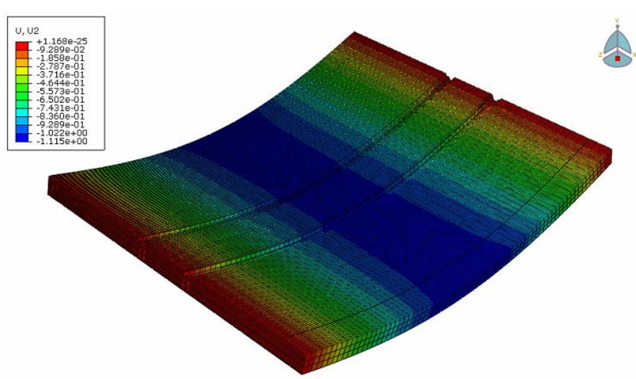

Figure 119 Long Term Deflection

Deflections at the edge:

$$\delta_{short,edge,fem} = 2.6 * \alpha * \frac{\varphi}{\eta_{ser,short}} = 5.6\ mm$$

$$\delta_{long,edge,fem} = \frac{1.1}{\eta_{ser,long}} = 2.15mm$$

This implies that the results obtained from hand calculations and FE calculations at the edge are roughly same.

Maximum deflections at the center

$$\delta_{short} = 5.26mm$$

$$\delta_{long} = 1.15mm$$

Total FEM short term deflections:

$$\delta_{short,FEM,max} = \delta_{short} * \alpha * \frac{\varphi}{\eta_{ser,s}} = 10\ mm < 13.28mm\ (\frac{L}{800})$$

Total FEM long term deflections:

$$\delta_{long,FEM,max} = \frac{\delta_{long}}{\eta_{ser,l}} = 2.3mm$$

Where

$$\eta_{ser,s} = 0.73,\ \eta_{ser,l} = 0.53, \alpha = 1.21\ \&\ \varphi = 1.29$$

Table 18 summarizes the short term and long- term deflections calculated after using appropriate conversion factors from JRC 2016.

Short Term Deflection	10mm
Long Term Deflection	2.3mm

Table 18 Total Deflection for Form III

From table 18, it can be observed that the values of total deflections for the preliminary design of the bridge are under the limit of L/800 as required.

6.3.2.2 Verification of ultimate limit state

(a)Facing Failure of the face

1.Top Face of horizontal panel

When the FRP panel is subjected to LM71 load, it is subjected to bending in the longitudinal direction. Due to this bending, stresses will develop on the faces. Faces of the FRP panel can be subjected to failure due to these bending stresses. The top face is subjected to compressive bending stresses.

Design bending moment:
Bending moment acting on a single HE650B girder of old steel bridge comprising of 4 such girders as calculated in section 1.5.2.2:

$$M_{ed,beam} = 1187.78\ kNm$$

Bending moment acting on the whole bridge:

$$\begin{aligned} M_{sd} &= 4 * M_{ed,beam} \\ &= 4751.12\ kNm \end{aligned}$$

Calculation of maximum compressive bending stresses at mid-span of the longitudinal edge of the bridge:

$$\sigma_{f,t} = \left(\frac{M_{sd}}{I_{yy}}\right) * \left(y_{cg} - \frac{t_{face}}{2}\right) = 5.1\frac{N}{mm^2}$$

The compressive strength of the laminate:

$$f_{f,rd,top} = \sigma_1 * \frac{\eta_{uls}}{\gamma_{m,uls}} = 95.55\frac{N}{mm^2}$$

Unity check:

$$UC_{top} = \frac{\sigma_{f,t}}{f_{f,rd,top}} = 0.05$$

Comparison with FEA

The results from the finite element analysis for compressive stresses at mid-span of the longitudinal edge of the bridge is shown in figure 120.

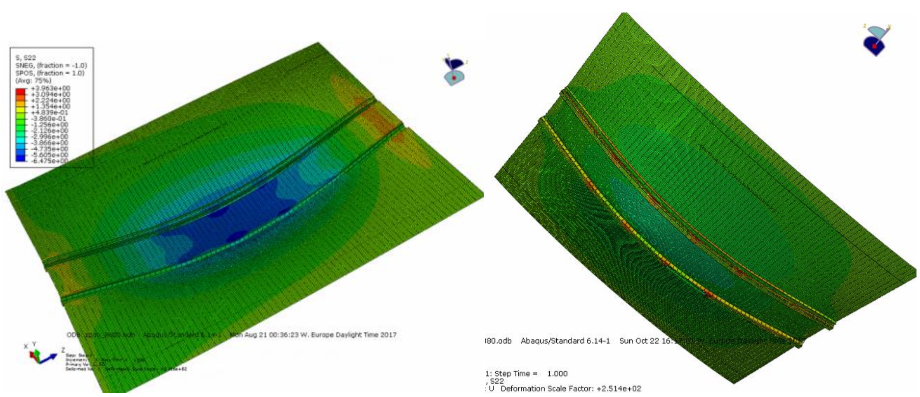

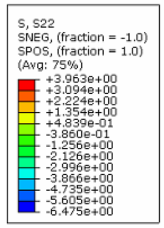

Figure 120 Bending stresses on top face of Form III

Check for FEA stresses at mid of longitudinal edge

$$\sigma_{ft,fem,edge} = 2.12 * \alpha * \varphi * \gamma_{Q1}$$

$$= 4.96\ MPa$$

Unity check for FEA stress:

$$UC_{top,fem,edge} = \frac{\sigma_{ft,fem,edge}}{f_{f,rd,top}} = 0.05$$

It can be observed that the maximum compressive stress is at position x=5.4m around mid-span, which is obvious since the bending moment is maximum at this position. The magnitude of compressive section stresses at the mid-distance of shell face is obtained and check for facing failure shows that it is safe from facing failure. The results obtained from hand calculations and FE analysis show a good match between them.

Check for maximum stress at x=5.4m

$$\sigma_{ft,fem,max} = 6.475 * \alpha * \varphi * \gamma_{Q1} = 15.16MPa$$

Unity check for maximum compressive bending stresses at x=5.4m:

$$UC_{top,fem,max} = \frac{\sigma_{ft,fem,max}}{f_{f,rd,top}} = 0.15$$

2.Bottom Face of horizontal panel

As described in the above section, similarly tensile bending stresses are developed due to longitudinal bending. The bottom face is subjected to tensile stresses since the curvature of this face is larger than the top face. Calculation of maximum tensile stresses at mid-span along the longitudinal edge of the bridge:

$$\sigma_{fb} = \left(\frac{M_{sd}}{I_{yy}}\right) * \left(y_{cg} - \frac{t_{face}}{2}\right) = 5.1\,\frac{N}{mm^2}$$

The tensile strength of the laminate:

$$f_{f,rd,bottom} = \sigma_1 * \frac{\eta_{uls}}{\gamma_{m,uls}} = 95.55\,\frac{N}{mm^2}$$

Unity check:

$$UC_{bottom} = \frac{\sigma_{f,t}}{f_{f,rd,bottom}} = 0.05$$

The results from the finite element analysis for tensile stresses at mid-span of the longitudinal edge of the bridge is shown in figure 121.

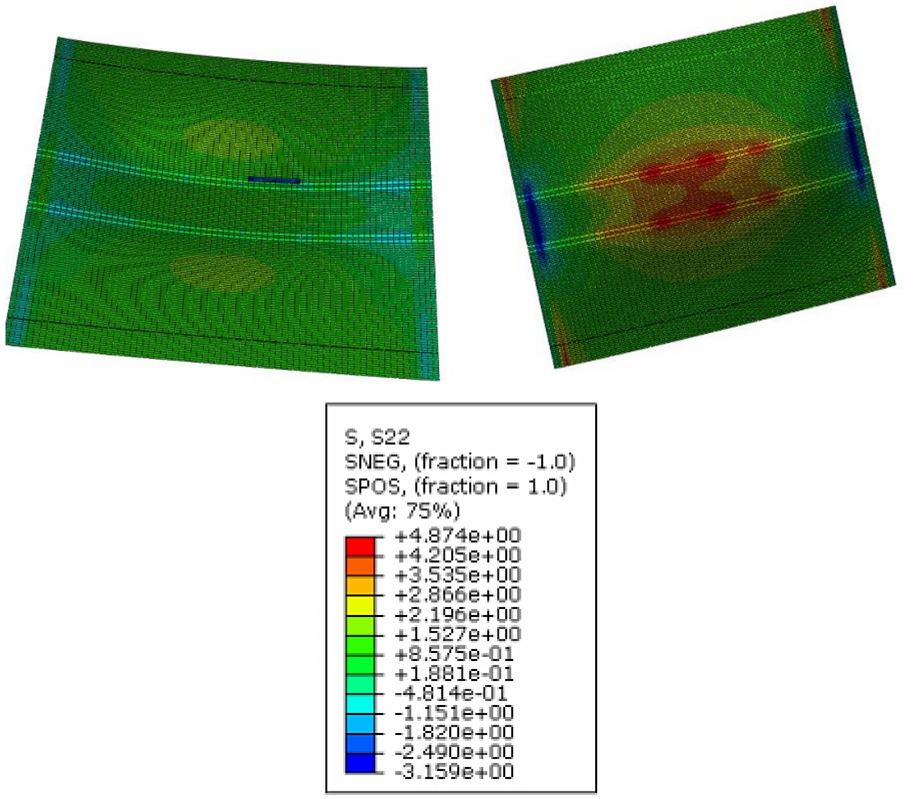

Figure 121 Bending stresses on bottom face of horizontal panel

Check for stresses at mid of longitudinal edge

$$\sigma_{fb,fem,edge} = 2.196 * \alpha * \varphi * \gamma_{Q1}$$

$$= 5.14MPa$$

Unity check for FEA stresses:

$$UC_{bottom,fem,edge} = \frac{\sigma_{ft,fem,edge}}{f_{f,rd,bottom}} = 0.05$$

It can be observed that the maximum tensile stresses are at position x=5.4m around mid-span, which is obvious since the bending moment is maximum at this position. Average of tensile section stresses at the bottom and top layer of shell face is obtained and check for facing failure is made. From the check, it can be inferred that the facing failure due to tensile stresses is not an issue here.

Check for maximum tensile bending stress at x=5.4m

$$\sigma_{fb,fem,max} = 4.87 * \alpha * \varphi * \gamma_{Q1} = 11.40MPa$$

Unity check for maximum compressive stresses at x=5.4m:

$$UC_{bottom,fem,max} = \frac{\sigma_{fb,fem,max}}{f_{f,rd,bottom}} = 0.12$$

(b) Transverse Shear Failure:

Transverse shear failure is an important shear failure assuming that the shear stresses are taken by the webs only.This failure can be critical due to the low shear strength of webs or insuffcent web thickness. The thickness of webs in this model is 10mm in the horizontal panel.These structural elements are subjected to shear stresses and a check should be made for their strength.As it is expected, the shear stresses would be maximum at the supports when bending takes place in the longitudinal direction. Similar behaviour is observed for this bridge, where the webs of the horizontal panel experience maximum shear stress at the extreme edge of the supports.

Calculation for maximum shear stress acting transversely on the webs at the support region:

Design shear forces:

The shear forces acting on the bridge due to the LM71 load model with positions is shown in the figure below

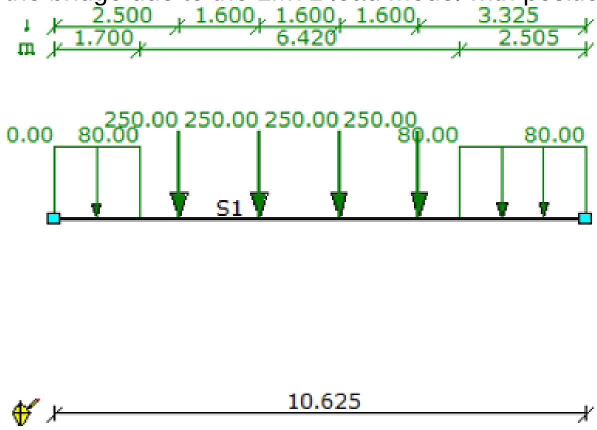

Figure 122 Load positions and magnitude

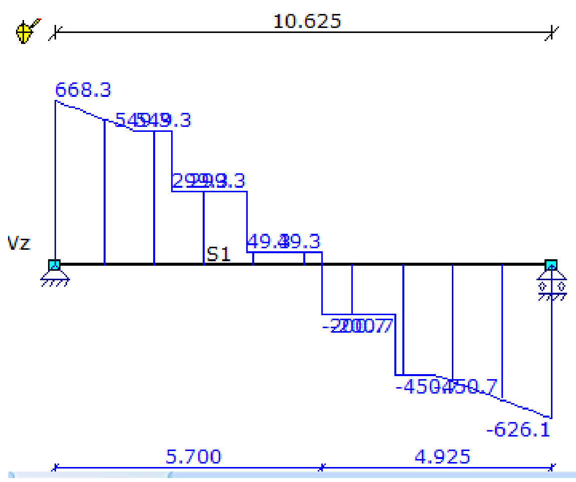

Figure 123 Shear force diagram

$$V_{ed} = 668.3 * \alpha * \varphi * \gamma_{Q,1} = 1564kN$$

Where $\alpha, \varphi, \gamma_{Q,1}$ are the correction, dynamic and partial load factors with magnitude equal to that in section 1.5.2.2.

Shear stress in the webs:

$$\tau_{v,ed} = \frac{V_{ed}}{N_{web} * h_{core} * t_{web}} = 1.9MPa$$

Design shear strength of the webs:

$$f_{c,v,d} = \tau * \frac{\eta_{uls}}{\gamma_{m,uls}} = 31.263 \frac{N}{mm^2}$$

Unity check:

$$UC_v = \frac{\tau_{v,ed}}{f_{c,v,d}} = 0.06$$

From the UC check, it can be observed that the webs at the supports are safe for this failure mode.

Comparison with FEA

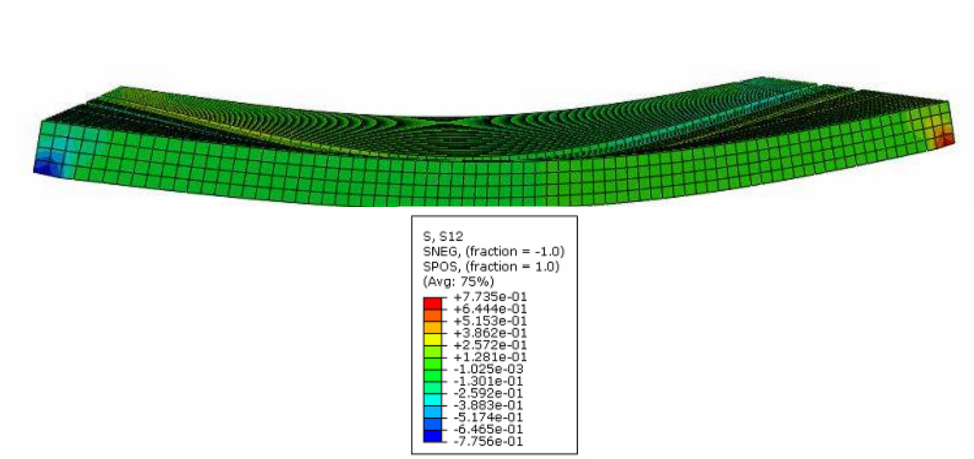

Figure 124 Transverse shear stresses acting on webs

Shear stresses acting transversely to webs from FEA:

$$\sigma_{c,vd,fem} = 0.82 * \alpha * \varphi * \gamma_{Q1} = 1.91MPa$$

Unit check from FEA:

$$UC_{bottom,fem} = \frac{\sigma_{c,vd,fem}}{f_{c,vd}} = 0.06$$

The above checks show that the stresses are within limits.

(c) Local Crushing of Core:

At the position x=2.512m, compressive forces are introduced by the axle load at the onset of the train, which can lead to crushing of webs. These webs support the face and this failure should be avoided. Maximum compressive stresses are encountered in the trough at the position where the axle load is acted.

1.Due to axle load of 250kN distributed by rail (140*320) mm^2 on the horizontal panel:

Design value of compressive stress on the webs:

$$f_{core} = \frac{\frac{250}{2}}{140 * 320} = 2.79MPa$$

Design value of compressive strength:

$$f_{c,c,d} = \sigma_2 * \frac{\eta_{uls}}{\gamma_{m,uls}} = 64.55MPa$$

Unity check:

$$UC_{loc,crush} = \frac{f_{(core)}}{f_{c,c,d}} = 0.04$$

<u>Comparison with FEA</u>:

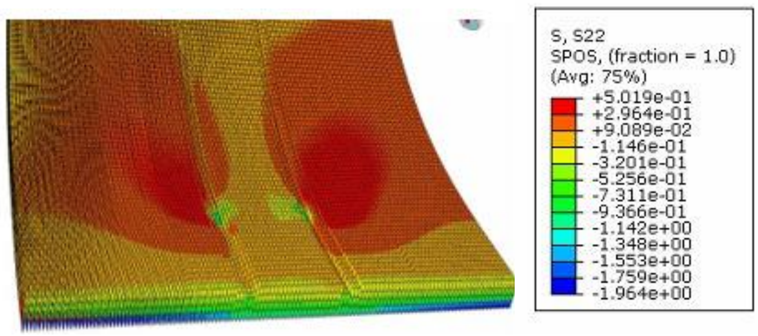

Figure 125 Compressive stresses due to axle load

Maximum compressive stress acting on the webs at the supports:

$$f_{loc,crush,fem} = 1.964MPa$$

Unit check:

$$UC_{loc,crush,fem} = \frac{f_{loc,crush,fem}}{f_{c,d}} = 0.03$$

The discrepancy between the results of the hand calculation and FEA is that the hand calculations are made assuming that the maximum compressive stresses would occur at the point of application of loads but in reality, the maximum stresses occur at one end of the support due to reaction forces.

2.Due to Jacket load:

During accidental situation, jacket loads can be resulted which come from machines that lift the train. These loads which are compressive in nature can be positioned at the sides of the bridge. This results in compressive reaction forces at the support which can lead to crushing of the web. Hence, a check is made which is within the allowable limit.

A jacket load of 500kN is subjected to a plate of 1.6m*0.7m for lifting the derailed train.

Design compressive stress acting on the webs:

$$f_{jacket} = \frac{500 * 10^3}{1600 * 700} = 0.44MPa$$

Unity check:

$$UC_{jacket} = \frac{f_{jacket}}{f_{c,c,d}} = 4.6 * 10^{-3}$$

<u>Comparison with FEA</u>

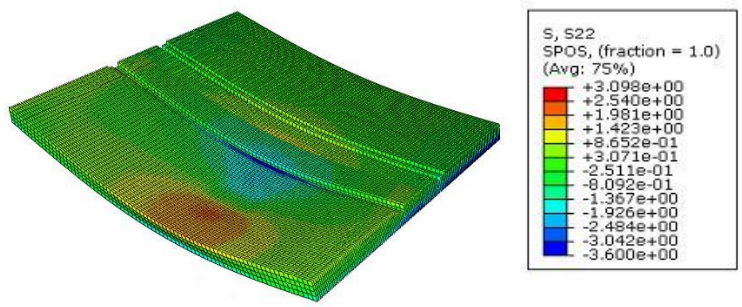

Figure 126 Compressive stresses due to accidental loads

Maximum compressive stress acting on the webs:

$$f_{acc,crush,fem} = 3.6MPa$$

Unity check:

$$UC_{acc,crush,fem} = \frac{f_{acc,crush,fem}}{f_{c,d}} = 0.03$$

(d)Local buckling of webs:

The stiffness of FRP panels is higher in the fiber direction as compared to the other perpendicular directions. When thin webs of 10mm with such property are subjected to vertical force, there is a tendency for them to buckle in weaker axis due to higher slenderness ration. These compressive forces will be maximum at the edges of the supports since the vertical reaction forces will be higher in that region. The phenomenon of secondary bending results in the increase of these vertical reaction forces. This creates a critical location for the webs at the extreme. Therefore, local buckling analysis of these webs is made and it is found that the webs are safe for buckling.

The nominal vertical stresses acting on the webs due to vertical reaction forces as a result of LM71 loads can be obtained from figure 127.

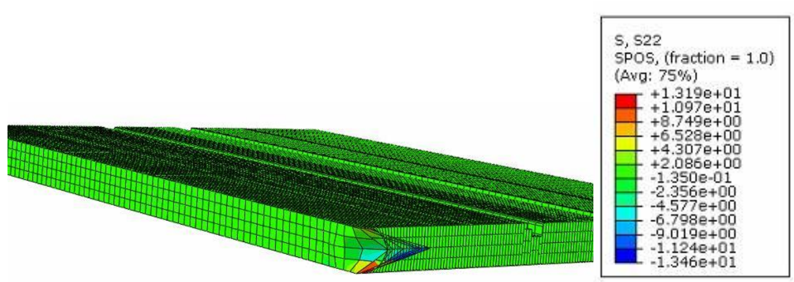

Figure 127 Local buckling compressive stresses on webs

$$\sigma_{v,nom,fea} = 13.46MPa$$

Eigenvalue buckling factor

$$\alpha_{cr,FEA} = 138$$

Critical stress for buckling:

$$\sigma_{buck,fem} = \sigma_{v,nom,fea} * \alpha_{cr,FEA} * \frac{\eta_{stab}}{\gamma_{m,glob}} = 823MPa$$

The critical stress for buckling of webs is too high, as compared to maximum vertical stresses acting on the webs. Therefore, the webs are safe from buckling.

6.4 Comparison between Form II and III

Both the structural design forms meet the deflection criteria prescribed by the Pro Rail guidelines and can be regarded as possible alternatives for the old steel bridge. Another aspect to keep in mind while replacing the old steel railway bridge is low mass and availability of depth section for new bridge structure to fit into the exisiting railway setup.

The depth of Form II bridge can be calculated as:

Total depth = Depth of ballast (325mm) + Depth of ballast mat (25mm) + thickness of faces of horizontal panel (60mm) *2 + depth of webs (450mm) + height of sleepers (233mm) + height of rail (160mm)

=1313mm

The depth of Form III bridge can be calculated as:

Total depth =thickness of faces of horizontal panel (120mm) *2 + depth of webs (480mm) +height of rail (160mm)

=880mm

Table 19 summarizes the depth of the bridge required for attaing flexural rigidity for comparison.

Available Depth for installation	**973mm**
Bridge with ballast (Form II)	1313mm
Bridge with embedded rail (Form III)	880mm

Table 19 Comparison between Form II and Form III

From the above table, it can be concluded that the bride with ballast roughly requires 1.5 times the depth of the bridge with embedded rail system while the weight of bridge with ERS system is 1.5 times the bridge with ballast rail track system. Inorder to meet the criteria of low weight and best fit into existing rail system, Form III is considered as the possible alternative for replacement. The calculation of fatigue resistance of Form III bridge is shown in Annex E. Utilisation of the fatigue resistance of upto 18% over 100 years lifetime is obtained. Therfore, it is concluded that the deflections are the dominating design criterion over strength and fatigue. A revised design of Form III is considered in chapter 7 with the aim to optimize it for this serviceability criteria.

7

Revised Design

This chapter deals with improving the design for the structural form III chosen for the potential replacement of the bridge. From Chapter 6, static calculations and Annex E fatigue analysis, it can be observed that neither ultimate limit state and fatigue limit state is governing for the design of FRP bridges but it is the SLS criterion that governs the design of FRP railway bridge. Therefore, from the results obtained from the static check of Form III of the bridge, some improvements in the design have been proposed which are as follows:

1. The depth of the section: Earlier the depth of the section was 880mm. The available depth for replacement is 973mm. Hence it is proposed that the depth of the section should be increased to 960mm including the thickness of bearings, head of the rail and miscellaneous works. This will enable to reduce the thickness of faces of the horizontal panel to 50mm.The UC ratio for the faces in bending is 0.02, hence increasing the depth and reducing the thickness of faces would not be critical since the earlier UC ratio is too low.
2. The spacing between webs: The UC ratio for the transverse shear stresses acting on the webs is 0.13 with the spacing between the webs of 50mm. It is proposed that the spacing between the webs should be doubled since failure due to shear stresses is not critical and UC ratio is too low for the material.

On the basis of these two observations, the revised design of Form III is shown in figure 128 below.

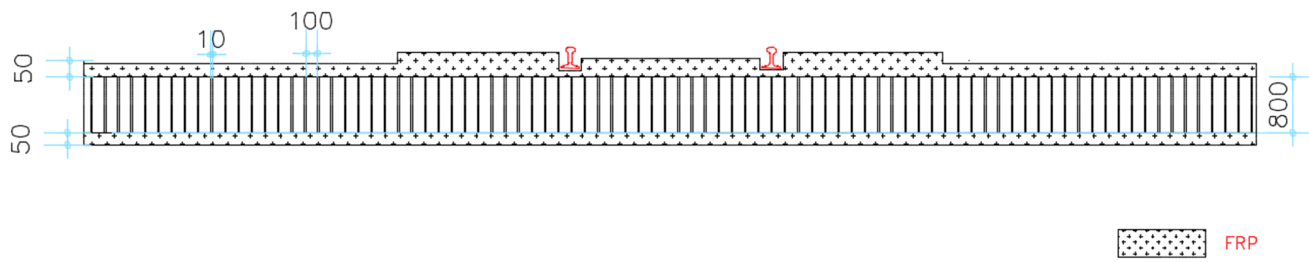

Figure 128 Revised design form III

To check this bridge for serviceability limit state, deflections are calculated for LM71 and dead loads in figure 129 below.

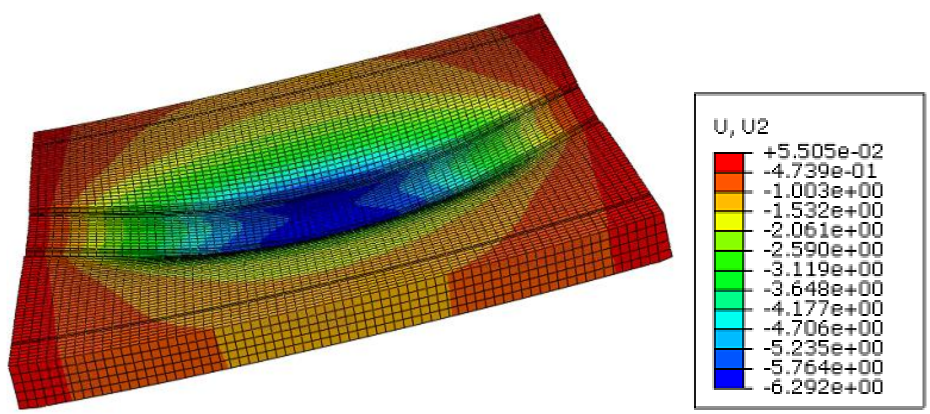

Figure 129 Deflection due to LM71

From the above figures, it can be observed that:

$$\delta_{LM71,max,fea} = 6.2mm$$

Total deflections:

$$\delta_{total} = \delta_{Lm71,amx,fea} * \alpha * \frac{\varphi}{\eta_{ser,short}} = 13.2mm < 13.28mm\ (\frac{L}{800})$$

Hence, it can be observed that the revised bridge structure meets the deflection criterion.

Cross-section Properties

To calculate the weight of this bridge structure, the area of cross-section is calculated.

Thickness of face

$$t_{face} = 50mm$$

Thickness of webs

$$t_{web} = 10mm$$

Spacing between webs

$$S_w = 100mm$$

Depth of webs

$$d_{web} = 800mm$$

Number of webs

$$N_w = 80$$

The width of the bridge:

$$b = 8800\ mm$$

Area of cross-section

$$A = \left(t_{face} * b * 2\right) + (N_w * d_{web} * t_{web})$$

$$= 1520000mm^2$$

Structural Weight of bridge per meter run

$$W_{bridge} = A * \rho_{ply} = 3\frac{ton}{m}$$

The structural weight of this revised Form III bridge is 3 ton/m as compared to the weight of the new steel rail bridge which is 1.23 ton/m. The new steel railway bridge is designed according to EN1991-2-2003 guidelines and its design adopts the OVS recommendations stated in Appendix B for safety and inspection. Hence, it becomes important to compare it with the state of the art steel rail bridges. This implies the weight of the FRP railway bridge is 2.4 times the weight of the new steel railway bridge.

Conclusions

Considering the main research question and sub-research questions posed in Chapter 1, the following conclusions can be made:

- Preliminary Design
  - Form II consisting of ballast should be optimized for increased inertia to maintain restricted depth by varying depth of vertical panels and horizontal panels. With the only increase depth of vertical panels for higher stiffness, these panel become so stiff that they restrain the longitudinal deflection but the transverse deflection which is restrained by the horizontal panel of low depth increases at the same time. An optimization study should be made for this form.
  - The junction between the horizontal and vertical panel for Form II possess high local stresses due to local bending. This can be a key issue for fatigue.
  - The webs running in the transverse direction of the span are the most efficient variants possible for the Form II bridge.
  - Influence of stresses due to the temperature difference between the steel plate and the FRP faces should be considered and a study be made for the durability of the FRP top face in Form III.
  - Serviceability criteria of deflections are dominating the design as compared to other design criteria such as strength and fatigue, which are only 20% utilized.

- Static FE analysis
  - From the static analysis, it can be recommended that the spacing of the webs can be increased by 2-3 times to optimise the material application.
  - The weight of the bridge with ballast is 1.5 times heavier the weight of the ERS, therefore the application of ERS system should be made when compared with ballast rail track system.
  - The weight of the final selected ERS Form III FRP rail bridge is around 2.4 times the weight of new steel bridge. This implies that the chosen ERS form is not the most optimal design solution for the application of FRP in short-span railway bridge. Further optimization is possible by adopting following approaches:
    1. Increasing the depth of the bridge section.
    2. Designing a hybrid bridge where steel/CFRP are combined with GFRP to gain desired flexural stiffness with low weight while the corrosion resistance and fatigue endurance are improved when compared to steel bridges.
    3. By choosing another form like Form II, where transverse deflections would be reduced by making use of space for non-structural parts.

  The Proper combination of the above-mentioned design optimization approaches would most probably lead to the competitive design of short-span FRP against steel bridge.

Main research question:

- The main research question is stated as: "*Is it feasible to replace the existing steel railway bridge such that the existing foundations can be reused?*"

  According to the results obtained from static and fatigue analysis, it can be observed that the feasibility of FRP railway bridge is not an issue. With the proposed design, the weight of the FRP bridge has been found to be 2.7 times the old steel bridge. This would not allow for the re-use of the existing foundations without further optimization of the bridge design.

Further Considerations

From the results obtained in this study, it can be observed that the further optimization of the bridge forms is required to attain increased flexural rigidity and achieve feasible design for short span FRP bridges. Some additional considerations are listed below that are needed to have a complete overview of the possibilities of such design as:

- The non-linear static analysis of the old steel railway bridge should be made to calculate its residual strength.
- A site inspection should be made to check the condition of corrosion of the steel bridge.
- The allowance for passenger and inspection path to be made only on one side and design the bridge for these requirements.
- The bearing is provided throughout the width of the bridge, this will lead to the extension of the masonry foundation. Feasibility of extending masonry foundation should be made as per its exact material properties and the current status of the masonry material.
- Dynamic analysis of the bridge for traffic safety serviceability requirement to ensure further verification for SLS.
- Passenger comfort analysis for the comfort criteria of the FRP railway bridge to ensure feasibility.

Appendices

A

Hand Calculations

A.1 Critical Loading Position

To calculate the maximum bending moment for the rail loadings, the first step is to find the critical load position of the LM71 along the span of the bridge such that it results in the maximum bending moment at the center of the simply supported beam bridge. The influence of UDL load is not considered in the calculation since it would be present at both the ends at equal lengths. This will have a minimum effect on the result.

Consider a simply supported beam of length L loaded with four concentrated loads separated by a_1, a_2 and a_3. R_A and R_B are the reaction forces at the supports and P_R is the resultant force of the four concentrated loads at a distance $\overline{x}$-x from the centerline, where x is the distance between P_3 and the center of the span and $\overline{x}$ =0.8m is the distance between P_3 and P_R. For LM 71 loading, here a_1, a_2 and a_3=1.6m each.

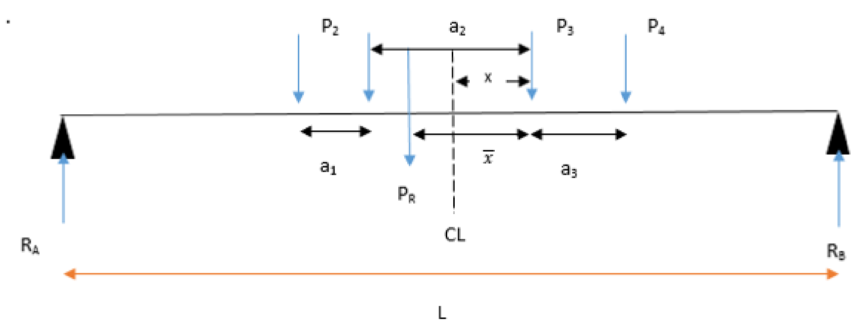

Figure 130 Simply supported beam with LM71 for critical loading position

BM at support A=0

Therefore,

$$R_B = \frac{P_R}{L}\left[\frac{L}{2} - (\overline{x} - x)\right]$$

Considering static equilibrium of the system,

$$R_A + R_B = P_R$$

this implies,

$$R_A = \frac{P_R}{L}\left[\frac{L}{2} + (\overline{x} - x)\right]$$

Bending moment at the center: -

$$M_{CL} = R_A\left(\frac{L}{2} + x\right) - P_1(a_1 + a_2) - P_2 * a_2$$

$$= \frac{P_R}{L}\left[\frac{L}{2} + (\overline{x} - x)\right]\left[\frac{L}{2} + x\right] - P_1(a_1 + a_2) - P_2 * a_2$$

For maximum bending moment,

$$\frac{dM_{CL}}{dx} = 0$$

$$0 = \frac{P_R}{L}\left(\frac{L}{2} + (\overline{x} - x)\right) + \frac{P_R}{L}\left(\frac{L}{2} + x\right)(-1)$$

For L=10.625m

$$x = 0.4m$$

This implies, resultant load P_R should be placed at a distance of $(\overline{x} - x)$=0.4m from the centerline to get the maximum bending moment at the centre.

A.2 Design of structural elements for Pathway

A separate design of structural elements required to support the pathway and cable ducts is made to reduce the width of the steel bridge. Since these elements are not connected to the box-girder section to avoid eccentric moments on the bridge, that is why they are not connected to the box section. A separate load bearing I-beams will be proposed that will carry the secondary beam spanning in the transverse direction to which the walkway paths and cable ducts will be connected. These I- beams will rest on the foundation at the same level as of the box-girder section.

A.2.2.1 Load calculations

To determine the dimension of these I sections, the load has to be calculated. The estimated load is a combination of:

1. Dead weight of passenger path and cable ducts & covers
2. Pedestrian load

The dead weight of non-structural elements for passenger path and cable covers:

Passenger Path:

The passenger path consists of a walking grid supported by thin steel plates of 6mm thick. There are several walking grids in the market. For this bridge, a walking grid from Bailey's company is considered as shown in figure 130 (Source: http://www.baileybridge.com) with weight in figure 131. For 1 meter wide and 1 meter long grating, the approximate weight can be taken as 21.3kg/m^2. Since we have 2 paths each 1m wide for passenger and inspection, the total weight of the gratings would be 21.1*2=42.2 kg/m. For the design of I-beams running in the longitudinal direction of the bridge, this load can be assumed as 42.2*9.81=0.414kN/m running towards the longitudinal direction for a span of 10.625m.

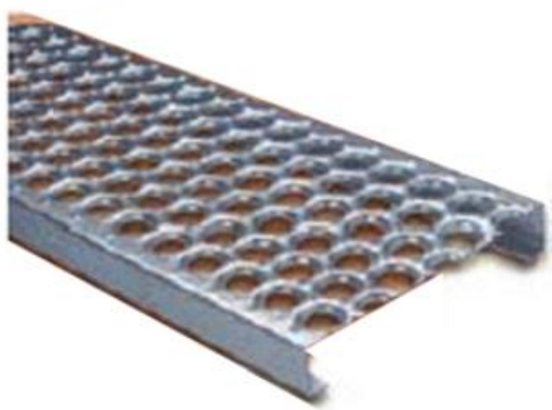

Figure 131 Walkpath grating(Source:http://www.baileybridge.com)

990 x 1000	40/2	H64020991001	21,1
1000 x 1000	40/2	H64021001001	21,3
1010 x 1000	40/2	H64021011001	21,5
1020 x 1000	40/2	H64021021001	21,7

Figure 132 Walkpath weight(Source:http://www.baileybridge.com)

The dead weight of cable ducts and covers:

The weight of the cable ducts including covers can be referred from the ProRail document 43KBK 01 which gives the value of 35kg/m (0.343kN/m).

Hand rail

The FRP handrail is considered from a steelflooring.ie company that deals in FRP materials. This hand rail is shown in figure 133 below. The weight of this handrail is 8.68 kg/m.

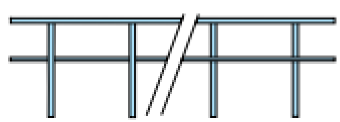

Figure 133 FRP handrail (Source: steelflooring.ie)

Pedestrian Load:

For the pedestrian load, a uniformly distributed load of 5kN/m (spanning longitudinally) or 5kN/m^{2}as per 5.3.2.1(1) EN1991-2-2003 is considered.

Therefore, total bearing load for I-beams (q) = (0.414+0.343+5) = 5.75kN/m

A.3.2.2 Selection of beams

<u>Beam in longitudinal direction:</u>

Maximum bending moment in the longitudinal direction = $1.5 * q * \frac{L_s^2}{8} = 121.85\ kNm$,where 1.5 is the partial safety factor considered.

This would lead to $W_{section,reqd} = 518510.63\ mm^3$

Considering I beams of section HEB220: $W_{section,actual} = 3 * 258.5 * 1000 = 775500 mm^3 > W_{section,reqd}$

<u>Beams in transverse direction:</u>

The secondary beam can be supposed to be resting upon the 3 I- beams as proposed above. Assuming the load from crowd load and passenger gratings to be acting in the transverse direction, the resulting loading in the transverse direction would be, q = (0.414+5)=5.414kN/m

Length of span (L_c) = width/3 =966.67mm

Maximum sagging moment = $1.5 * q * \frac{L_c^2}{8} = 0.95\ kNm$

This leads to $W_{section,required} = 4042.55 mm^3$

Considering IPE beam 180 with $W_{section,actual} = 22200 mm^3$

A beam with much higher requirements is chosen so that it fits in the available depth and within allowable allowances to the HEB220 beams.

B

Geometrical Layout

B.1 Introduction

In this section, the guidelines that influence the geometric layout of the high-speed rail bridge will be discussed. A typical layout of the steel bridge will be used for the design of FRP railway bridge, in which the geometrical clearance to be adopted for safety, track inspection and maintenance, depth of section etc to be included will be mentioned.

B.2 Geometrical Clearances

The following guidelines control the layout of the bridge structure in The Netherlands. The visual of the layout is described in figure 134 of high speed (200km/hr) rail track steel bridge for Embedded rail system and in Figure 135 for Ballast rail track system railway bridges in The Netherlands.

B.2.1 Lateral Clearances

- The lateral clearance from the center of the rail track should be a minimum of 2000mm and maximum of 2150mm according to OVS00030-1 art 4.1.4. See label (2) in figure 134.
- For design speed of 200km/hr, the minimum distance from the center of the track to the center of passenger path should be 2750mm (OVS00030-1 art 3.3.3).
- A passenger path of 1000mm should be provided.
- An additional space of 100mm for hand rail base plate should be provided wherever possible.

B.2.2 Vertical Clearances

- The vertical clearance of the rail head should be a minimum of BS+100mm.
- The vertical clearance of the top of passenger path should be a maximum of BS+400mm and minimum of BS-150mm (OVS00030-1 art 3.3).
- Ballast mat of 20-40mm should be used according to OVS00056-5.1 art. 2.2.6 or a ballast of depth 350mm can be used on the bridge.

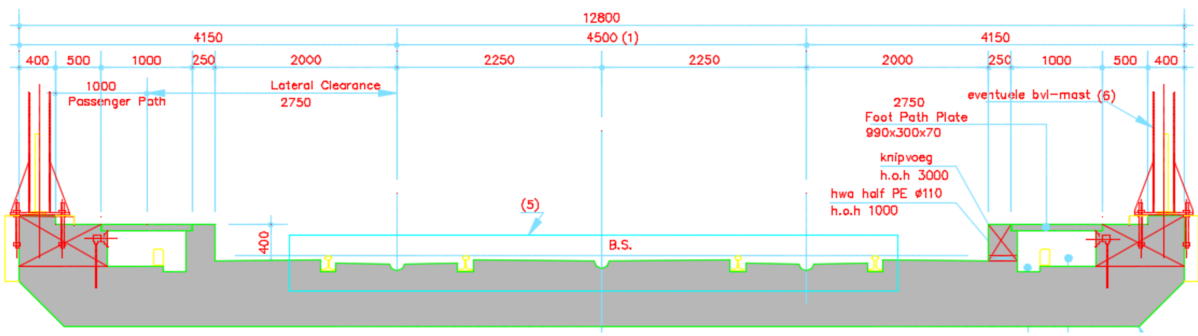

Figure 134 Typical Layout of Embedded Rai Track Bridge System in The Netherlands

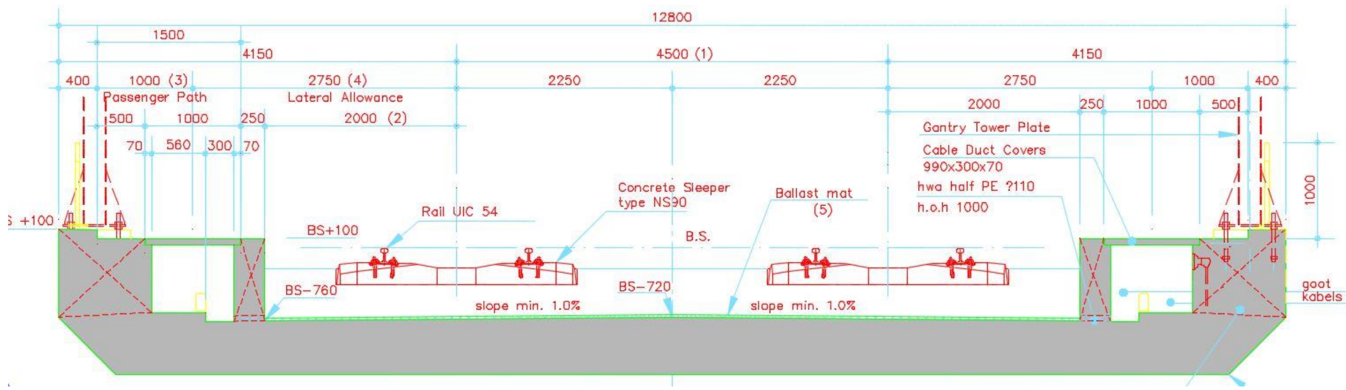

Figure 135Typical Layout for Ballast rail track Bridge system in The Netherlands

C

Loads & Combinations

C.1 Introduction

In this section, the study will consider the type of loads and load combinations that need to be considered for the safe functioning of the bridge superstructure according to NEN EN1991-2, OVS00030-06 (National) and EN1991-2 Eurocodes.

C.2 Loads

C.2.1 Permanent Load

The permanent load consists of the dead weight of the bridge superstructure. This permanent load adds to the creep deflection in the structure.

Dead load:
Structural weight

$$\rho_{FRP} = 2022\frac{kg}{m^3}$$

Structural Weight of Form II Bridge:

$$W_{Form\ II} = 7461.18\frac{kg}{m} * 9.81 = 73.19\ kN/m$$

Structural Weight of Form III bridge:

$$W_{Form\ III} = 5681\frac{kg}{m} * 9.81 = 55.73\ kN/m$$

Non-structural weight:

$$Weight\ of\ FRP\ walkway\ gratings\ 60mm\ thick = 12.69\frac{kg}{m^2} * (1 * 0.06 * 4) = 3\frac{kg}{m}$$

$$Weight\ of\ FRP\ platform = 0.45\frac{kN}{m^2} * (0.125 * 0.4) * 2 = 4.58\ kg/m$$

$$Weight\ of\ FRP\ handrail = (0.87 * 0.025)m^2 * 1.7\frac{g}{cc} = 0.36\frac{kg}{m}$$

$$W_{rail} = 54.77\frac{kg}{m} * 2 = 109.54\frac{kg}{m}$$

$$Total\ non-structural\ weight = 117.48\frac{kg}{m} = \frac{1.15kN}{m}$$

The density of Ballast:

$$\rho_{ballast} = 22\frac{kN}{m^3}$$

The weight of Ballast:
Width of ballast

$$W_{ballast} = 4m$$

$$W_{ballast} = \rho_{ballast} * h_{ballast} * 4m = 30.8\frac{kN}{m}$$

Total Dead Load:
For Variant II

$$W_{dead,II} = (W_{footpath} + W_{footpath,support}) + W_{rail} + W_{FormII} + W_{ballast} = 105\frac{kN}{m}$$

For Variant III

$$W_{dead,III} = (W_{footpath} + W_{footpath,support}) + W_{rail} + W_{Form\,IV} = 57.66\frac{kN}{m}$$

C.2.2 Variable Load

The variable load consists of train axle loads vertical loads, wind load, horizontal loads and aerodynamic actions.

C.2.2.1 Vertical Loads

Vertical Loads comprise of rail axle loads. These loads are defined by load models expressed in EN1991-2. Rail load models represent the static effect of the normal rail traffic conditions by means of concentrated and unfirmly distributed loads. For simply supported and small span bridge LM71 will be used to analyze the static behaviour of the FRP bridge and old steel rail bridge as well. Figure 136 shows the rail load model LM 71 below. This load model is multiplied by a factor to obtain “classified vertical loads” to account for heavier/lighter rail traffic in a specific country. In the Netherlands, according to NEN EN1991-2, this factor is assumed to be 1.21.

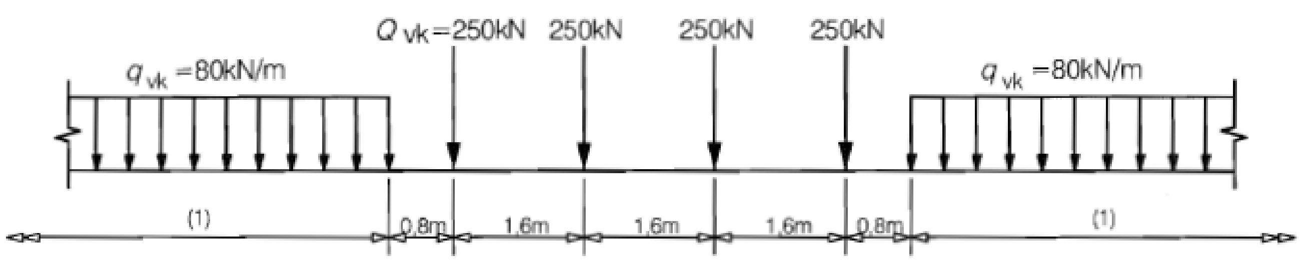

Figure 136 LM71 (EN1991-2-2003)

In addition, this rail load model is further multiplied by partial safety factor Partial safety factor;

$$\gamma_{Q1} = 1.50$$

Eq 11 (Table A1.2(A), EN1990-2002)

C2.2.2 Dynamic Effects

To consider the dynamic effects of moving rail load model, the dynamic factor is introduced to account for increment or decrement in the values of stresses and deflection/acceleration of the bridge. This factor multiplies the static real load model to magnify the static stresses/deflection such that they are equivalent to real dynamic stresses. In this case, this dynamic factor is considered as a function of determinant length and for the carefully maintained track, it can be described as in equation below.

$$Dynamic\ Factor, \varphi_2 = \frac{1.44}{(L_\varphi - 0.2)^{\frac{1}{2}}} + 0.82$$

Eq 12 (6.4) EN1991-2-2003

$$Determinant\ Length, L_\varphi = 10.625m$$

Eq 13 (Table 6.2 (5.1), EN1991-2-2003)

$$\varphi_2 = 1.29$$

Eq 14

C2.2.3 Centrifugal Forces

Centrifugal forces are considered for bridges with curved over the whole or just part of it. In this case, the bridge is horizontal and straight, therefore centrifugal forces are not considered.

C2.2.4 Nosing Force

The nosing force is considered as a concentrated force which acts horizontally at the top of the rails and perpendicular to the center-line of the track. It can be applied on both straight and curved track as well. The characteristic value of the nosing force is 100kN multiplied by a factor (1.21) according to (2) P 6.5.2 NEN EN1991-2-2003.This force is always applied in combination with vertical traffic load explained in section D2.1.1.

C2.2.5 Actions due to traction and braking

Actions due to traction and braking forces are considered at the top of the rails in the longitudinal direction of the track. These actions are considered as uniformly distributed over the corresponding influence length La,b for tractive forces. Braking forces are considered for the whole structural element considered. The direction of the traction and braking forces is taken in the direction of travel of track.

The characteristic value of tractive force is considered as:

$$Q_{lak} = \frac{33kN}{m} * L_{a,b}(m) \leq 1000kN\ for\ LM71$$

Eq 15 Eq(6.20) EN1991-2-2003

The characteristic value of braking forces is considered as:

$$Q_{lbk} = \frac{20kN}{m} * L_{a,b}(m) \leq 6000kN\ for\ LM71$$

Eq 16 (6.21) EN 1991-2-2003

C2.2.5 Special Accidental Situation Loads

Actions due to accidents or emergency are critical for safety in case of the derailment of the train. Numerous accidental load cases are recommended in OVS guidelines to consider during the design of a bridge. Only case relevant to our study will be discussed here.

OVS00030-06 recommends checking the bridge for jacket load on the side edge of the bridge. The jacket load is a result of the machine equipment required to lift the derailed load. This load consists of a concentrated load of 500kN (Figure 137) acting on a plate of 0.70m*1.60 m2

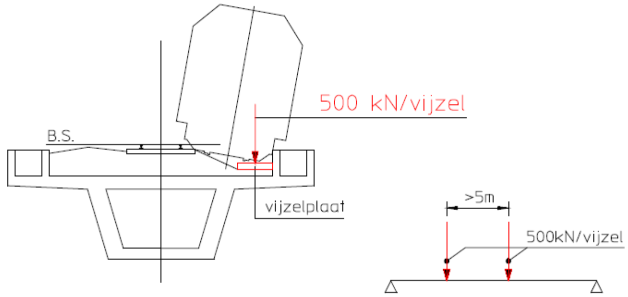

Figure 137 Accidental Jacket Load(OVS00030-06)

- Another design situation to be considered due to a derailment is the check for stability in terms of the overturning of the bridge superstructure. A uniformly distributed load is distributed at the edge of the bridge for a maximum length of 20m.Figure 138 shows the accidental load and its position according to EN1991-2-2003.

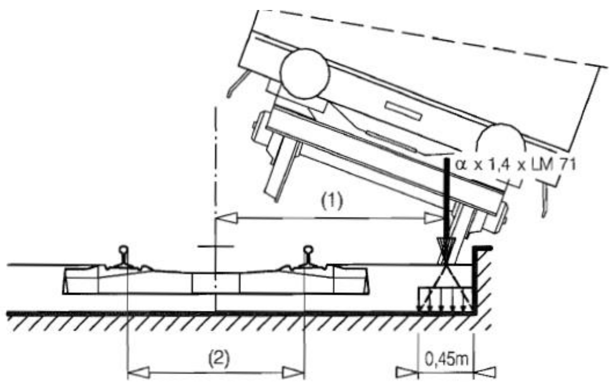

Figure 138 Equivalent Accidental Design Load (EN1991-2-2003)

$$q_{A2d} = \alpha * 1.4 * LM71$$
$$= 1.21 * 1.4 * LM71$$

Eq 17

C2.2.6 Wind Load

Actions due to wind acting on the bridge superstructure are calculated according to NEN-EN 1991-1-4. The bridge is located in Zwolle region, which lies in zone III. Therefore from Table NB.1 in figure 139 and Figure 140 NB.1 from EN-EN 1991-1-4, base wind velocity is calculated as below:

Windgebied	$v_{b,0}$ m/s
I	29,5
II	27,0
III	24,5

Figure 139 Table NB.1-Waarden voor $v_{b,o}$ voor toepassing in Nederland

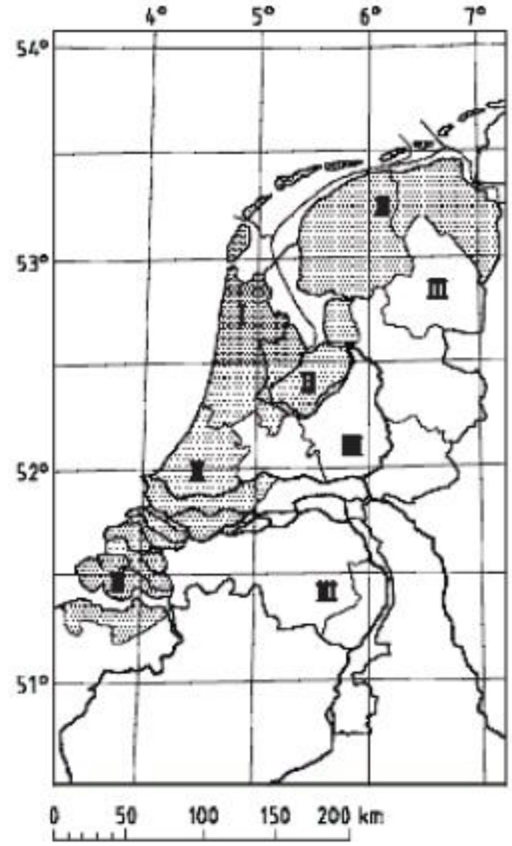

Figure 140 Figuur NB.1- Indeling van Nederland in windgebieden

$$v_{b,0} = c_{dir} * c_{season} * v_{b,0}$$

Where

$$c_{dir} = 1\,, c_{season} = 1$$

Mean wind velocity:

$$v_m(z) = c_r(z) * c_o(z) * v_b$$

Where:

$$c_r(z) = k_r \ln\left(\frac{z}{z_0}\right)$$

$$c_0(z) = 1$$

$$k_r = 0.19 * \left(\frac{z_0}{z_{0,II}}\right)^{0.07}$$

The peak velocity is calculated as:

$$q_p(z) = \big(1 + 7 * I_v(z)\big) * 0.5 * \rho * v_m^2$$

Where wind turbulence is calculated as:

$$I_v(z) = \frac{k_l}{c_o(z) * \ln\left(\frac{z}{z_0}\right)}$$

Wind pressure that is going to act on the structure can be calculated as follows:

$$w_e = q_p(z) * c_{pe}$$

C2.2.7 Snow Load

The snow load acting on the structure is 10kN*m as a variable load.

C2.2.8 Temperature Load

The effect of loads due to the thermal difference is should be taken into account by using a suitable partial load factor as per 2.3.1.2 JRC,2016 while conversion factors estimated in section F.1.1 take thermal variation in account too.

C.3 Load Combinations

In this section, the combination of loads will be described for the bridge superstructure. An overview of the combination of loads is given below in Table 24.

Number of Tracks on Structure	**Groups of Loads**	**Vertical Forces**	**Horizontal Forces**	
		LM71	Traction Braking	Nosing Forces
1	g11	1	0.5	0.5
	G12	1	1	0.5
	G13	1	0.5	1

Table 20 Load Combinations

C.4 Load Factors

Load factor for ULS:

For ultimate limit states, load factors and load combinations are calculated according to equation 6.10a and 6.10b of EN1990 which is as follow:

$$\Sigma\gamma_{G,j}G_{k,j} + \gamma_P\, P + \gamma_{Q,1}\psi_{0,1}Q_{k,1} + \Sigma\gamma_{Q,i}\psi_{0,i} * Q_{k,i}$$

$$\Sigma\xi_j\gamma_{G,j}G_{k,j} + \gamma_P\, P + \gamma_{Q,1}\psi_{0,1}Q_{k,1} + \Sigma\gamma_{Q,i}\psi_{0,i} * Q_{k,i}$$

Load Factor for SLS:

Similar to ULS, SLS load factors for combination are determined by equation 6.15b of EN1990

$$\Sigma G_{k,j} + P + \psi_{1,1}Q_{k,1} + \Sigma\psi_{0,i} * Q_{k,i}$$

C.5 Fatigue Loads

In this section load models for Fatigue Limit state will be discussed as mentioned in Appendix D of EN 1991-2-2003. For the new design of railway bridge, it is recommended to consider heavy traffic mix of 25t(250 kN axle load) for fatigue load analysis.

For fatigue load analysis, the Eurocode recommends using real fatigue train models which represent the real traffic load situation. Table D.2 of EN 1991-2-2003 gives the details of the type of service trains to be considered for this heavy traffic mix. This table is shown in figure 141 below.

Train type	Number of trains/day	Mass of train [t]	Traffic volume [10^6t/year]
5	6	2160	4,73
6	13	1431	6,79
11	16	1135	6,63
12	16	1135	6,63
	51		24,78

Figure 141 Heavy Traffic mix with 25t axles

Figure 142-145 shows the Load models associated with the train type mentioned in the above figure 141. These are then defined in the FE model to calculate fatigue stresses. Type 5 and 6 are part of standard and light traffic mix whereas type 11 and 12 are part of Heavy traffic mix.

$\Sigma Q = 21600\text{kN} \quad V = 80\text{km/h} \quad L = 270{,}30\text{m} \quad q = 80{,}0\text{kN/m'}$

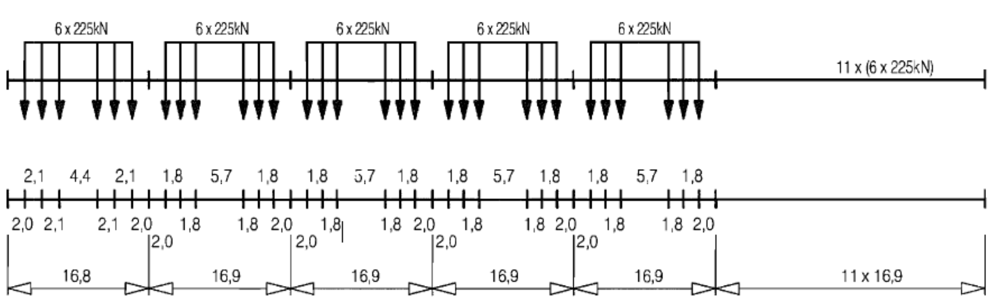

Figure 142 Type 5: Locomotive Hauled Freight Train

$\Sigma Q = 14310\text{kN} \quad V = 100\text{km/h} \quad L = 333{,}10\text{m} \quad q = 43{,}0\text{kN/m'}$

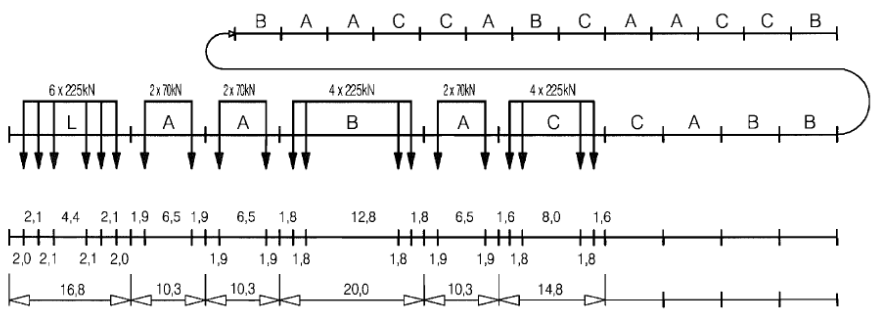

Figure 143 Type 6 Locomotive Hauled Freight Train

$\Sigma Q = 11350\text{kN} \quad V = 120\text{km/h} \quad L = 198{,}50\text{m} \quad q = 57{,}2\text{kN/m'}$

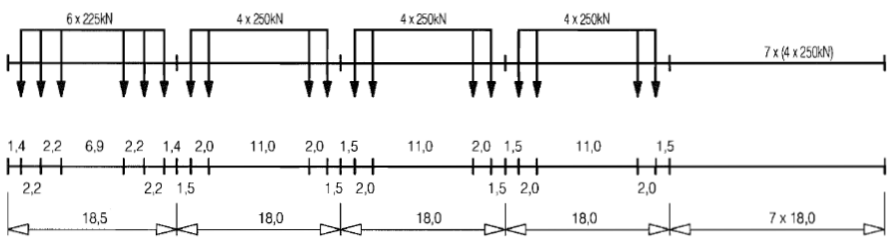

Figure 144 Type 11: Locomotive Hauled Freight Train

$\Sigma Q = 11350\text{kN} \quad V = 100\text{km/h} \quad L = 212{,}50\text{m} \quad q = 53{,}4\text{kN/m'}$

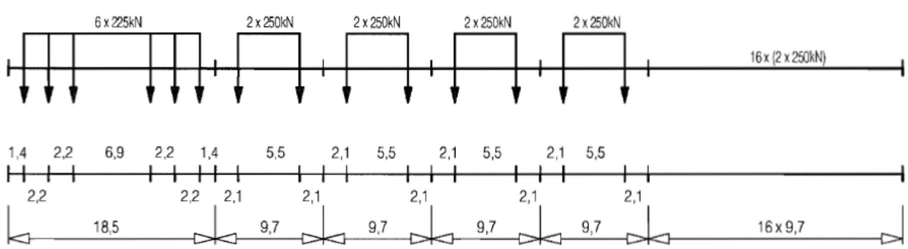

Figure 145 Type 12: Locomotive Hauled Freight Train

C.6 Real high-speed train models

To analyse the behaviour of bridges when subjected to high speed trains, real high-speed trains in operation are suggested to take into account. The moving force model described in the section 2.7.2.2 will represent these real train models. In this section, the study will have a look at the operational high-speed trains in The Netherlands and make choice of the appropriate real train model for our dynamic transient analysis.

Name	Type	Amount	Company
VIRM	double deck coach	872 [a]	NS
SLT	lightweight train	648 [b]	NS
ICM	single deck coach	581 [c]	NS
Stadler GTW	lightweight train	338 [d]	Arriva, Veolia, Breng and Connexxion
ICR	single deck coach	277 [e]	NS
DDZ / NID	double deck coach	240 [f]	NS
SGM	lightweight train	240 [g]	NS
Thalys PBKA	high speed train	170 [h]	NS
ICE 3M	high speed train	136 [i]	NS
DM '90	diesel train	106 [j]	NS
Thalys PBA	high speed train	100 [k]	NS
DDM-1	double deck coach	66 [l]	NS
DD-AR	double deck coach	57 [m]	NS
Mat '64 / Plan V	single deck coach	48 [n]	NS
Talent	lightweight train	48 [o]	DB Regio NRW
LINT 41/H	diesel train	12 [p]	Syntus, Arriva and Veolia
Protos	lightweight train	10 [q]	Connexxion

Figure 146 Inventory of rail trains in the Netherlands (B.Komen,2012)

Figure 146 shows the rail inventory of trains in The Netherlands. It is important to keep in mind that while considering the rail models, the train with maximum velocity will be considered for the analysis. The reason being that the higher velocity trains may have multiple resonant velocities that may be critical fir the bridge. Out of all the trains mentioned in Figure 146, for this thesis study, ICE3M train is used. This train has the maximum speed of 350km/hr. To design the bridge for next 100 years of service life and keeping in mind the Trans- European rail network expansion shown in figure 9 of section 1.3, it becomes essential for us to consider this train which is capable to attain a high speed in the near future.

C.6.1 Train description

The ICE-3M is a distributed traction, high speed multiple unit train which is composed of 8 cars to a total length of 200.32m. It is also possible to join the two units of this train to a form a single train of 400.64m. Each 8-car unit is symmetric at the middle between the first 4 cars and the remaining 4. A schematic view of one half of the train is described in figure 147.

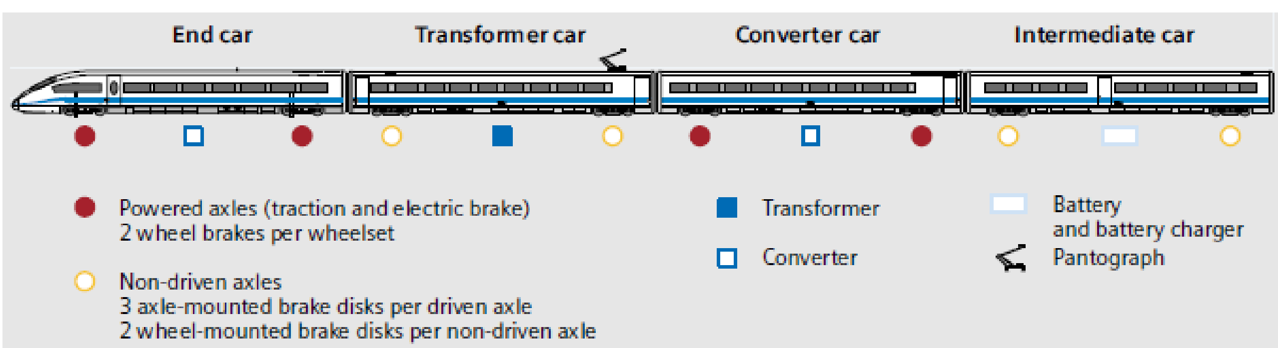

Figure 147 Schematic view of ICE-3M train (Goicolea, 2014)

C.6.2 Geometry

In this section, the geometry of the rolling stock is described as follows:

- Distance between bogie centers in one car: 2a* = 17.375 m
- Distance between axles in one bogie: 2a+ = 2:5 m

- Distance between bogie centers from adjacent cars: (u1 + u2) = 7.4 m
- Distance from nose to first bogie center: u3 = 4.76 m
- length of intermediate cars: L = 24.775 m
- length of end cars: L = 25.835 m

C.6.3 Axle loads

To model the ICE 3M train as a load model for transient dynamic analysis as per the geometry described above, the following distribution of axle loads is obtained in figure 148. The distance mentioned in the figure is the distance between the consecutive axles of the train.

axle	distance (m)	load (t)
1	3.51	15.5
2	2.5	15.5
3	14.875	15.5
4	2.5	15.5
5	4.9	15.5
6	2.5	15.5
7	14.875	15.5
8	2.5	15.5
9	4.9	15.5
10	2.5	15.5
11	14.875	15.5
12	2.5	15.5
13	4.9	13.5
14	2.5	13.5
15	14.875	13.5
16	2.5	13.5

axle	distance (m)	load (t)
17	4.9	13.5
18	2.5	13.5
19	14.875	13.5
20	2.5	13.5
21	4.9	15.5
22	2.5	15.5
23	14.875	15.5
24	2.5	15.5
25	4.9	15.5
26	2.5	15.5
27	14.875	15.5
28	2.5	15.5
29	4.9	15.5
30	2.5	15.5
31	14.875	15.5
32	2.5	15.5
	3.51	
total	200.32	480.00

Figure 148 Axle Load Distribution of ICE-3M((Goicolea, 2014)

D

Variant study for Form II

D.1 Variant Study

To understand the influence of the webs orientation, a variant study is done for the structural design form II. The main objective of this study is to study the effect of webs orientation in this system on a global and local deflection and flow of forces around the corners. In this study, the conceptual design form II is further investigated for deflection resulting from LM 71 and creep using material and conversion factors in JRC 2016. Alongside, they are optimised for the reduced mass system.

For this 4 variants are modelled in ABAQUS with similar FRP face dimensions and the deformation behaviour is analysed. The cross-section of the bridge considered for the variant study is shown in figure 149.

The details about Finite element model are discussed in Chapter 6 in detail, section 6.2.

Table 24 below shows the variant FEM models modelled. These models are compared based on deflection (Short and Long Term) and Bending Stresses at the corners. This offers optimization of FRP material for best expected stiffness.

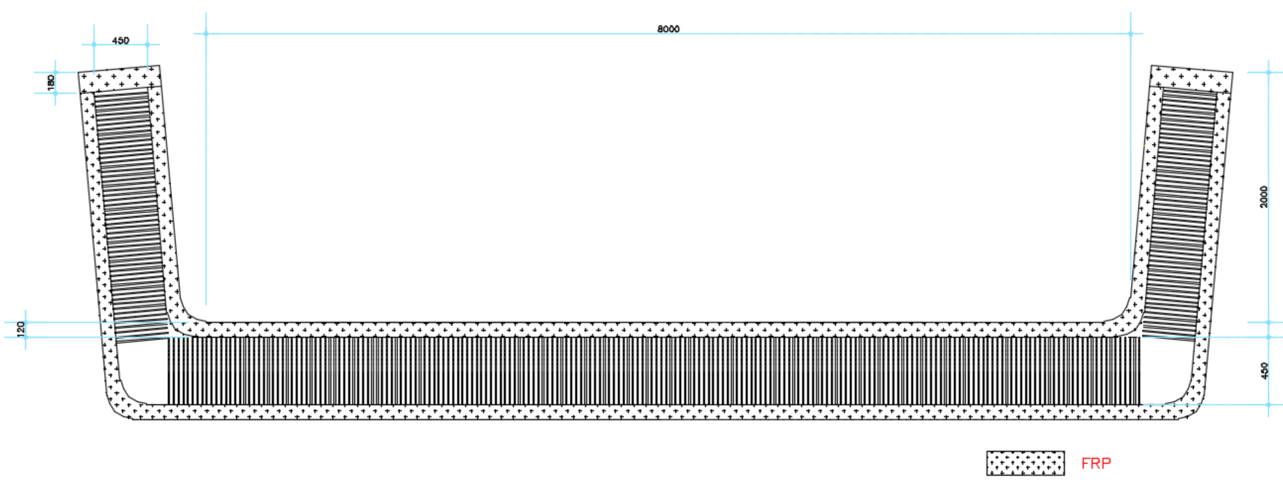

Figure 149 Cross-section of bridge for Form II

FEM Model	Description
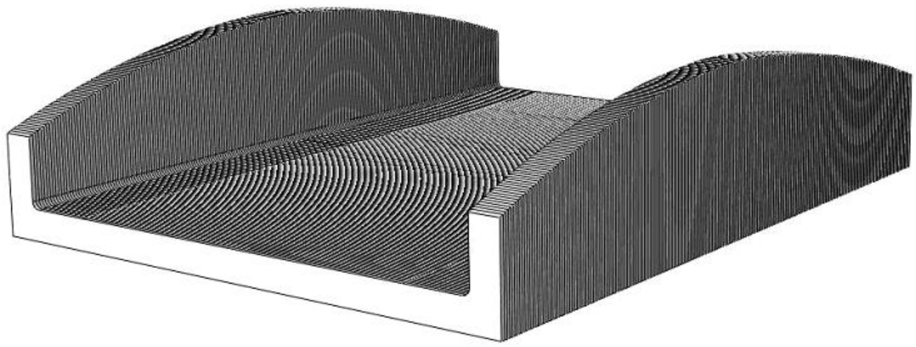	Webs running parallel to cross-wise direction of span in both horizontal and vertical FRP panel **VARIANT 1**
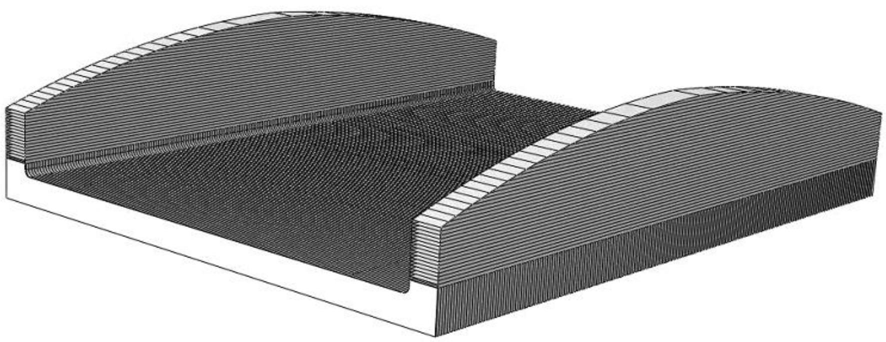	Webs in cross wise direction of span for horizontal panel and Webs in the direction of span for vertical panel **VARIANT 2**
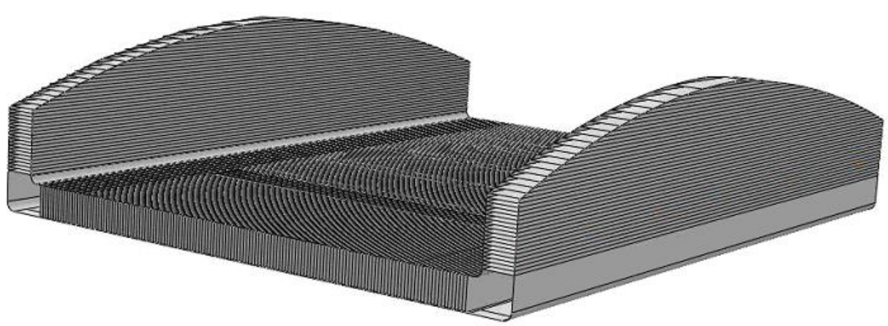	Webs running in the span direction for both Panels **VARIANT 3**
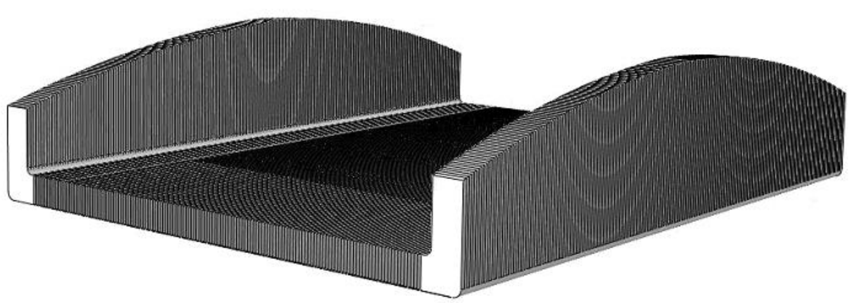	Webs running in the span direction for horizontal panel and in cross wise to span direction in vertical panel **VARIANT 4**

Table 21 Variants for Form II

D.1.1 Comparison based on Deflection

From the finite element analysis, deformed shape of the respective models is achieved and deflection due to short term and long term (Creep) are plotted on the table below.

Deformed Model	Maximum short- term deflection around mid-span
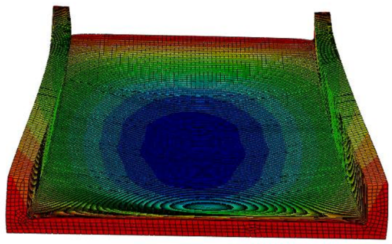 **VARIANT 1**	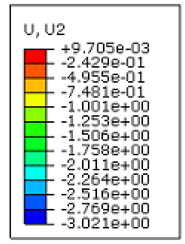 $\delta_{short} = 3mm$
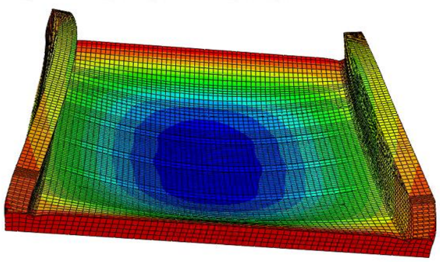 **VARIANT 2**	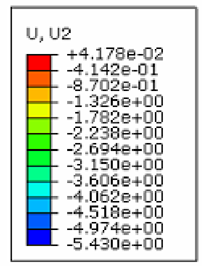 $\delta_{short} = 5.4mm$
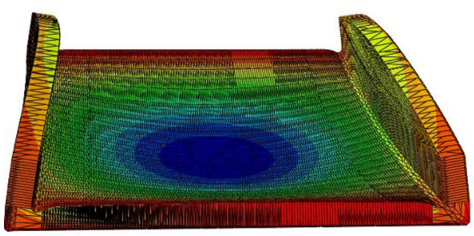 **VARIANT 3**	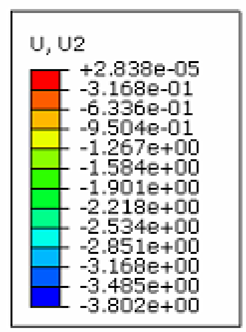 $\delta_{short} = 3.8mm$

Table 22 Bending Deformations of variants

<table>
<tr><th>Deformed Model</th><th>Maximum long -term deflection around mid-span</th></tr>
<tr><td>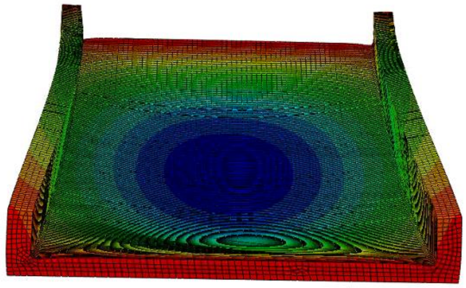
Variant 1</td><td>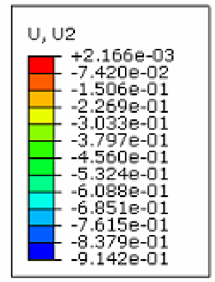
$\delta_{long} = 0.9mm$</td></tr>
<tr><td>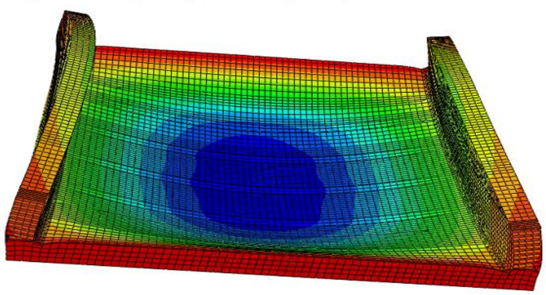
Variant 2</td><td>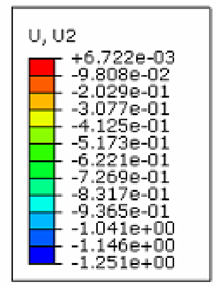
$\delta_{long} = 1.25mm$</td></tr>
<tr><td>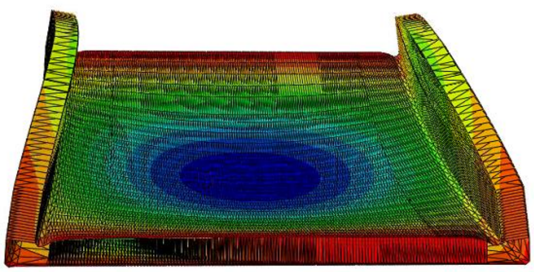
Variant 3</td><td>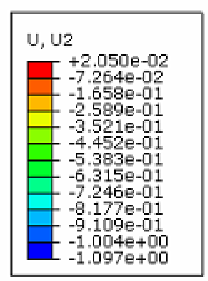
$\delta_{long} = 1.1mm$</td></tr>
<tr><td>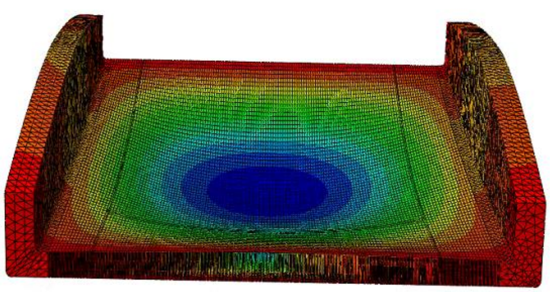
Variant 4</td><td>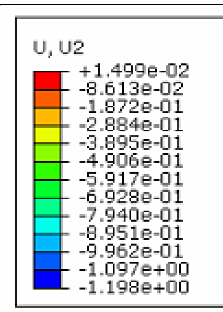
$\delta_{long} = 1.2mm$</td></tr>
</table>

Table 23 Creep Deformations OF Variants

The total deflection of the structure is defined as the sum of short-term deflection and long-term deflection and can be modelled as:

$$\delta_{total} = \delta_{short} * \alpha * \frac{\varphi}{\eta_{ser,s}}$$

Where

$$\eta_{ser,s} = 0.73,\ \eta_{ser,l} = 0.6, \alpha = 1.21\ \&\ \varphi = 1.29$$

Variant	Total Deflection	Deflection Limit
Variant 1	7mm	**13.3mm**
Variant 2	12.64mm	
Variant 3	8.89mm	
Variant 4	11.23mm	

Table 24 Total Deflection Comparison of Variants

From table 27, it can be seen that the deflections of all the variants are within limits but there is a slight difference between them though they have similar dimensions. The possible reason is the effect of webs on the stiffness of the cross-section. Since most of the stiffness is obtained from the faces but the webs in the vertical panel do have a significant role to play due to their higher lever arm. The influence of the orientation of these webs do affect the moment of inertia of the bridge system and hence the difference is observed.

Table 28 shows the moment of inertia of all the variants to highlight the influence of the webs orientation in determining the stiffness of the bridge structure. A difference in the values of the inertia can be observed.

Variant	Moment of Inertia (mm^4)
Variant 1	9.98E+11
Variant 2	8.20E+11
Variant 3	8.45E+11
Variant 4	9.12e+011

Table 25 Inertia properties of variants

The variant 1 gives most favourable structural behaviour because of balanced flexural stiffness in both bridge directions. Webs oriented transversally facilitate the local load transfer from the deck to the main load bearing elements of the bridge in the longitudinal direction, the vertical panels. The aligned transverse orientation of the webs in the deck and the vertical panels provide rigid longitudinal joint at the corner between the two major structural parts of the bridge. The resistance to lateral buckling of the "top chord" of the vertical panels is improved by this rigid joint. On the other hand, the local transverse deflections of the deck are reduced by clamping to the vertical panels.

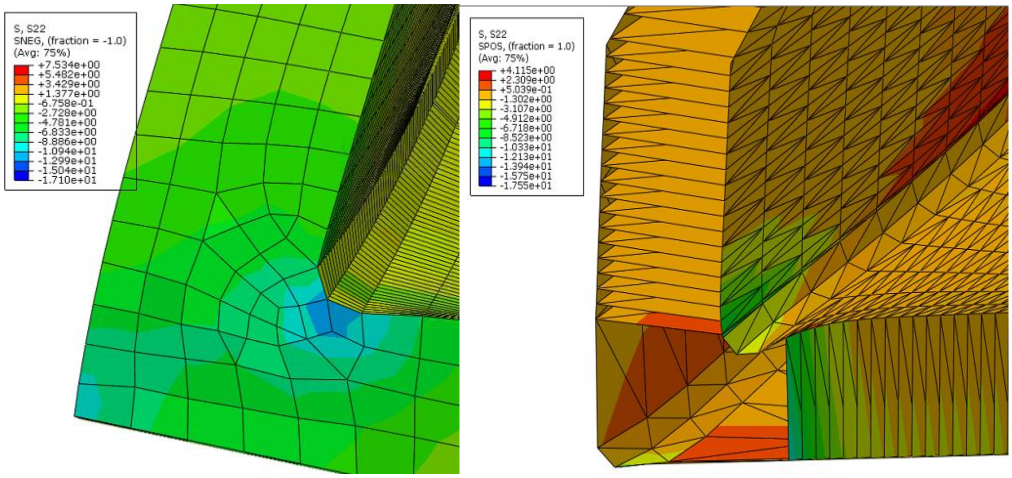

Figure 150 Bending Stresses for variants 1&3

Orienting the webs in the transverse direction in the deck and the vertical panels provide better corner detail leading to low stresses induced by local bending of the facings when compared to e.g. variant 3 where all the webs are oriented longitudinally. This can be evident from figure 150 which shows the bending stresses at the junction of the vertical and horizontal panel. The stresses are high in variant 3 around 17.5 MPa whereas in variant 1 they are around 8MPa

E

Fatigue Analysis

The main objective of this chapter is to answer if the chosen FRP bridge can satisfy fatigue limit state damage. Since the existing steel bridges fail in fatigue, therefore this study is essential to calculate the working life of the FRP bridges so that they are feasible to replace. To answer this question, critical details subjected to higher stresses in the static analysis are subjected to moving fatigue loads described in Appendix C of EN1991-2-2003 and fatigue damage is calculated for its service life. In addition, fatigue utilization ratios are calculated to understand the magnitude of damage observed.

E.1 Introduction

FRP material is known to have excellent fatigue properties in the aeronautical industry. In the civil infrastructure industry, the application of FRP decks on steel bridges is a common practice to improve the service life of fatigue affected steel bridges. In contrast, the fatigue behaviour of FRP material due to its limited application is not well recognised in the academia and civil industry. In this chapter, emphasis will be laid to understand the nature of fatigue response of FRP railway bridges. How does FRP behaves against cyclic stresses when the bridge is designed according to stiffness criterion and no given guidelines from Eurocode are applicable to it.

E.2 Fatigue critical details

Fatigue life assessment is performed on a structural element like connection details or change in the laminate properties in case of fibers reinforced with polymers. Before assessing the damage in these structural elements, it is essential to first identify these potential points of fatigue critical details.

In this section, emphasis will be paid to identifying such locations with the aid of static finite element analysis made in chapter 6. The potential source of these critical locations on the bridge structure can be attributed to:

- Normal stresses acting perpendicular to the longitudinal direction of the bridge
- Maximum shear stresses at the supports
- High bending stresses at the mid-span of the bridge

It is not only these locations but other potential sources as well that should be looked after through the static finite element analysis.

In the following sections, the study will identify the critical details and assess their damage in the subsequent sections.

E.2.1 Critical locations

The critical locations are generally considered to be the locations where the static stresses are high or where local peak stresses are encountered in the structure. In chapter 6, the location of the maximum bending, shear and normal stresses was observed for the bridge from static analysis. These critical locations along with locations in their vicinity of 250mm (to account for unexpected peak stresses) are considered for fatigue analysis. These critical points are chalked out in figure 151. The critical locations which are a result of normal stresses, shear stresses and bending stresses are marked with ‘V’,’S’ and ‘B’ respectively. The description of these details follows the figure 151 below.

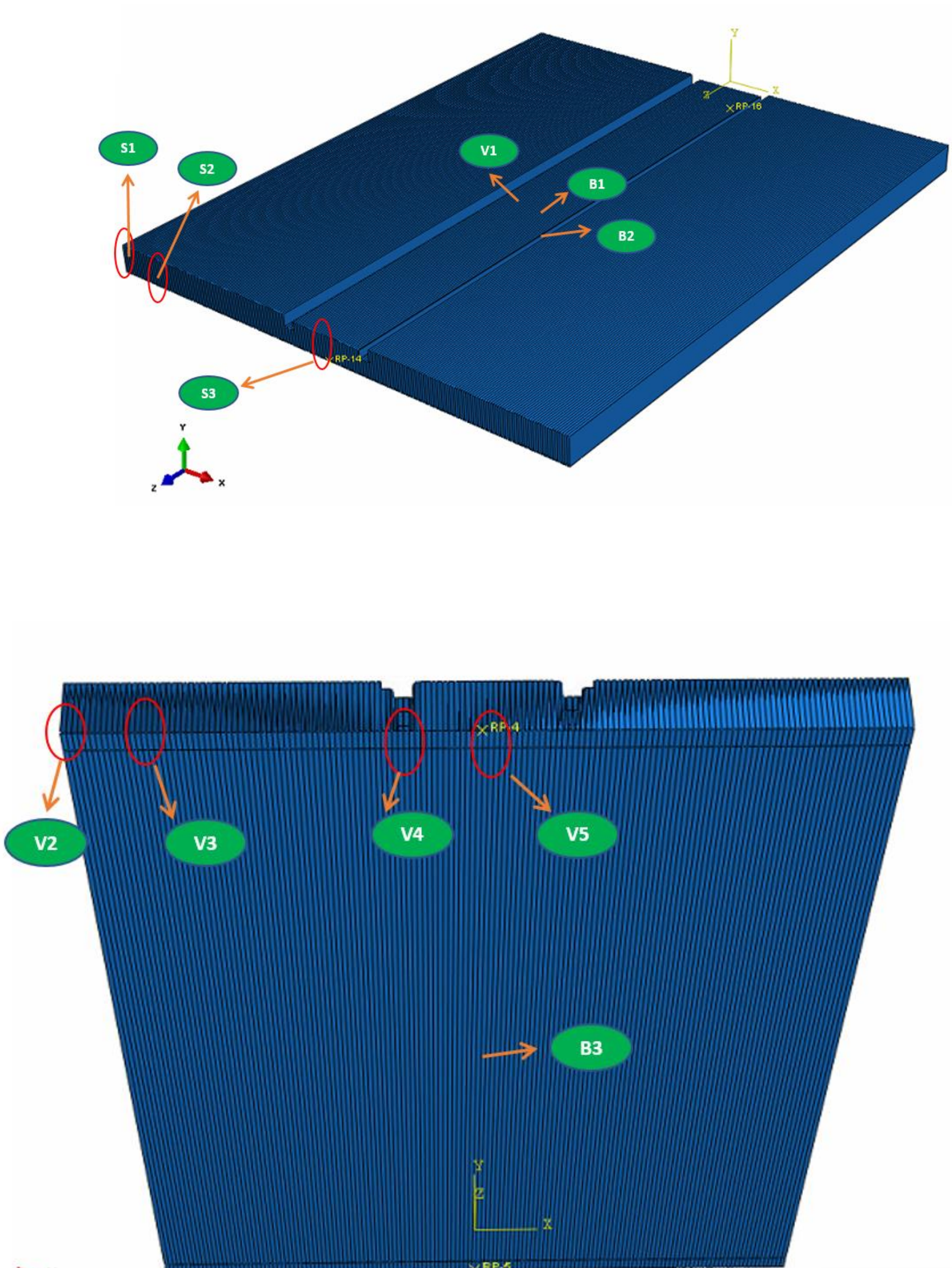

Figure 151 Critical Fatigue details

- V1 is the detail which comprises of the interface between the top face of the panel and the web. This detail is located at the mid-span of the bridge. The importance of this detail is to analyse the vertical stresses due to the direct application of axle loads near the ERS groove.
- V2 is the detail which comprises of the interface between the bottom face of the panel and the web at the extreme edge of the supports. High vertical stresses from the reaction forces on this location make it critical to analyse for cyclic stresses.
- V3 is the detail which has similar structural element configuration as of V2 and in the vicinity of the V2 to check for any critical stresses.
- V4 and V5 also have the same structural element configuration as of V2. V4 is located at the bottom of the grove of ERS and V5 at the middle of the supported edge.
- S1and S2 are the locations of webs at the extreme edges of the supports and its vicinity (500mm). Shear stresses acting vertically on these webs are maximum at these locations.
- S3 is the detail similar to V1 but at the middle of the supported edge. This detail is chosen to analyse the repeated stresses acting longitudinally to the web-face interface. These stresses will be higher because simply supported beams experience maximum shear stresses at the supports.
- B1 and B3 are the locations at the mid-span of the bridge. B1 and B2 are the points at the center of the top and bottom face respectively. These details are subjected to maximum compressive and tensile bending stresses respectively. B2 is the location directly on the groove surface of the top face near B2.

E.3 Influence line diagram

In this section, the study will proceed to the next step that leads to an assessment of fatigue analysis. The methodology of performing fatigue calculations for FRP railway bridges has been discussed in section 2.6. Here, we will follow the same steps and calculate the damage experienced by the critical locations at the end of their service life.

The first and foremost step is to have a plot of influence line diagrams for the bending, shear and normal stresses acting on the bridge elements. A unit load of 1kN is moved across the bridges in a total of 55 steps of 200mm each in the ABAQUS. Figure 152 shows the load steps modelled in the finite element software.

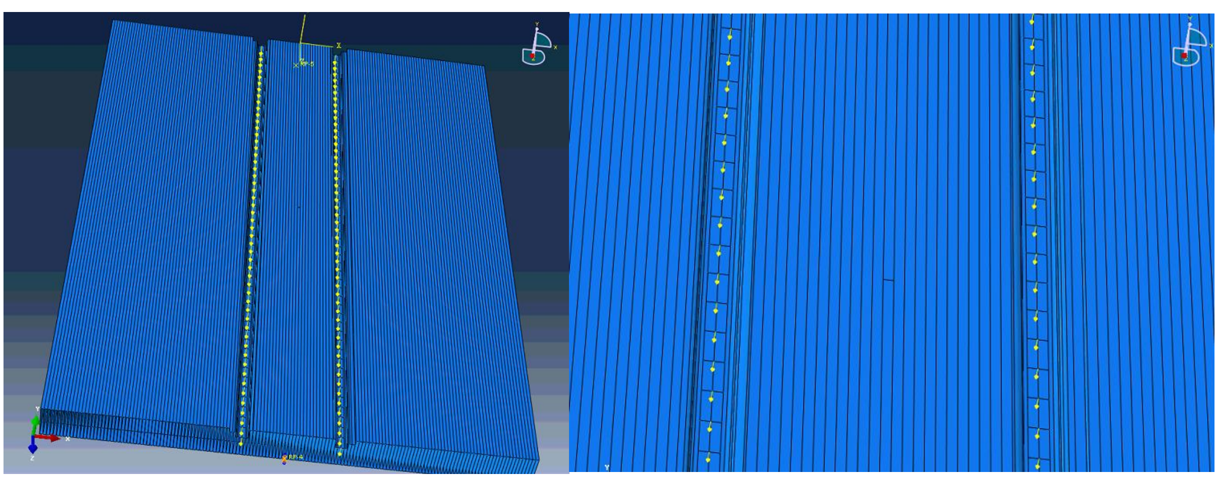

Figure 152 Load steps for ILD

Using these load steps, the static general analysis is run and desired stresses are calculated. These stresses are plotted against the position of the load in the graphs to obtain influence line diagrams. Figure 153-163 shows the plot of the influence line diagram obtained for all the critical points described above.

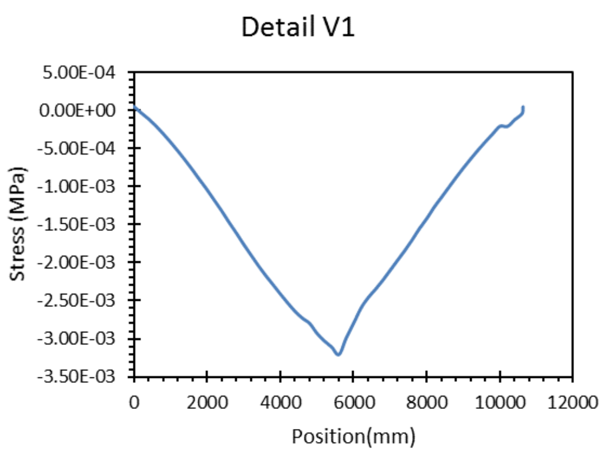

Figure 153 ILD for detail V1

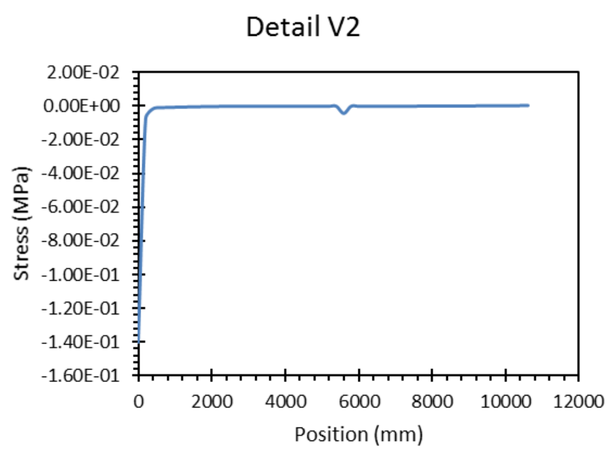

Figure 154 ILD for detail V2

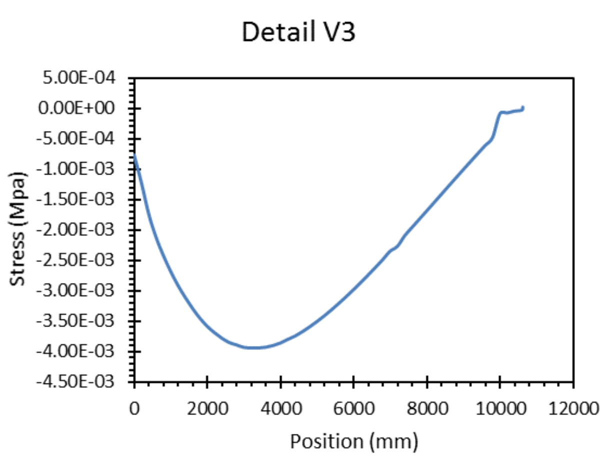

Figure 155 ILD for detail V3

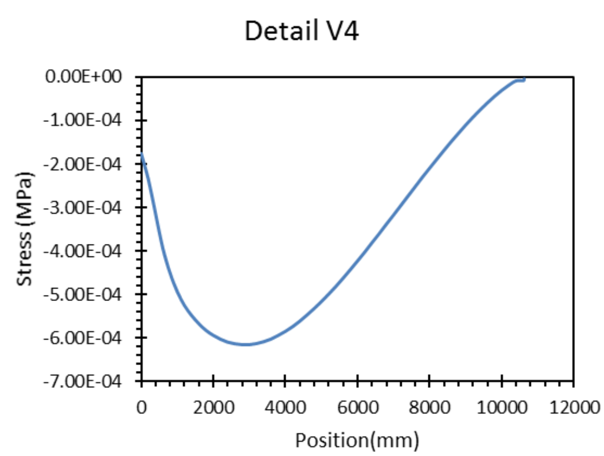

Figure 156 ILD for detail V4

*Note: '+ve' stands for tensile stresses and '-ve' stands for compressive stresses. In some plots, shear stresses are +ve/-ve. In actual, shear stresses acting on the structural elements will be both positive and negative depending upon which side of the supports the details are located. For ease of work, only one side of the support is considered to calculate the stresses. The other support will have the opposite nature of stress as well.

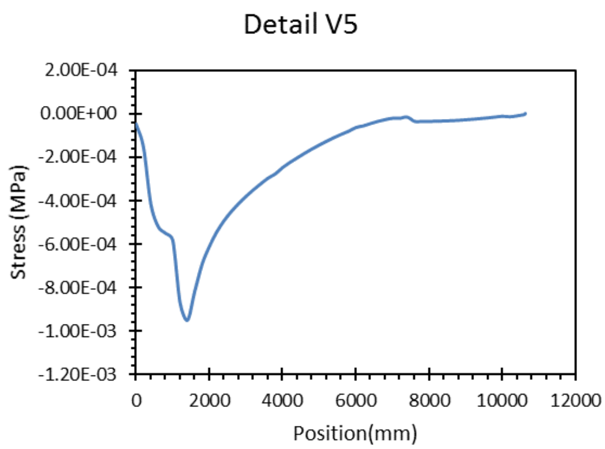

Figure 157 ILD for detail V5

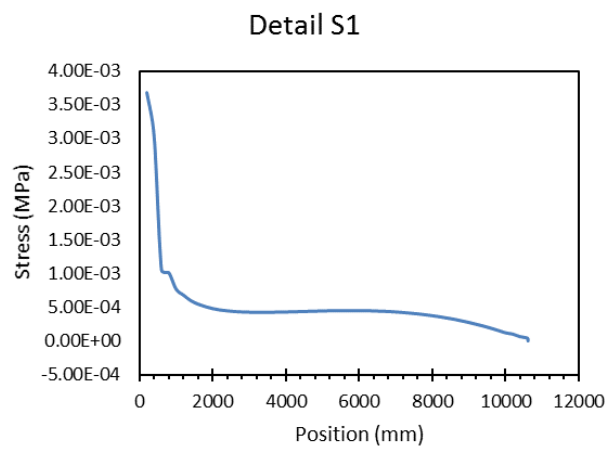

Figure 158 ILD for detail S1

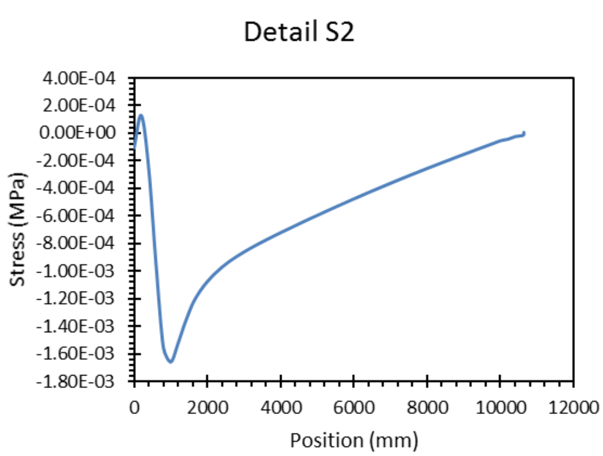

Figure 159 ILD for detail S2

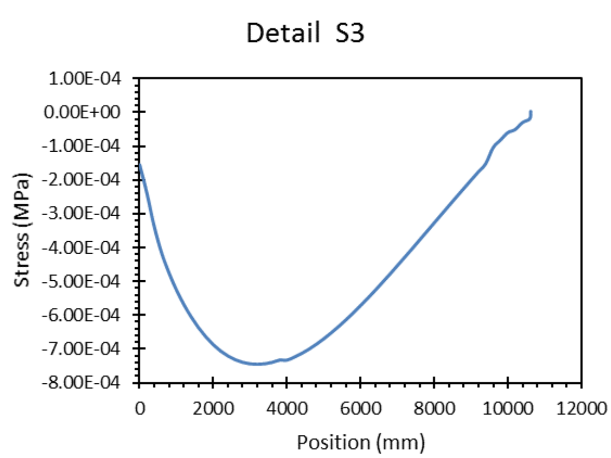

Figure 160 ILD for detail S3

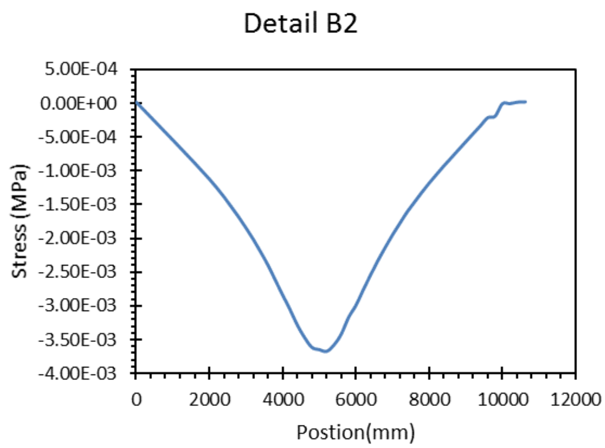

Figure 161 ILD for detail B2

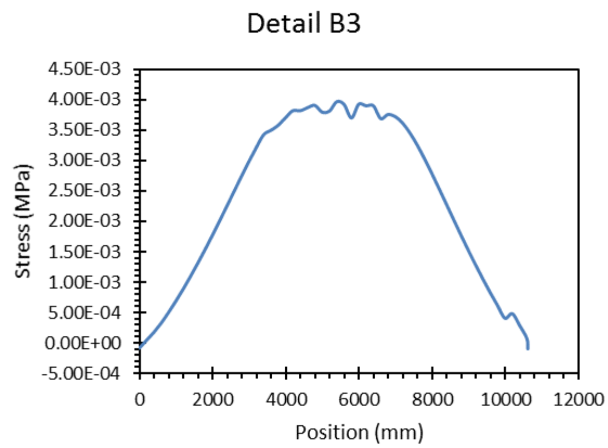

Figure 162 ILD for detail B3

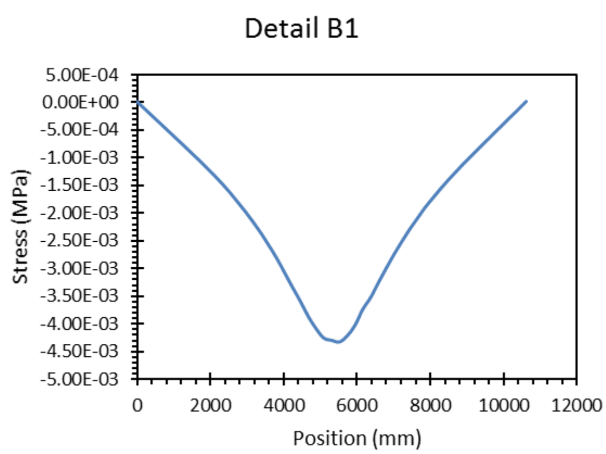

Figure 163 ILD for detail B1

E.3.1 Discussion of ILD plots

- Figure 153 describes the influence line plot for the vertical stresses at detail V1. The unit load passes from x=0 to x=L length of the bridge. When the unit load reaches the mid-span, it can be observed that the compressive stresses are maximum. From x=0 to x=mid-span as the load approaches the location of the detail the vertical stresses increase linearly and then decrease linearly to zero when the load departs from the mid-span.
- Figure 153-158 describes the influence line plot for the vertical stresses at detail V2, V3, V4 and V5. The unit load passes from x=0 to x=L length of the bridge. Therefore, at x=0, the vertical stresses are maximum since the point of action of the unit load is on the location of the detail V2. With the passage of load, the stresses acting on detail V2 decrease. For details V3, V4 and V5 also similar trend are followed but the maximum stresses are experienced at a distance of around 2000mm. This is because the finite element software does not distribute the stresses instantaneously. The stresses are spread out at an angle of 45 degrees and hence the maximum is obtained at a certain distance from the supports.
- Figure 158-160 describes the influence line plot for shear stresses at details S1, S2 and S3. The unit load passes from x=0 to x=L length of the bridge. Therefore, the shear stresses around the support are maximum since the point of action of the unit load is on the location of the detail. With the passage of load away from the supports, the stresses acting on these details decrease to zero.
- Figure 161-163 describes the influence line plot for bending stresses at detail B1, B2 & B3. The unit load passes from x=0 to x=L length of the bridge. Therefore, at x=0, the bending stresses are zero at supports and at x=L/2, the bending stresses are maximum at the mid-span since the point of action of the unit load is on the location of the detail. With the passage of load away from the location of the details, the stresses acting on these details decrease.

E.4 Stress histograms

After plotting of influence line diagram, formulation of stress histograms is the next step. These stress histograms give an idea of the number of times a certain value of stresses acting due to fatigue train load models (section C.5) will be faced by the structural member. The fatigue load model is passed over the influence line to establish the time history response (stress vs time step). Subsequently, stress histogram is constructed using rainfall counting method.

For example, the time history plots of detail B1 when train load models 5,6,11 and 12 passes over the influence line shown in figure 164-167 below.

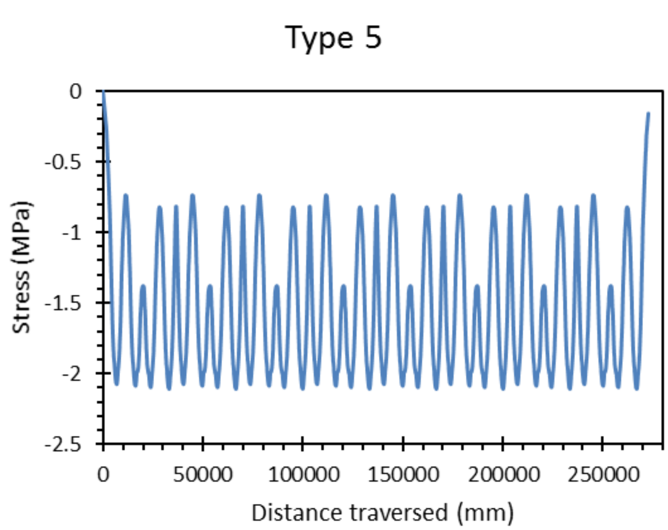

Figure 164 Stress-history of B1 due to Type 5 load model

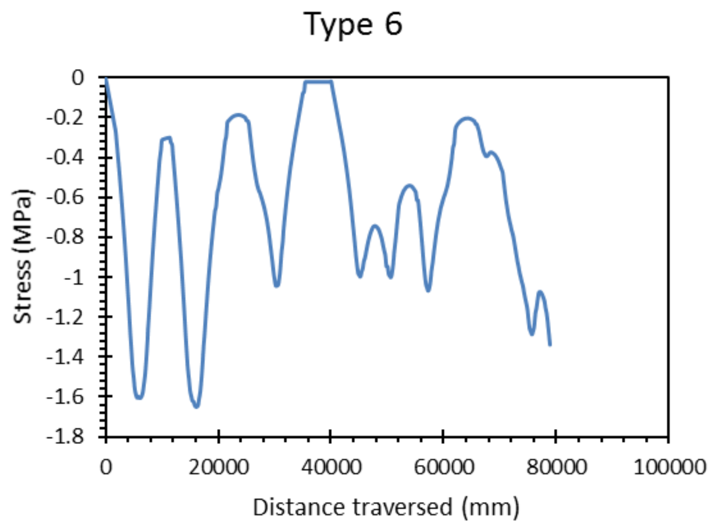

Figure 165 Stress-history of B1 due to Type 6 load model

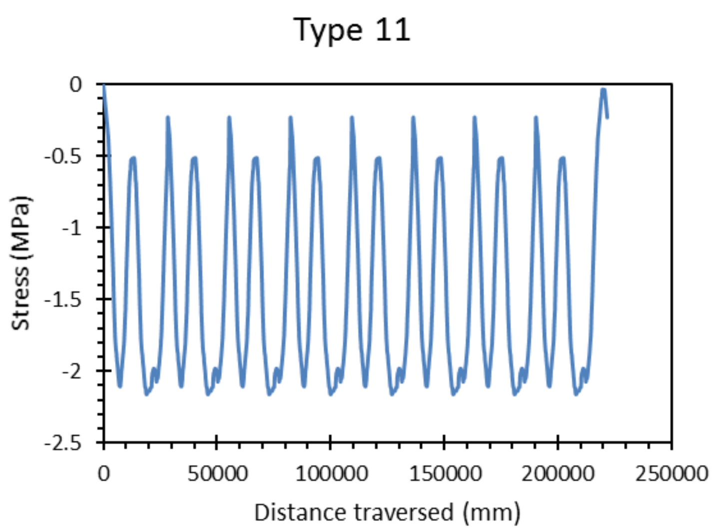

Figure 166 Stress-history of B1 due to Type 11 load model

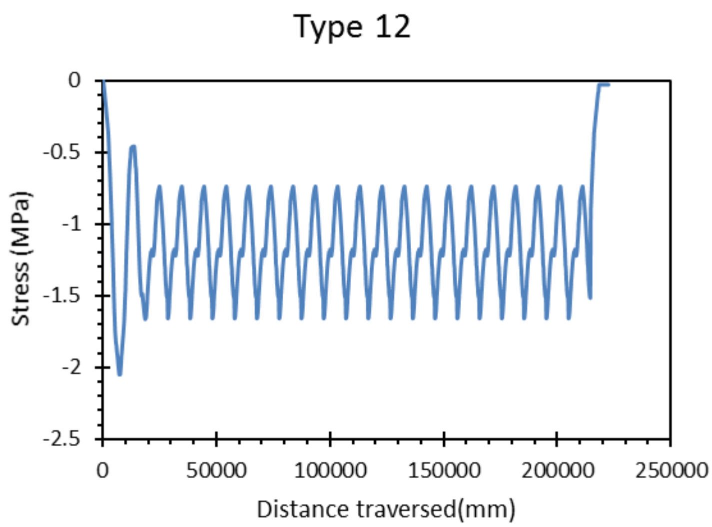

Figure 167 Stress-history of B1 due to Type 12 load model

These time history plots are then constructed into stress-histogram plots using rainfall counting method as shown in figure 168.

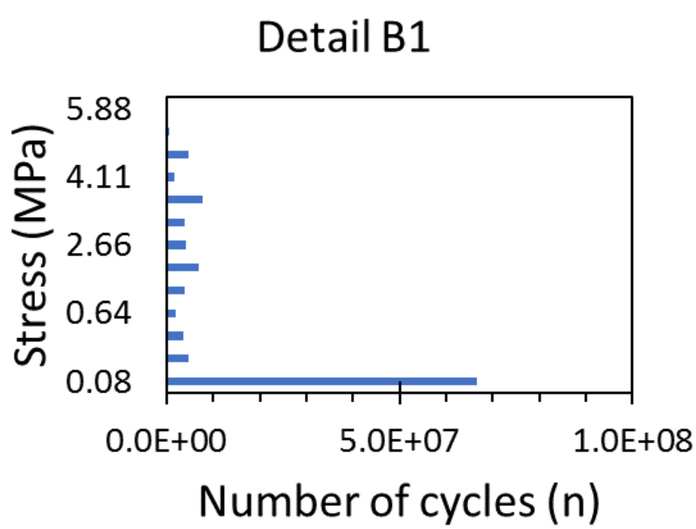

Figure 168 Stress-histogram for B1

Details about the time history response and stress histogram for other details described in this report are reported in Appendix F.

E.4.1 Discussion for stress-history plots and stress histogram

For the detail B1 the stress history plots are obtained when the fatigue train models type 5,6,11 and 12 run across the bridge. A clear pattern is obtained from the passage of these load models. At x=0, it can be observed that the bending stresses are zero for all type of loadings. The maximum is obtained at the mid-span for all the stress-history. The stress history obtained from type 5,11, and 12 have a repeated pattern due to the repeated axle loadings in their load model configuration. Hence, the bending stresses repeat themselves with time. For type 6, this pattern is not observed due to different axle load configuration for each coach which does not follow any definite pattern. The maximum bending stresses are obtained for the interface between the two bogies. The reason is that the distance between the axles of the 2 bogies is less than the intermediate distance between the axles of each bogie itself. As a result, for that interface, maximum loads are present on the bridge deck. Therefore, maximum stresses are obtained for these bogie-bogie load configuration interface.

After the plots of these stress history are obtained, using a J-rain excel template available on the internet for free usage of students. Rainfall counting of stresses from the stress-history plots of all these details is made and a number of cycles of repeated cyclic stresses are obtained. The resulting data between the repeated cyclic stresses and number of cycles is plotted on a chart known as stress-histogram plot for detail B1. It can be observed that the maximum number of repeated stresses are of low magnitude. Another observation is that the highest stresses have a low number of cycles since there occurrence is limited due to load configuration.

E.6 Damage calculation using S-N curves

To calculate the fatigue damage of the critical details, two most important parameters are R-ratio, 'n_i' and 'N_i' for each of the detail class.

R-ratio is the ratio of minimum and maximum stress that occurs in a cycle. For detail subjected to only tensile forces, R=0.1 is considered. For details subjected to only compressive stresses, R=10 is considered. R=-1 is considered for details subjected to both tensile and compressive stresses.

n_i - is the number of cycles occurring in a load of a specific size and *R* value. For all the details, this can be obtained from their respective stress-histograms.

N_i - being the number of cycles to failure for a specific size and *R* value. This is calculated by the equation

$$\log(N) = a\frac{log(1.1 * \gamma_m * \sigma_{\max})}{\eta_c\ B}$$

Where the terms a,B can be obtained from table 4 of section 2.6.3, γ_m and $\eta_c$from section 6.2 of Chapter 6 and $\sigma_{\max}$ from the stress-histograms of the respective details in appendix E.

Table 20 shows the value of the above-mentioned parameters and the damage calculated for all the details. A similar approach is followed for rest of the details and damage calculation has been made (refer F.3, Appendix F).

Detail B1		R=10	
$\Delta\sigma_i\ (MPa)$	n_i	N_i	D_i
0.07	65992000	1.91E+54	2.41E-48
0.63	4599000	1.26E+37	5.294E-31
0.35	3504000	4.98E+41	7.02E-36
0.56	1898000	1.05E+38	1.45E-32
1.12	3796000	4.03E+32	5.43E-28
1.4	6716000	7.26E+30	2.61E-25
2.31	4088000	8.83E+26	4.29E-21
2.73	3796000	4.36E+25	8.68E-20
3.01	7592000	7.53E+24	6.05E-19
3.57	1533000	3.49E+23	1.88E-16
4.62	4562500	3.37+21	1.73E-16
4.97	584000	9.05E+20	8.38E-15
5.81	219000	5.44E+19	7.50E-14
		D	8.38E-14

Table 26 Damage calculation for detail B1

Table 21 shows the results obtained for number of cycles to failure N_i, number of cycles of stresses n_i, stress range $\Delta\sigma_i$ and damage encountered D_i for each stress range. Then the damage is calculated as the sum of individual D_i obtained from each stress range.

For detail B1 the damage is 8.38E-14, which is very low. This makes sure that the service life of the bridge will not be any issue because of bending stresses.

The damage for all the details is summarized in table 21 below.

Detail	Damage
V1	1.45E-10
V2	9.52E-11
V3	1.33E-12
V4	3.93E-19
V5	7.11E-17
S1	2.69E-09
S2	2.02E-09
S3	4.94E-16
B1	8.38077E-14
B2	2.65E-18
B3	2.19E-14

Table 27 Damage for detail B1

Table 22 shows the damage values for all the details described in the section 7.2.1. From this table, it can be inferred that the damage for all the details is < 1 and therefore, the bridge will be operation during its whole service life against fatigue stresses.

E.7 Damage calculation using Equivalent stress levels

Another life prediction method to compare the severity of the fatigue loads on the bridge structure is to examine the fatigue resistance utilisation ratio. This ratio is derived from the basic S-N logarithmic curve formulation, a standard equivalent load and Miner's damage summation obtained in the previous sections.

The formulation of the equivalent stress used is expressed as:

$$S_{eq} = \left(\frac{\Sigma n_i S_i^m}{\Sigma n_i}\right)^{\frac{1}{m}} * \left(\frac{1}{M}\right)^{\frac{1}{m}}$$

Where

S_{eq} = equivalent maximum stress at selected R-value

S_i = Maximum stress at cycle i

N_i=Number of cycles with Si

M=value of Miner's sum at failure (~1)

m=slope of the S-N curve at selected R-value (m=4.7E-05 for R=0.1 and 1.67E-06 for R=10)

Fatigue utilisation ratio is expressed as:

$$Fatigue\ utilisation\ ratio = \frac{\gamma_F * S_{eq}}{\eta_c * \frac{S_{ult}}{\gamma_m}}$$

Where $\gamma_F = 1$

$\gamma_m = 2.03$

$\eta_c = 0.81$

S_{ult} is the ultimate compressive/tensile strength of the FRP laminate when subjected to fatigue loads

$$S_{ult,comp} = 440MPa\ and\ S_{ult,tension} = 700MPa$$

Table 22 summarises the value of fatigue utilisation ratio for all the details concerned and comparison with the UC ratios for static results is made.

Details	S_{eq}(MPa)	FUR	UC
V1	1.86	0.006	0.18
V2	0.89	0.003	0.18
V3	0	0	0.15
V4	0	0	0.11
V5	0	0	0.002
S1	0	0	0.13
S2	0	0	0.10
S3	0	0	0.04
B1	0	0	0.08
B2	0	0	0.08
B3	0	0	0.05

Table 28 Fatigue utilization ratio and comparison with static results

Table 22 compares the fatigue utilization ratio and unity ratio for the details considered. From these ratios, it can be observed that the UC ratio of these detail is really low (<1). The UC ratio is obtained by using factors which increase the magnitude of LM71 load by 2.5 times. Therefore, the fatigue utilization ratio will no amplification factor will be subjected to low utilization of the FRP material. That is why out of all the details only V1 and V2 are utilized against stresses. This can be only increased by improving the UC ratio of these details by making sure that the deflection criteria is satisfied.

F

Stress History & Histograms

F.1 Introduction

In this appendix, the plot of the stresses due to the passage of train loads will be presented below against time and the resulting histograms are plotted after that for each detail.

F.2 Stress Histograms

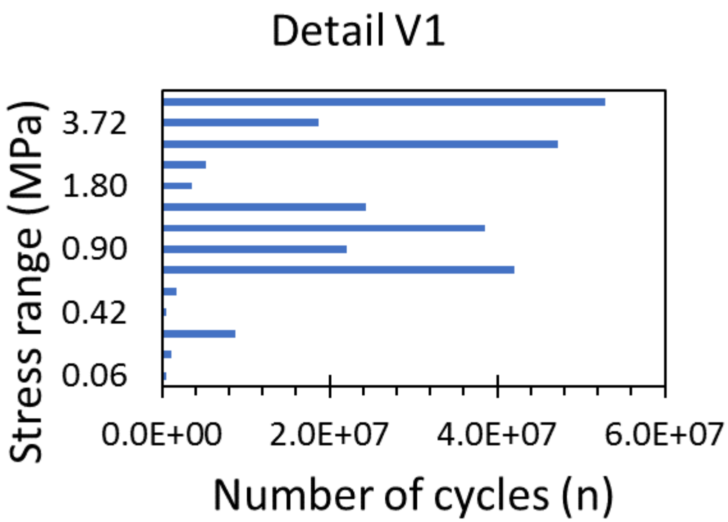

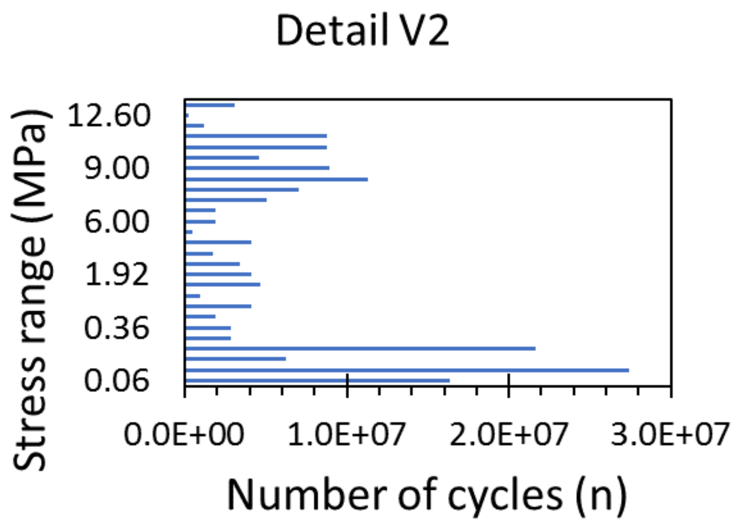

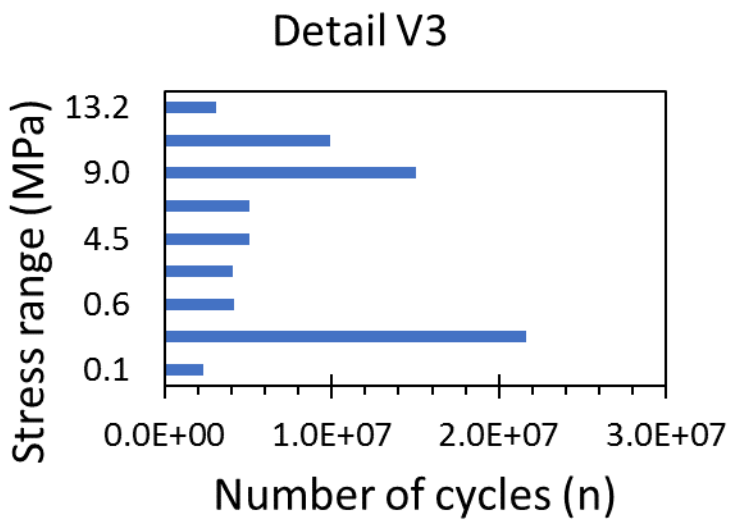
Detail V3
Stress range (MPa)
13.2
9.0
4.5
0.6
0.1
0.0E+00
1.0E+07
2.0E+07
3.0E+07
Number of cycles (n)

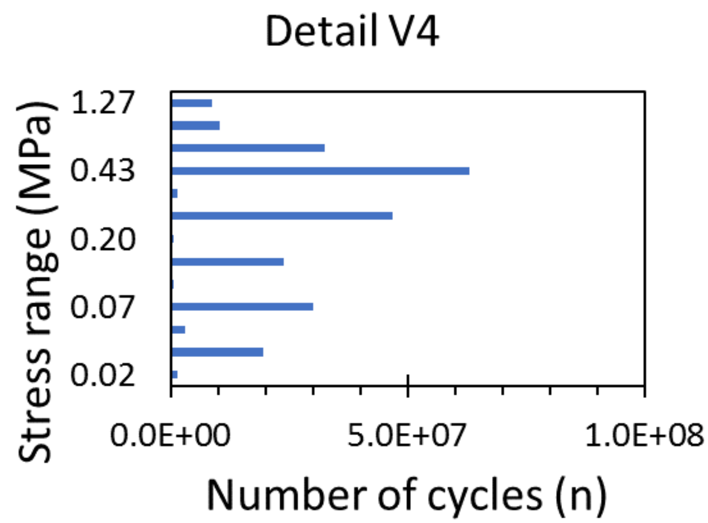
Detail V4
Stress range (MPa)
1.27
0.43
0.20
0.07
0.02
0.0E+00
5.0E+07
1.0E+08
Number of cycles (n)

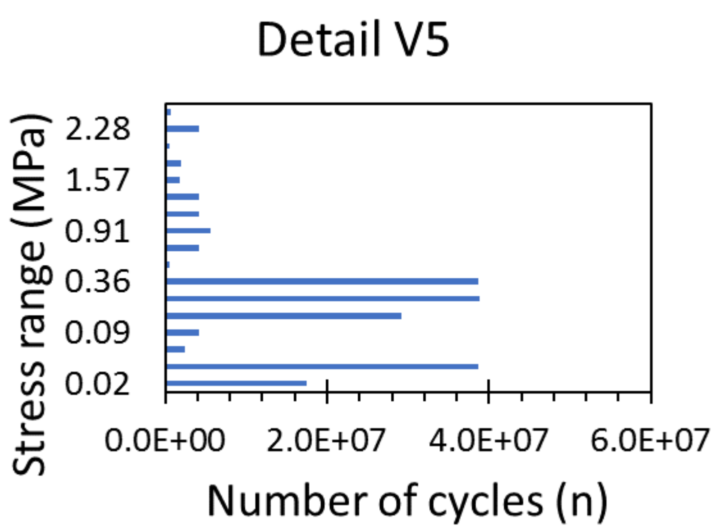
Detail V5
Stress range (MPa)
2.28
1.57
0.91
0.36
0.09
0.02
0.0E+00
2.0E+07
4.0E+07
6.0E+07
Number of cycles (n)

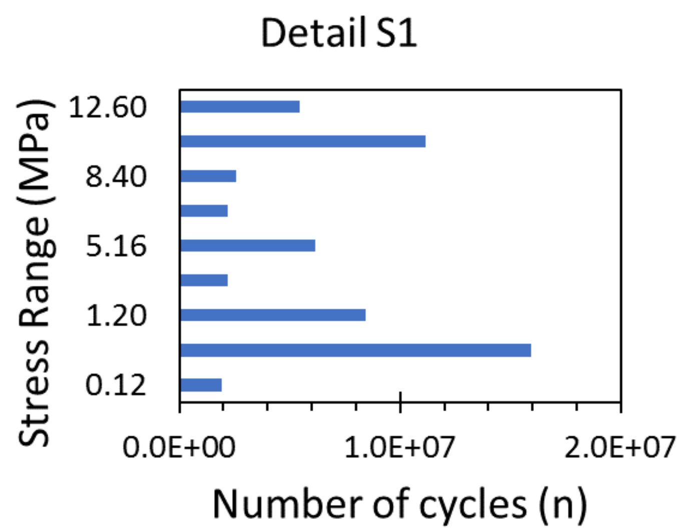
Detail S1
Stress Range (MPa)
12.60
8.40
5.16
1.20
0.12
0.0E+00
1.0E+07
2.0E+07
Number of cycles (n)

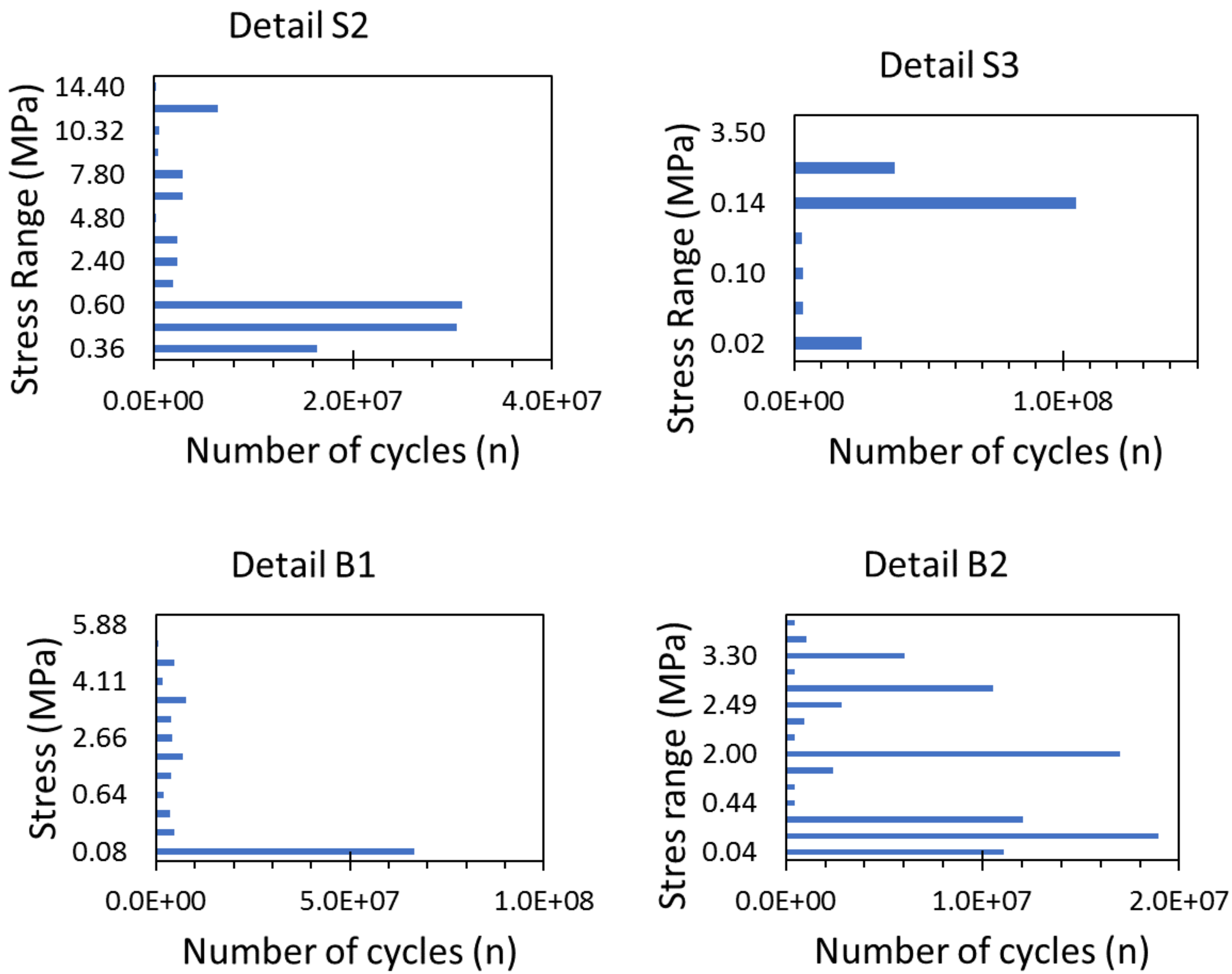

Detail S2
14.40
10.32
7.80
4.80
2.40
0.60
0.36
Stress Range (MPa)
0.0E+00
2.0E+07
4.0E+07
Number of cycles (n)
Detail S3
3.50
0.14
0.10
0.02
Stress Range (MPa)
0.0E+00
1.0E+08
Number of cycles (n)
Detail B1
5.88
4.11
2.66
0.64
0.08
Stress (MPa)
0.0E+00
5.0E+07
1.0E+08
Number of cycles (n)
Detail B2
3.30
2.49
2.00
0.44
0.04
Stres range (MPa)
0.0E+00
1.0E+07
2.0E+07
Number of cycles (n)

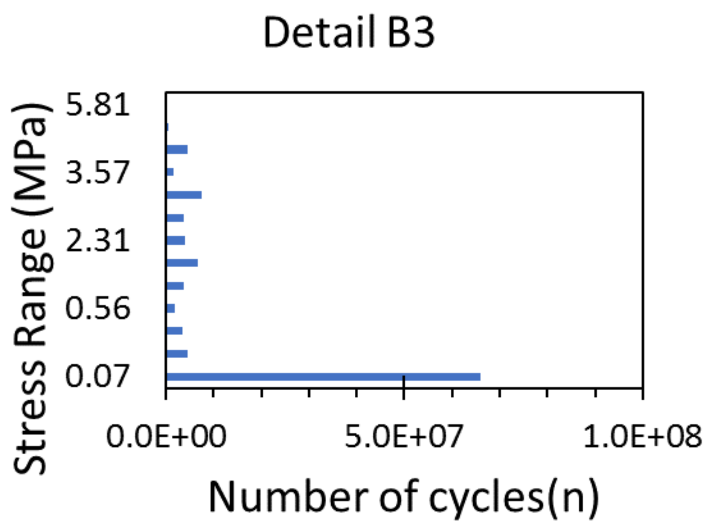

Detail B3
Stress Range (MPa)
5.81
3.57
2.31
0.56
0.07
0.0E+00
5.0E+07
1.0E+08
Number of cycles(n)

F.3 Damage calcualtions

Detail V1		R=10	
$\Delta\sigma_i\ (MPa)$	n_i	N_i	D_i
0.06	584000	4.0389E+38	1.44594E-33
0.12	1168000	3.94424E+35	2.96128E-30
0.3	8760000	4.13583E+31	2.11807E-25
0.42	584000	1.42982E+30	4.08442E-25
0.54	1752000	1.15834E+29	1.5125E-23
0.54	41975000	1.15834E+29	3.62371E-22
0.9	22046000	7.00407E+26	3.1476E-20
1.2	38544000	3.94424E+25	9.77223E-19
1.44	24382000	6.37016E+24	3.82753E-18
1.8	3504000	6.83991E+23	5.12287E-18
2.52	5256000	2.36467E+22	2.22272E-16
3	47304000	4.13583E+21	1.14376E-14
3.72	18688000	4.81223E+20	3.88344E-14
7.632	52925000	3.64243E+17	1.45301E-10
		D	1.454E-10

Detail V2		R=10	
$\Delta\sigma_i\ (MPa)$	n_i	N_i	D_i
0.06	16352000	4.0389E+38	4.04863E-32
0.12	27448000	3.94424E+35	6.95901E-29
0.18	21608000	6.83991E+33	3.15911E-27
0.36	2847000	6.6796E+30	4.26223E-25
0.54	1898000	1.15834E+29	1.63855E-23
0.6	4124500	4.0389E+28	1.02119E-22
1.8	4672000	6.83991E+23	6.8305E-18
1.92	4088000	3.58726E+23	1.13959E-17
3.24	3431000	1.91569E+21	1.791E-15
4.2	4088000	1.42982E+20	2.85909E-14
4.86	474500	3.3221E+19	1.42831E-14
6	1898000	4.0389E+18	4.6993E-13
6.6	1898000	1.55717E+18	1.21888E-12
7.8	5037000	2.92974E+17	1.71926E-11
8.76	7008000	9.17771E+16	7.63589E-11
9	8942500	7.00407E+16	1.27676E-10
9.72	4562500	3.24424E+16	1.40634E-10
10.2	8760000	2.00343E+16	4.37251E-10
10.8	8760000	1.1312E+16	7.74402E-10
11.4	1168000	6.5876E+15	1.77303E-10
12.6	219000	2.42142E+15	9.04428E-11
13.2	3066000	1.52067E+15	2.01621E-09
		D	9.529E-11

Detail V3		R=10	
$\Delta\sigma_i\ (MPa)$	n_i	N_i	D_i
0.12	2336000	3.94424E+35	5.92257E-30
0.18	21608000	6.83991E+33	3.15911E-27
0.6	4124500	4.0389E+28	1.02119E-22
1.92	4088000	3.58726E+23	1.13959E-17
4.5	5073500	7.17217E+19	7.07388E-14
7.8	5037000	2.92974E+17	1.71926E-11
9	15074500	7.00407E+16	2.15225E-10
10.2	9928000	2.00343E+16	4.95551E-10
13.2	3066000	1.52067E+15	2.01621E-09
		D	1.33E-12

Detail V4		R=10	
$\Delta\sigma_i\ (MPa)$	n_i	N_i	D_i
0.02	1401600	2.38493E+43	5.8769E-38
0.03	19491000	4.13583E+41	4.71272E-35
0.04	2920000	2.32903E+40	1.25374E-34
0.07	30003000	8.6456E+37	3.47032E-31
0.09	474500	7.00407E+36	6.77463E-32
0.1	23725000	2.44217E+36	9.71473E-30
0.2	584000	2.38493E+33	2.44871E-28
0.3	46720000	4.13583E+31	1.12964E-24
0.4	1423500	2.32903E+30	6.11198E-25
0.43	62926000	1.13003E+30	5.56851E-23
0.5	32521500	2.50078E+29	1.30045E-22
0.73	10220000	5.6826E+27	1.79847E-21
1.27	8760000	2.23737E+25	3.91531E-19
		D	3.93517E-19

Detail V5		R=10	
$\Delta\sigma_i\ (MPa)$	n_i	N_i	D_i
0.01	17520000	2.8607E-37	2.8607E-37
0.03	38748000	6.4787E-34	6.4787E-34
0.07	2372500	4.06204E-32	4.06204E-32
0.09	4088000	6.51853E-31	6.51853E-31
0.10	29163500	2.87932E-29	2.87932E-29
0.18	38887100	6.34957E-27	6.34957E-27
0.36	38748000	6.4787E-24	6.4787E-24
0.54	474500	4.57496E-24	4.57496E-24
0.72	4088000	6.99921E-22	6.99921E-22
0.91	5621000	8.96297E-21	8.96297E-21
0.96	4088000	1.16737E-20	1.16737E-20
1.33	4088000	2.94822E-19	2.94822E-19
1.56	1752000	6.33078E-19	6.33078E-19
2.0	1898000	8.03825E-18	8.03825E-18
2.27	4088000	6.21655E-17	6.21655E-17
2.76	693500	7.45454E-17	7.45454E-17
		D	7.1153E-17

Detail S1		R=0.1	
$\Delta\sigma_i\ (MPa)$	n_i	N_i	D_i
0.12	1898000	3.94424E+35	4.81208E-30
0.6	15914000	4.0389E+28	3.94018E-22
1.2	8468000	3.94424E+25	2.14693E-19
4.2	2190000	1.42982E+20	1.53166E-14
5.16	6168500	1.82507E+19	3.37988E-13
7.2	2190000	6.52305E+17	3.35733E-12
8.4	2591500	1.39631E+17	1.85596E-11
9.9	11132500	2.70037E+16	4.12258E-10
12.6	5475000	2.42142E+15	2.26107E-09
		D	2.6956E-09

Detail S2		R=0.1	
$\Delta\sigma_i\ (MPa)$	n_i	N_i	D_i
0.36	16352000	6.6796E+30	2.44805E-24
0.42	30368000	1.42982E+30	2.1239E-23
0.6	30952000	4.0389E+28	7.66348E-22
1.2	1898000	3.94424E+25	4.81208E-20
2.4	2372500	3.85179E+22	6.15947E-17
4.26	2409000	1.24074E+20	1.94159E-14
4.8	219000	3.76152E+19	5.82212E-15
5.4	2847000	1.15834E+19	2.45782E-13
7.8	2883500	2.92974E+17	9.84216E-12
9.6	474500	3.67336E+16	1.29173E-11
10.32	584000	1.78229E+16	3.27668E-11
12	6424000	3.94424E+15	1.62871E-09
14.4	219000	6.37016E+14	3.437016E-10
		D	2.02E-09

Detail S3		R=0.1	
$\Delta\sigma_i\ (MPa)$	n_i	N_i	D_i
0.02	25039000	2.38493E+43	1.04988E-36
0.06	3431000	4.0389E+38	8.49489E-33
0.1	3139000	2.44217E+36	1.28533E-30
0.12	2774000	3.94424E+35	7.03305E-30
0.14	104901500	8.44297E+34	1.24247E-27
0.28	37412500	8.24508E+31	4.53755E-25
3.5	438000	8.85309E+20	4.94742E-16
		D	4.94742E-16

Detail B2		R=0.1	
$\Delta\sigma_i\ (MPa)$	n_i	N_i	D_i
0.02	949000	2.38493E+43	3.97915E-3
0.05	12045000	2.50078E+39	4.8165E-3
0.1	2810500	2.44217E+36	1.15082E-3
0.22	474500	9.19493E+32	5.16045E-2
0.43	10512000	1.13003E+30	9.30239E-2
0.94	18943500	4.53416E+26	4.17795E-2
1	17009000	2.44217E+26	6.96472E-2
1.112	474500	8.44749E+25	5.61705E-2
1.2	474500	3.94424E+25	1.20302E-2
1.245	474500	2.72949E+25	1.73842E-2
1.37	474500	1.0485E+25	4.5255E-2
1.46	1058500	5.54941E+24	1.90741E-1
1.65	11096000	1.63281E+24	6.79564E-1
		D	2.65731E-18

Detail B3		R=0.1	
$\Delta\sigma_i\ (MPa)$	n_i	N_i	D_i
0.07	8.6456E+37	7.63302E-31	7.63302E-31
0.63	2.47953E+28	1.85478E-22	1.85478E-22
0.35	8.85309E+30	3.95794E-25	3.95794E-25
0.56	8.05184E+28	2.35723E-23	2.35723E-23
1.12	7.86313E+25	4.8276E-20	4.8276E-20
1.46	8.44297E+24	7.95455E-19	7.95455E-19
2.31	5.64489E+22	7.24195E-17	7.24195E-17
2.73	1.06206E+22	3.57419E-16	3.57419E-16
3.01	4.00046E+21	1.89778E-15	1.89778E-15
3.57	7.26262E+20	2.11081E-15	2.11081E-15
4.62	5.51259E+19	8.27651E-1	8.27651E-14
4.97	2.6559E+19	2.19888E-14	2.19888E-14
		D	2.19E-14

References

(n.d.). Retrieved from www.statictools.eu: http://www.staticstools.eu/profil_HEB.php?profil=HE650B&act=zobraz

Aref, A. J. (2007). Advanced Composite application in structural engineering. University at Buffalo.

(2015). *Assessment of existing structures in case of reconstruction,NEN8700.* Delft: Nederlands Normalisatie-instituut.

(2015). *Assessment of existing structures in case of reconstruction,NEN8701.* Delft: Nederlands Normalisatie-instituut.

Bjorklund, L. (2004). *Dynamic Analysis of a Railway Bridge subjected to High Speed Trains.* Stockholm: Royal Institute of Techology.

Burnside, P. B. (n.d.). *Design optimization of and all-FRP bridge.* Proceedings of 38th Int. SAMPE Symposium.

cholsta, M. (2012). *Feasibility study on fiber reinforced polymer cylindrical truss.* Delft: Delft University of Technology.

compositeadvantage. (n.d.). *https://cdn2.hubspot.net/hub/457166/file-2256956858-pdf/marketing_and_web_documents/FiberSPAN_Deck_for_Pedestrian_Bridges_Brochure.pdf?t=1487373635425.* Retrieved from www.compositeadvantage.com.

Dan Frangopol, Y. T. (n.d.). *Maintenance and Safety of Ageing Infrastructure.* CRC Press.

Delft, W. (1997). Fatigue behavior of fibreglass wind turbine blade material under variable amplitude loading. *Aerospace Sciences Meeting & Exhibit*.

(2003). *Eurocode 1: Actions on structures - Part 2: Traffic loads on.* Brussels: EUROPEAN COMMITTEE FOR STANDARDIZATION.

(2006). *Eurocode 3 - Design of steel structures - Part 1-4: General rules.* Brussels: EUROPEAN COMMITTEE FOR STANDARDIZATION .

(2006). *Eurocode 3 - Design of steel structures - Part 2: Steel Bridges .* Brussels: EUROPEAN COMMITTEE FOR STANDARDIZATION .

(2005). *Eurocode 3: Design of steel structures - Part 1-9: Fatigue .* Brussels: EUROPEAN COM MITTEE FOR ST Al"OAROIZATI00i .

Goicolea, J. M. (2014). *Simplified Mechanical Description of AVE S-103 - ICE3 Velaro E High Speed Train.* Madrid: Technical University of Madrid – UPM.

GÜRTLER, H. W. (2004). *COMPOSITE ACTION OF FRP BRIDGE DECKS ADHESIVELY BONDED TO STEEL GIRDERS.* EPFL.

Heinen, T. a. (2002). *Reliable Optimal Use of Materials for Wind Turbine Rotor Blades.* EESD.

Hollaway, L. (2010). A review of the present and future utilisation of FRP composites in the civil infrastructure with reference to their important in-service properties. *Construction and Building Materials, vol. 24*, 2419–2445.

Ir. Arie Bleijenberg, P. D. (2017, June). *TNO TIME.* Retrieved from www.tno.nl: https://time.tno.nl/en/articles/how-can-we-keep-european-civil-structures-safe/

J, C. (1996). *Structural Design of Polymer Composites.* London: E & FN SPON.

Jing Ji, W. Z. (2012). Analysis and Comparison on Dynamic Characteristics of the Bridge subjected to moving load based on ansys. *Journal of Convergence Information Technology(JCIT)*.

K.H. Oostermeijer, A. (2000). *Dynamic behaviour of railway superstructures.* doi:HERON, Vol. 45, No. I (2000) lSSN0046-7316

Kok, L. (2013). *Feasibility study for FRP in large hydraulic structures.* Delft: TUDelft & Witteveen Bos.

(2012). *kunstwerken: deel 6, aanvullingen op NEN-EN normen,OVS00030-6.* ProRail.

LUDVIGH, E. (2001, March). ELASTIC BEHAVIOUR OF CONTINUOUSLY EMBEDDED RAIL. *PERIODICA POLYTECHNICA SER. CIV. ENG. VOL. 46, NO. 1*, pp. 103-114.

Ma´rio Garrido, J. R. (2013). Creep behaviour of sandwich panels with rigid polyurethane foam core and glass-fibre reinforced polymer faces: Experimental tests and analytical modelling. *Journal of Composite materials*, 1-13.

Mallick, P. (2007). *Fibre Reinforced Composites Material,Manufacturing and Design.* CRC Press .

MARA, V. (2015). *Development of connections for fibre reinforced bridge.* Chalmers University of Technology.

Movares. (2010). Strengtening Bridges. *IABSE WC2 Workshop Stockholm* .

(2011). *Nederlandse norm NEN-EN 1991-2+C1.*

Nijsen, D. ,. (2002). *Optimal and relianle use of Composte Materials for Wind turbines.*

Nijsen, D. (2002). Alternative fatigue lifetime prediction formulations for variable-amplitude loading. *Journal of Solar Energy Engineering,vol 124*, 396-403.

Nijssen, W. (2010). Strength and fatigue of wind turbine rotor laminates and subcomponents. *Aerospace Sciences meeting including the New horizons forum and Aerospace Exposition*.

NWO. (n.d.). *Metal Fatigue in steel bridges*. Retrieved from Toegepaste en technische Wetenschappen: http://www.stw.nl/nl/node/257

Oliver Wyman, I. (2016). *Assessment of European Railways:Characteristics and Crew related safety.* Newyork: Oliver Wyman,Inc.

P.W.Bach. (1992). Fatigue Properties of glass and Glass/carbon-polyester composites for wind turbines. *ECN-C-92-072*.

Pellegirino, C. (2012). Fatigue Damage Estimation in Existing Railway Steel bridge using detailed loading history. *ISRN*. doi:10.5402/2012/231674

Reijneveld. (2010). Changes in the soil phosphorus status of agricultural land in the Netherlands during the 20th century.

SNIJDER, H. (2010). Strengthening the Caland Bridge Rotterdam for Increased Load. *International Workshop Strengthening of steel bridges*.

Wahl, N. (2001). *Spectrum fatigue lifetime and residual strength for fibreglass laminates.* Montana State University.

WILLIAM F. ALBERS, O. H.-E. (2007). *DYNAMIC ANALYSIS OF THE BENTLEY CREEK BRIDGE WITH FRP DECK.* NEWYORK: TRANSPORTATION RESEARCH AND DEVELOPMENT BUREAU.

Woraphot Prachasaree, 1. A. (2015). Parametric Study on Dynamic Response of Fiber Reinforced Polymer Composite Bridges. *International Journal of Polymer Science*.